Louisiana Transportation Research

Development of an Accelerated Creep Testing Proceedure for Geosynthetics

by

Khalid Farrag, Ph.D., P.E.
John Oglesby, P.E.

LTRC
Louisiana Transportation Research Center

Sponsored Jointly by Louisiana State University and the Louisiana Department of Transportation and Development

TECHNICAL REPORT STANDARD PAGE

1. Report No.	2. Government Accession No.	3. Recipient's Catalog No.
307		

4. Title and Subtitle	5. Report Date
DEVELOPMENT OF AN ACCELERATED CREEP TESTING PROCEDURE FOR GEOSYNTHETICS	September 1997
	6. Performing Organization Code

7. Author(s)	8. Performing Organization Report No.
Khalid Farrag, Ph.D., P.E. **John Oglesby. P.E.**	

9. Performing Organization Name and Address	10. Work Unit No.
Louisiana Transportation Research Center	11. Contract or Grant No. **92-10GT**

12. Sponsoring Agency Name and Address	13. Type of Report and Period Covered
Louisiana Transportation Research Center **4101 Gourrier Ave.** **Baton Rouge, LA 70808**	**Final Report**
	14. Sponsoring Agency Code

15. Supplementary Notes

Conducted in cooperation with the U.S. Department of Transportation, Federal Highway Administration

16. Abstract

The report presents a procedure for predicting creep strains of geosynthetics using accelerated creep tests at elevated temperatures. Creep testing equipment was constructed and tests were performed on two types of geosynthetics: High Density Polyethylene (HDPE) geogrid, and Polyester (PET) geogrid) typically used in soil reinforcement applications.

Creep strains at room temperature were first measured in 10,000 hour tests at various loading levels (15 percent to 40 percent of ultimate strength of the geogrid T_{max}). Accelerated creep tests were then conducted at the same loads for 1,000 hours at various controlled-temperatures up to 72°C (160°F). Test results showed that temperature increased creep strains with a higher temperature effect in the HDPE geogrid than in the PET geogrid when tested at the same loads.

The procedure for extrapolating creep strains from elevated temperature tests using the Arrhenius Equation was evaluated. The results showed limitations associated with the estimation of the equation parameters and the corresponding predictions of creep strains.

An interpretation procedure based on shifting the 1,000 hour temperature curves to form creep response curves (master curves) at longer times was applied. Shift factors were established through comparison of the master curves with the 10,000 hour test results at room temperature. The master curves were compared with the analytical relationship of the temperature-shift factors known as the WLF equation. Creep curves were then established to predict creep response up to 100,000 hours (2 cycles shift on the log-time scale from the 1,000 hour test results).

The testing program and analysis demonstrated the applicability of applying the shift factors to the HDPE geogrid to predict the response at longer time intervals. The analysis was applicable to creep loads lower than 40 percent T_{max}. For the PET geogrid, the increase of creep strains at elevated temperatures was not sufficient to successfully establish the master curves in a form consistent with the WLF equation. This is mainly due to fact that creep tests were performed at temperatures close to the glass-transition temperature of the PET geogrid (75°C). Tests at higher temperatures would be required to obtain more measurable response of creep strains and to evaluate the applicability of temperature-shift factors in predicting creep strains for the PET geogrid.

17. Key Words	18. Distribution Statement
Geosynthetics, geogrid, creep, creep testing, temperature, temperature shift.	Unrestricted. This document is available through the National Technical Information Service, Springfield, VA 21161.

19. Security Classif. (of this report)	20. Security Classic. (of this page)	21. No. of Pages	22. Price
Unrestricted		106	

DEVELOPMENT OF AN ACCELERATED CREEP TESTING PROCEDURE FOR GEOSYNTHETICS

by

Khalid Farrag, Ph.D., P.E.

and

John Oglesby, P.E.

Louisiana Transportation Research Center
4101 Gourrier Ave.
Baton Rouge, LA 70808

LTRC PROJECT NO. 92-10GT
STATE PROJECT NO. 736-99-0188

conducted for

LOUISIANA DEPARTMENT OF TRANSPORTATION AND DEVELOPMENT
LOUISIANA TRANSPORTATION RESEARCH CENTER

in cooperation with

U.S. DEPARTMENT OF TRANSPORTATION
FEDERAL HIGHWAY ADMINISTRATION

September, 1997

ABSTRACT

The prediction of the long-term performance of geosynthetics is usually based on 10,000 hour extension creep tests. Creep tests at elevated temperatures accelerate testing duration to a reasonable time frame (1,000 hour), and the results can be extrapolated to predict creep response at longer time intervals.

The report presents a procedure for accelerated creep testing of geosynthetics at elevated temperatures. Creep testing equipment was constructed and tests were performed on two types of geosynthetics typically used in soil reinforcement applications: High Density Polyethylene (HDPE) geogrid, and Polyester (PET) geogrid.

Creep strains at room temperature were first measured in 10,000 hour tests at various loading levels (15 percent to 40 percent of ultimate strength of the geogrid T_{max}). Accelerated creep tests were then conducted at the same loads for 1,000 hours at various controlled-temperatures up to 72°C (160°F). The results showed that temperature increased creep strains for both types of geogrids with a higher temperature effect in the HDPE geogrid than in the PET geogrid.

The procedure for extrapolating creep strains from elevated temperature tests using the Arrhenius Equation was evaluated. The results showed limitations associated with the estimation of the equation parameters and the corresponding predictions of strains.

An interpretation procedure based on shifting the 1,000 hour temperature curves to form creep response curves (master curves) at longer times was applied. Shift factors were established through comparison of the master curves with the 10,000 hour test results at room temperature. The master curves were compared with the analytical relationship of the temperature-shift factors known as the Williams, Landel and Ferry (WLF) equation. Creep curves were then established to predict creep response up to 100,000 hours.

The testing program and analysis demonstrated the applicability of applying the shift factors to the HDPE geogrid to predict the response at longer time intervals. The analysis was applicable to creep loads lower than 40 percent T_{max}. The procedure did not accurately estimate creep response at the higher loading levels where accelerated creep failure occurred.

For the PET geogrid, the increase of creep strains at elevated temperatures was not sufficient to successfully establish the master curves in a form consistent with the WLF equation. This was mainly due to fact that creep tests were performed at temperatures up to 72°C (160°F) which is close to the glass-transition temperature of the PET geogrid (75°C). Near the glass-transition temperature, geogrid polymer exhibits less effect to change in its creep strains than at higher temperatures. Tests at temperatures higher than 75°C would be required to obtain more measurable response of creep strains and to evaluate the applicability of temperature-shift factors in predicting creep strains for the PET geogrid.

ACKNOWLEDGMENT

The development of an accelerated creep testing procedure for geosynthetics was supported by the Louisiana Transportation Research Center (LTRC), the Louisiana Department of Transportation and Development (LA DOTD), and the Federal Highway Administration (FHWA). The financial support and cooperation provided by these agencies are gratefully appreciated.

The authors are grateful to Joe Baker, director of LTRC; William Temple, former associate director-research at LTRC; Harold "Skip" Paul, associate director-research at LTRC; Paul Griffin and Curtis Fletcher, former managers of geophysical systems at LTRC; and Mark Morvant, manager of geophysical systems at LTRC for their effective collaboration and cooperation.

The authors are also grateful to Dr. Mehmet Tumay, associate dean for research and professor of civil engineering at LSU, for his cooperation.

Appreciation is extended to Hadi Shirazi, geotechnical research engineer at LTRC, for his assistance in performing the testing program, and to William Tierney, research associate at LTRC, for his assistance in the construction of the testing equipment.

SIGNIFICANCE OF RESEARCH AND IMPLEMENTATION

The growing use of geosynthetics as reinforcement elements for the stabilization of permanent highway embankments, walls, and slopes makes it necessary to evaluate the long-term performance of these materials. The inherited creep characteristics of such materials requires the evaluation of their creep strains under the anticipated design loads. Creep strains are usually estimated from the results of extension creep tests for a duration of 10,000 hours, which are usually extrapolated to one order of time cycles (i.e. up to 10 years). Longer testing duration is usually required to predict creep response for the life-time of the structure.

The investigation of the applicability of temperature-controlled accelerated creep tests in predicting creep strains to longer time intervals offered a practical and economical solution for testing various geosynthetics in reasonable time frames. The proposed research aimed to establish a testing procedure and analysis of accelerated creep tests. The report can help the geotechnical engineers in evaluating creep strains at longer time frames from accelerated tests for many geosynthetics used in soil reinforcement applications.

The interpretation procedure of creep test results provided the shift factors and established master curves for the High Density Polyethylene (HDPE) geogrid that could be used to predict creep strains at longer time intervals. The procedure is applicable for testing other types of polyethylene (PE) and polypropylene (PP) geogrids and geotextiles as their creep properties demonstrate a measurable response to temperature increase. Further tests at higher temperatures may be required to demonstrate the applicability of the procedure on polyester (PET) geosynthetics.

TABLE OF CONTENTS

LIST OF TABLES

Table Page

LIST OF FIGURES

Figure Page

Figure Page

INTRODUCTION

The main design concern for the long-term stability of geosynthetic-reinforced soil structures is the prediction of the creep behavior of geosynthetics under the design loads. The long-term stresses and strains in the reinforcement should not exceed their corresponding allowable design values during the life of the structure. The current state-of-practice design methods and standards usually incorporate an allowable load for creep, or a factor of safety along with the safety factors for other degradation mechanisms, to obtain the allowable long term strength of geosynthetics *[1],[2]*. The safety factor for creep load is determined from unconfined creep tests with a minimum duration of 10,000 hours *[3],[4]*. It is a general practice that the geosynthetics creep data from these tests is extrapolated up to one order of time magnitude (i.e. up to 10 years) *[1],[5]*. Creep performance for longer duration, however, can be predicted in accelerated creep tests. In these tests, geosynthetics are subjected to creep loads at elevated temperatures. The results of these tests can be shifted to extrapolate creep behavior (at the same loading levels) to longer time intervals using time-temperature superposition principles.

Accelerated creep testing procedures have been established for testing time-temperature behavior of plastic pipes. Task Force 27 guidelines *[2]* referenced a testing procedure on plastic pipes (ASTM D 2837-1990) as a guide for running accelerated creep tests on geosynthetics. However, this testing procedure is related to failure modes associated with plastic pipes which are not directly applicable to geosynthetic materials *[1]*. Additionally, analytical methods for extrapolating creep data from accelerated tests have not yet been standardized. Some research on the temperature-dependent creep behavior of geosynthetics has been done *[6],[7],[8],[9]* and they demonstrated the effect of temperature on creep strains of geosynthetics and the applicability of extrapolating creep strains to longer time intervals.

Various factors influence geosynthetics strength and physical properties and affect the role of temperature on their creep behavior. These factors are mainly related to the polymer type, its chemical and chain structure, the nature of its intermolecular cohesive

forces, its manufacturing process, and the degree of orientation and crystallinity of the polymer *[10],[11]*. Consequently, temperature-creep relationships vary for each type of polymer used in soil-reinforcement applications. Moreover, extrapolation of strains from elevated temperature tests is limited to temperature ranges and loading levels which do not alter the physical nature of the polymeric specimens.

The report presents the newly developed accelerated creep testing equipment. The testing procedure and the analytical methods used to predict creep at longer time intervals are also evaluated.

A discussion concerning the principals of geosynthetic time-temperature dependency is presented in chapter 1. It also includes a review of the current procedures for extrapolating strains to longer time intervals.

Creep testing equipment was constructed at LTRC to permit geosynthetic testing under various controlled temperatures and extension loads. Chapter 2 illustrates details of the equipment and the testing program. The results of the testing program are presented in chapter 3.

Chapter 4 discusses the analytical procedures for predicting creep strains from elevated temperature tests using the Arrhenius Equation. The parameters associated with the application of the Arrhenius Equation are presented, and the applicability of the equation to predict creep strain-rates at longer time intervals is also assessed.

An interpretive procedure based on applying shift factors on the temperature-creep curves to establish master curves at longer time intervals is presented in chapter 5. This procedure was based on the temperature dependancy of the shift factors known as the WLF equation. Creep test results at elevated temperatures on the HDPE geogrid were used in predicting creep strains at longer time intervals. The procedure was evaluated through comparisons with the 10,000 hour creep test results at room temperature.

The extrapolation procedure was used in establishing creep strain curves up to 200,000 hours from the 1,000 hour temperature-creep tests. The results of the analytical procedures are discussed in chapter 6 and show the applicability of the procedure on the HDPE geosynthetic within the tested ranges of temperatures and loading levels.

OBJECTIVES

The objectives of the research are:

i) to develop testing equipment and a standard testing procedure for accelerated creep test of geosynthetics at controlled elevated temperature,

ii) to evaluate time-temperature relationships of geosynthetics used in reinforced soil applications, and

iii) to develop an analytical procedures for predicting creep strains at longer time intervals from the accelerated tests at elevated temperature.

SCOPE

The testing program was performed using two types of creep testing equipment. The first type consisted of five loading frames to test geosynthetic specimens at various creep loads in room temperature. The second type of testing equipment consisted of two creep loading frames with ovens for testing geosynthetics in various controlled and elevated temperatures. An instrumentation array and a data acquisition system were utilized in monitoring the applied loads, the specimens' elongation, and the temperatures surrounding the specimens.

Creep tests for various durations ranging from 1,000 to 10,000 hours were performed on two types of geosynthetics commonly used in soil reinforcement applications: High Density Polyethylene (HDPE) geogrid and Polyester (PET) geogrid. These tests were performed at various loading levels ranging from 15 percent to 40 percent of the tensile strength of the geogrid and at temperatures ranging from 24^{o}C (75^{o}F) to 72^{o}C (160^{o}F).

Two analytical procedures were used in predicting creep strains at longer time intervals. These procedures are commonly used in establishing time-temperature relationships for polymers and they are the Arrhenius Equation and the time-shift principal based on the WLF Equation.

CHAPTER I

TIME-TEMPERATURE DEPENDENCY OF GEOSYNTHETICS

A. Introduction

The growth of geosynthetic applications in geotechnical engineering has created a substantial number of new products in the market. Polymers most commonly used in soil reinforcement applications today are Polyethylene (PE), Polypropylene (PP), and Polyester (PET) *[11]*. The physical properties of these polymers are mainly influenced by their chemical and molecular chain structure, molecular weight and distribution, and manufacturing process *[11],[12]*.

Chapter 1presents the principles of time-temperature relationships of geosynthetics. It discusses the influence of polymer types and characteristics on their long-term behavior and their temperature dependency, and also presents an introduction to the principals of extrapolating creep test results to longer time intervals which will be applied to the results of the testing program in subsequent chapters.

B. Effect of Geosynthetic Type on Long-term Properties

Load-elongation properties of different polymers are schematically shown in figure 1. The figure shows the high strength and low elongation properties of PET in comparison with the Polyolefines (PE and PP fibers). This is mainly due to the strong intermolecular cohesive forces of the PET *[12]*. In addition, for the same polymer type, strength also increases at high molecular weight (the total mass of the molecular chains with respect to their number in the fiber). Higher average molecular weights and narrow distributions result in an increase in strength and durability *[12],[13]*.

Polymer structure is mainly characterized by long-chain molecules arranged in two phases: the Crystalline Region, where the filaments are mostly oriented, and the

Amorphous Region, where the filaments are randomly interweaved. Figure 2 shows the two phase structure of a drawn polymer. The degree of crystallinity of the polymer (defined as the portion of the polymer chains that are crystalline) changes according to polymer type and manufacturing process. Polyolefines have a high degree of crystallinity (70-85 percent) while PET usually has a lower crystalline percentage (30 -40 percent) *[14]*.

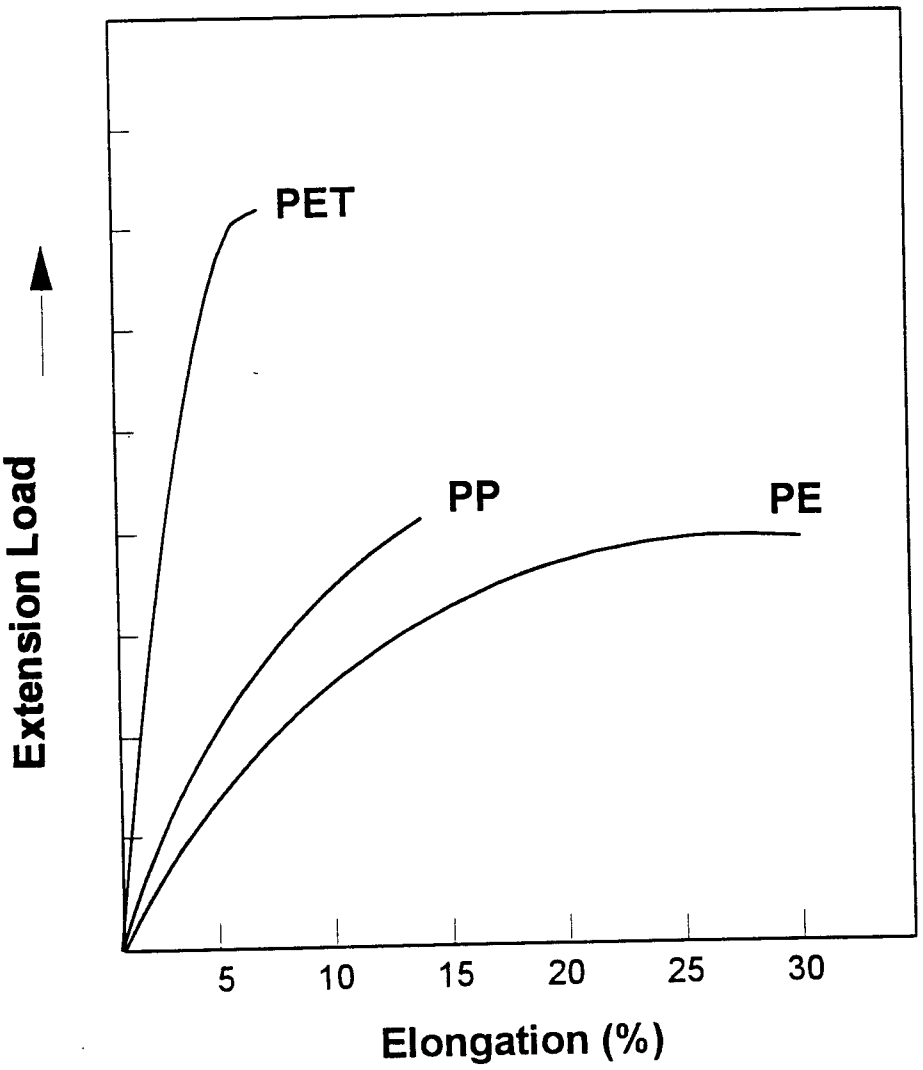

Figure 1

Schematic of load-elongation curves for different polymers (*reproduced after [12]*)

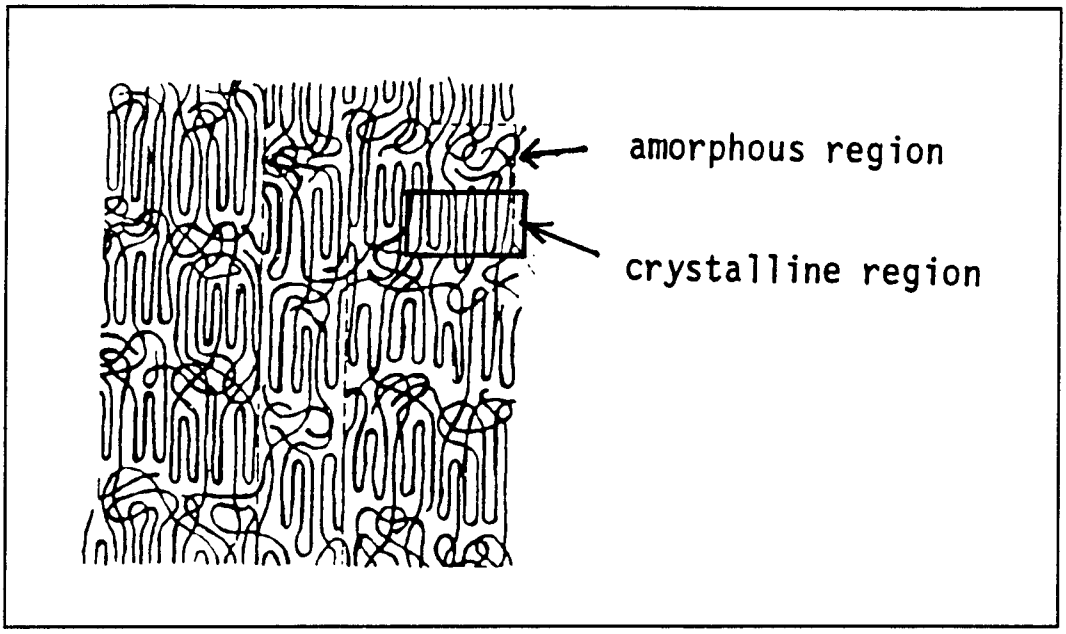

Figure 2

The two phase structure of a drawn polymer *[15]*

The structure of the polymer plays an important part in the long-term deformation characteristics. The degree of crystallinity and the orientation of the fibers affect the stress-strain properties of the polymer. Short-term stress-strain behavior is mostly determined by the deformation of the amorphous regions. Conversely, long-term deformation of the polymer is mostly determined by the deformation of the crystalline regions *[14]*. Creep in PE and PP occurs by slippage of the chains in the crystalline region. On the other hand, creep in PET usually occurs as a result of chain breakage at the interface between the crystalline and amorphous regions *[15]*. Figure 3 shows creep characteristics of various polymers at loading level of 60% T_{max}.

Temperature accelerates the time-dependent deformation process in polymers. The increase in temperature expedites the rearrangement and displacement of the polymer chains with respect to each other *[12]*. Accordingly, polymers with strong intermolecular bonds, such as PET, are more resilient to the increase in temperature than PE and PP polymers. A schematic of the effect of temperature on tensile strength of different polymers is shown in figure 4.

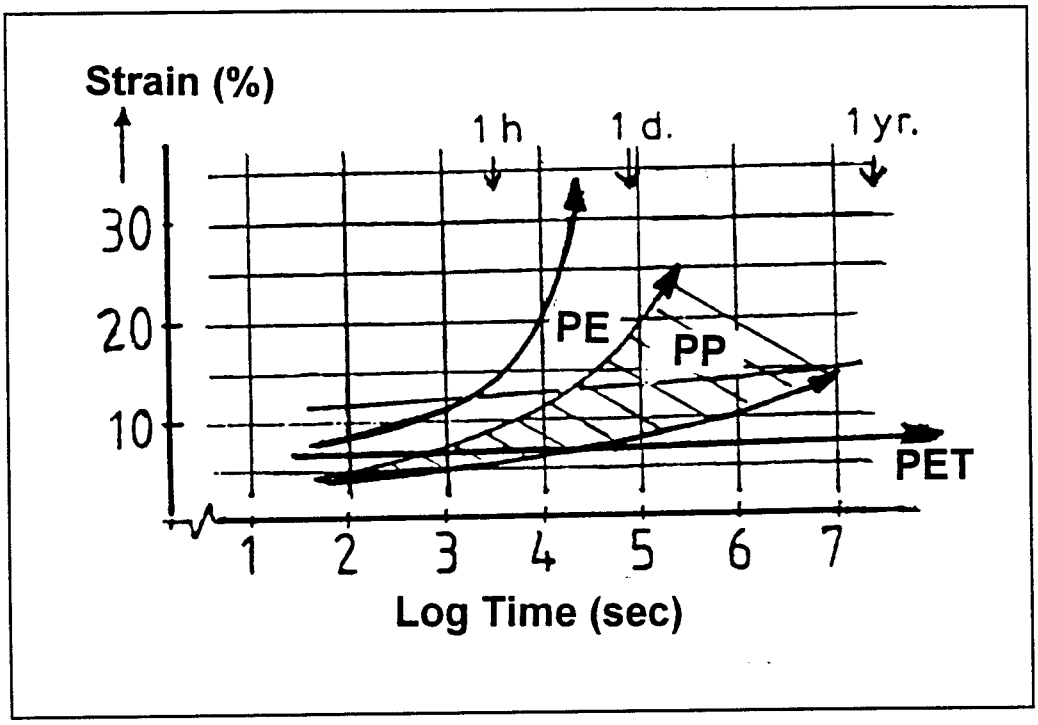

Figure 3

Creep at 60% loading for various types of polymers *[14]*

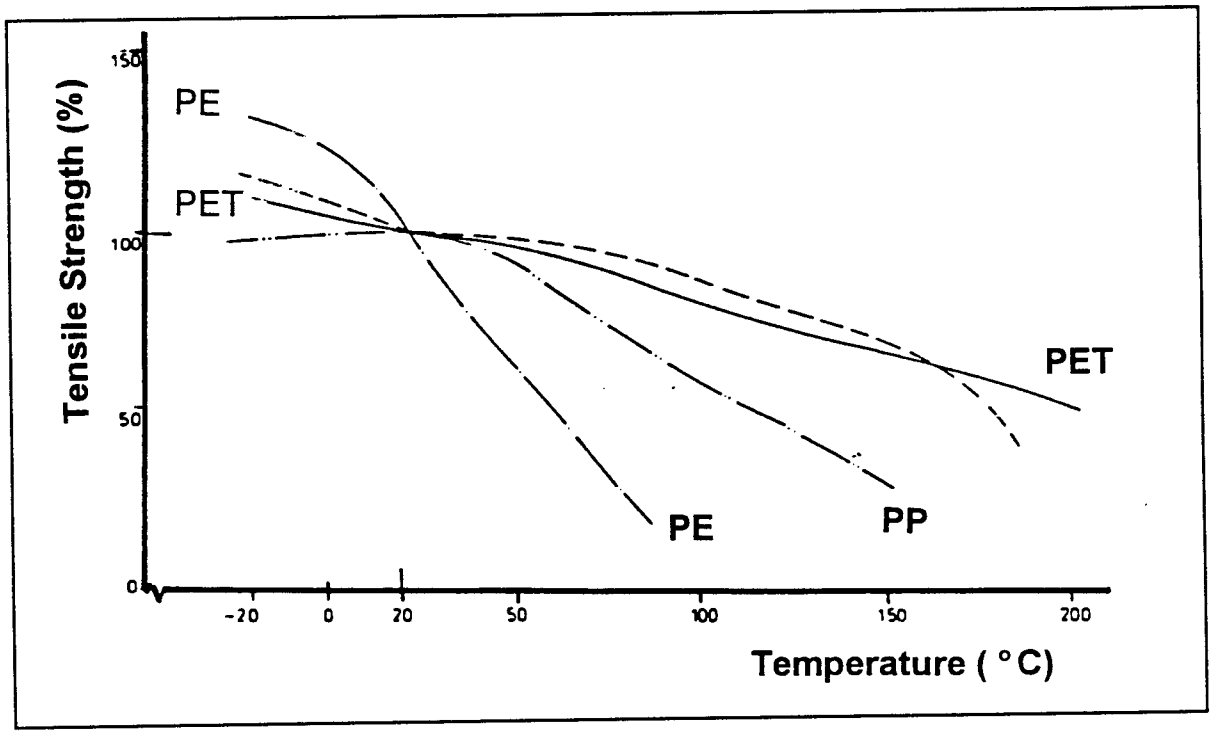

Figure 4

Schematic of the change of tensile strength with temperature *[12]*

C. Strain-Time-Temperature Relationships in Geosynthetic Polymers

Figure 5 shows a typical behavior of tensile strength properties of polymers with temperature. The figure shows the tensile modulus E of three different polymers; namely: an amorphous polymer Polystyrene (PS), and two crystalline polymers: PE and PVC. The modulus was measured after 10 seconds of tensile loading of the specimen at various temperatures *[16]*.

Polymers behavior with a change in temperature can generally be defined by three regions: the glassy region, the transition region, and the rubbery region. The glassy region is characterized when polymers are hard and brittle at low temperatures. As a polymer is heated to the transition region, the thermal energy is sufficient to cause movement of the polymer chains, which results in a drastic decrease in the tensile modulus. The temperature at which this movement occurs is defined as the glass-transition temperature (T_g). As the temperature is further increased, the polymer reaches the rubbery region where it exhibits slight reduction in its modulus. As temperature further increases, the modulus correspondingly decreases until the specimen reaches a state of thermal degradation.

The exact shape of the modulus-temperature curve depends on the degree of crystallinity of the polymer. Non-crystalline polymers closely exhibit the behavior of the PS polymer with temperature change. For highly crystalline polymers (as in PE), the polymer exhibits slight and gradual decrease in its modulus as temperature increases from its T_g value until it reaches its melting temperature ($T_{m)}$. At this point, the modulus rapidly decreases as the polymer looses its crystallites and behaves like an amorphous polymer. PVC has a lower degree of crystallinity than PE and its behavior is located between the PE and the amorphous PS polymer.

The value of T_g depends on many factors. The major factors that affect T_g are the molecular structure of the polymer, the rate of cooling from the melt during manufacturing process, the degree of crystallinity, and the presence of additives

[16],[17]. Table 1 shows typical glass-transition and melting temperatures for various polymers used in geosynthetics *[18]*. It should be noted that some polymers used in the geosynthetics industry are processed and treated by additives to reach a T_g below room temperatures such as PE, PP, and flexible PVC membranes in order to maintain their rubbery state at the normal temperature range of applications. PET, nylon, and rigid PVC, on the other hand, are in their glassy state at room temperature since their glass temperature is well above 70°C (160°F) *[17]*.

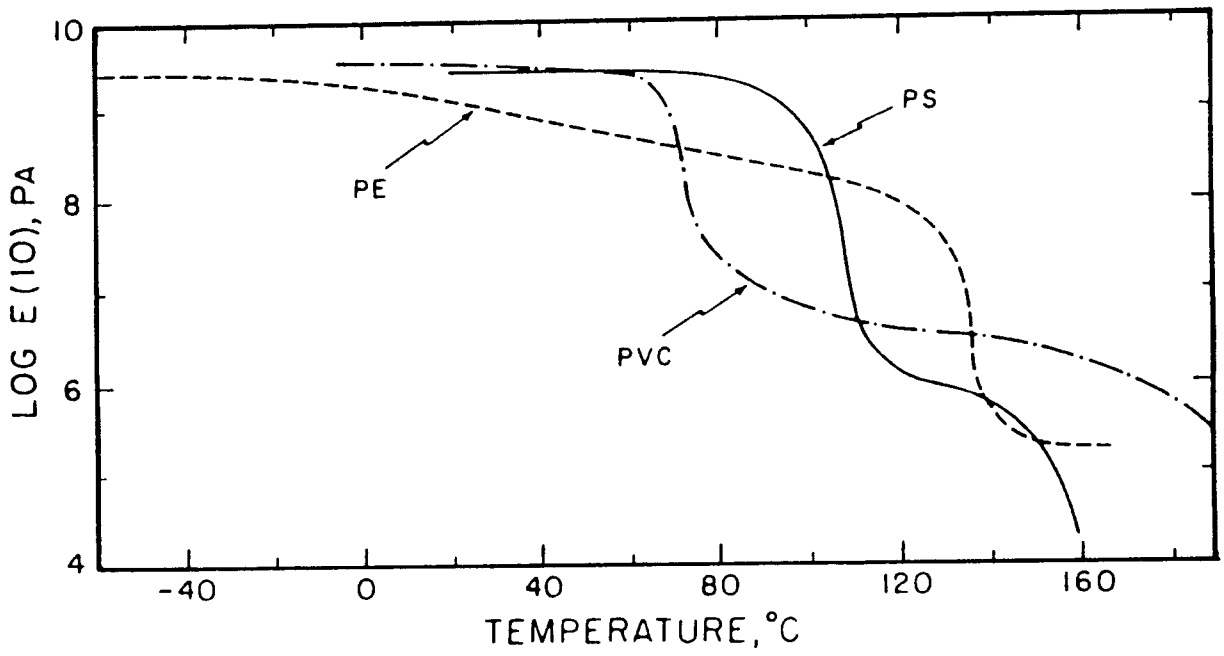

Figure 5

Tensile modulus E versus temperature for different polymers *[16]*

Table 1

Thermal transition limits of polymers used in geosynthetics *[18]*

Polymer	Glass Transition		Melting Range	
	°C	°F	°C	°F
Low density Polyethylene	-80	-112	60-100	140-212
Medium Density Polyethylene	-80	-112	80-120	176-248
High Density Polyethylene	-80	-112	100-140	212-284
Polypropylene	-10	14	100-165	212-330
Polyethylene terephthalate	75	167	200-260	390-500
Polyvinyl chloride (PVC)	80	176	--	

When tensile modulus E is plotted versus time for different temperatures, the behavior will be as shown in the left side of figure 6 *[16]*. The value of E decreases as temperature increases from T_1 to T_7 in the figure. When the experimental logarithmic curves of E along the time axis are shifted until the modulus values overlap, a single curve is obtained as shown in the right side of the figure. This curve, the master curve, represents E for longer time intervals at the reference temperature. The modulus E along the master curve can be expressed as:

$$E\ (\ T_O\ ,\ t\ )\ =\ E\ (\ T\ ,\ \frac{t}{a_T}) \qquad (1)$$

where T_o is an arbitrary reference temperature, T is the shifted temperature, and the horizontal distance shifted represents the logarithm of the shift factor a_T at time t.

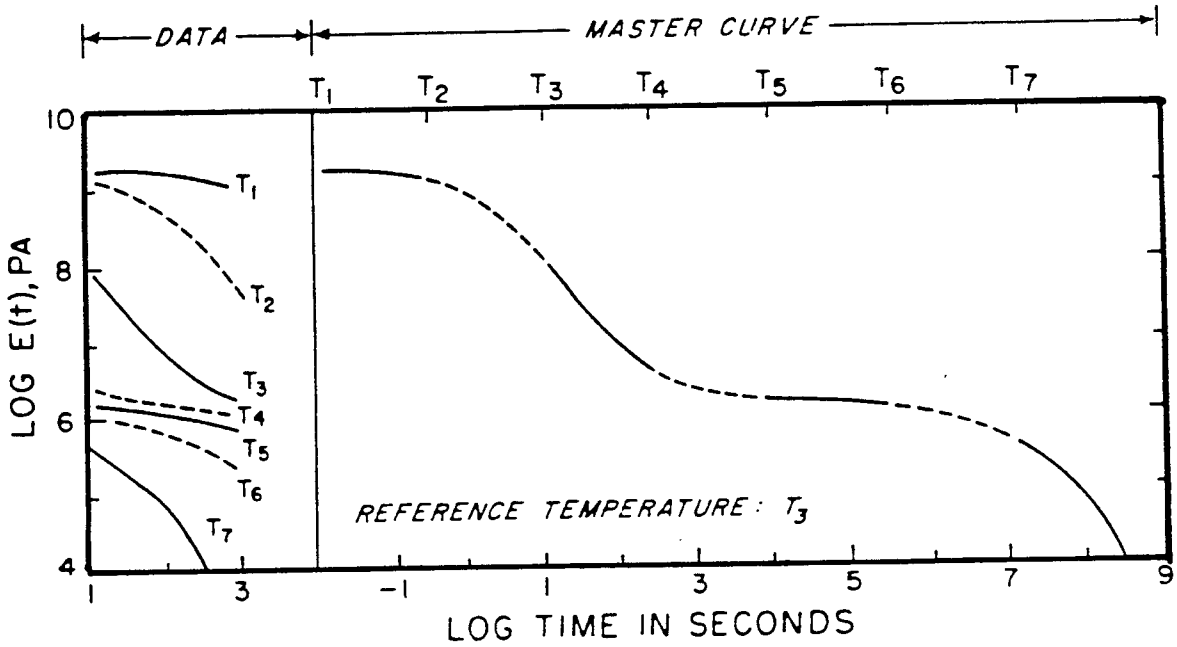

Figure 6

Construction of the master curve from experimental E values *[16]*

D. Modeling Strain-Time-Temperature Superposition

Extension creep is the increase of strain with time when a material is subjected to a constant extension load. This effect is due to the molecular rearrangement in the polymer induced by the stress. If polymer specimens are subjected to various constant extension loads (σ) and strains (ϵ) at particular times t_a and t_b, they can be plotted with respect to stresses in an isochronal plot as in figure 7. Polymers would show a linear visco-elastic creep at low stress levels and a non-linear creep rate at higher stress levels and time periods. In visco-elastic creep the molecules slowly recover their former arrangement and strains return to zero when stresses are released.

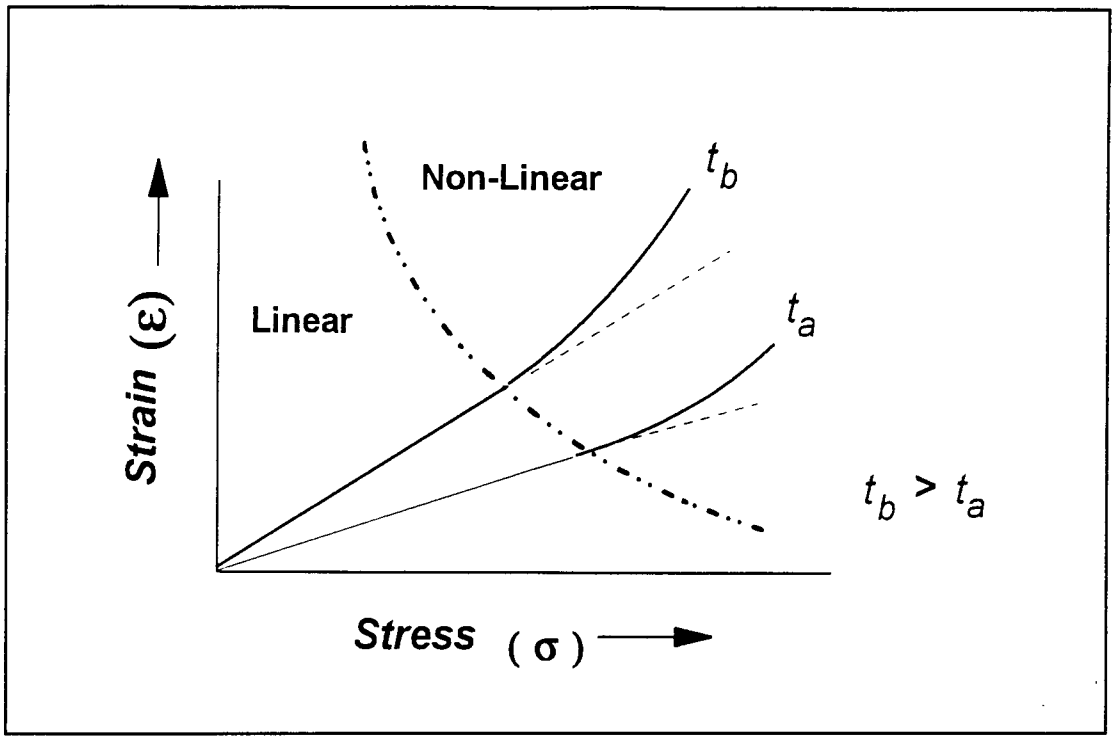

Figure 7

Isochronal plots for constant creep loads (σ) at different time *t*

In the linear visco-elastic zone, figure 7 shows that, for any time *t* :

$$\frac{\epsilon_1(t)}{\sigma_1} = \frac{\epsilon_2(t)}{\sigma_2} = J(t) \qquad (2)$$

where *J (t)* , creep compliance, is the reciprocal of the tensile modulus *E(t)* .

An increase in temperature from T_o to T results in the same relationship of the creep compliance *J(t)* with a constant time shift equal a_T. Figure 8 illustrates the shift of the creep curve along the log-time scale with a shift factor log a_T. The principal of shifting the creep compliance *J(t)* (or other visco-elastic function) against the logarithm of time is known as the time-temperature superposition. Different methods have been established for the superposition procedure *[20]*.

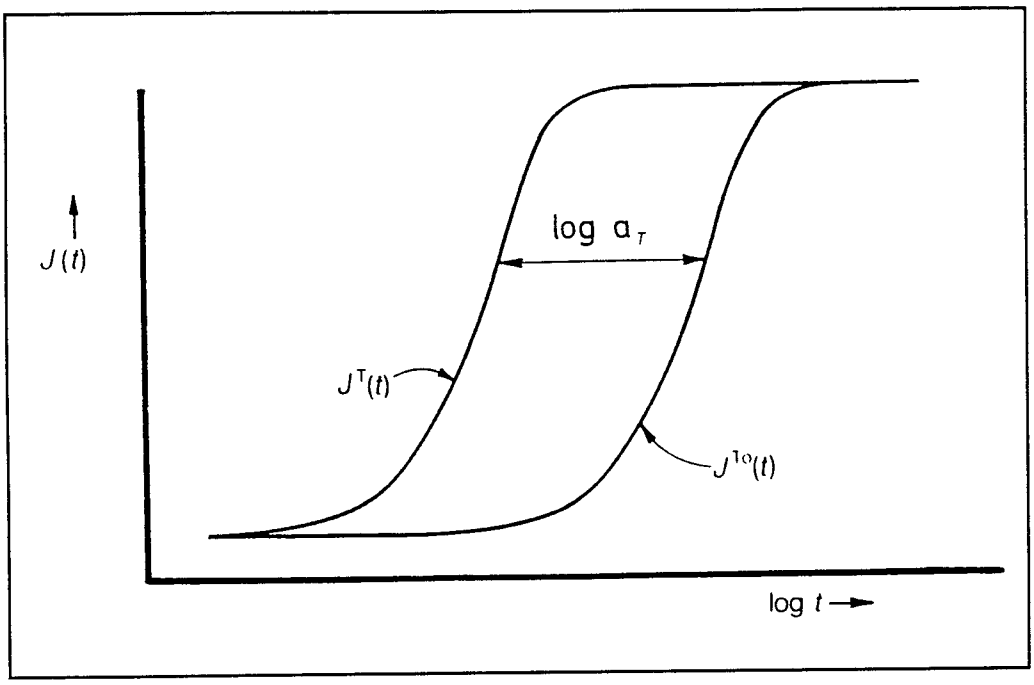

Figure 8

Variation of creep compliance J(t) with time and temperature *[19]*

An empirical equation for the shift factor a_T was proposed by Williams, Landel and Ferry *[21], [22]* in the form known as the WLF equation:

$$Log\ a_T = \frac{-C_1\ (\ T\ -\ T_g\ )}{(\ C_2\ +\ T\ -\ T_g\ )} \qquad (3)$$

where C_1 and C_2 are constants that slightly change according to the polymer type, and T_g is the glass transition temperature of the polymer.

The determination of the shift factors to predict creep response at longer time intervals was carried out in this report by applying the WLF time-shift principals on the experimental results. The application of the WLF procedure on the creep test results is further discussed in chapter 5.

CHAPTER II
TESTING EQUIPMENT AND PROGRAM

A. Design Considerations

This chapter presents the creep testing equipment and testing program for the evaluation of time-temperature-deformation characteristics of geogrid reinforcement. The creep testing equipment was constructed to permit evaluating long-term strength properties of a wide range of geosynthetic materials currently being used in highway applications. These materials consist of various polymers and differ in their manufacturing process and geometry. As a result, they demonstrate different stress-strain characteristics and exhibit different time-temperature responses.

These variations result in the development of different creep testing equipment to accommodate the various requirements of clamping mechanisms, specimen dimensions, temperature ranges, loading levels, testing durations, and methods of creep measurements. Accordingly, various procedures were suggested and practiced for different types of geogrids according to their flexural stiffness *[23],[24]*, as well as for different geotextiles *[25],[26],[27]*.

Creep testing equipment was designed and constructed to offer the flexibility of testing various types of geosynthetics without sacrificing the robustness of the loading mechanism or the accuracy of the monitoring system. Therefore, the creep testing equipment was constructed at LTRC with the following design considerations:

❒ **Frame dimensions**: The height of the loading frame was made adjustable to accommodate the length of the specimen and the expected elongation during the test. The height of the frame used in the testing program was 102 cm (40 in) .

The width of the loading frame was designed to test geosynthetic specimens of the

same dimensions of 20 cm (8 in) as in short-term testing procedure ASTM Wide Width D-4595. Running long-term tests on specimens of the same dimensions as in short-term tests permitted an appropriate comparison of test results without the possible effect of specimen dimensions on the results.

❒ **Loading system**: Most creep testing equipment utilized loads applied by dead weights hung from the bottom clamps *[8],[23],[24]*. This loading mechanism is the most economic, precise and stable method of applying creep loads. However, the applied loads are usually limited within the appropriate range of dead weights that can be placed on the loading frame. Accordingly, dead loads may not be an appropriate system for testing rigid geosynthetic specimens at high loading levels.

A lever loaded mechanism is usually used when higher loads are required *[25]*, since the lever increases the dead weights by multiple of the lever ratio. However, an elongation of the specimen results in a movement of the weights magnified by the same lever ratio and a mechanical damping system may be required to prevent possible vibrations of the weights.

Extension creep loads were also applied by pneumatic jacks with the loads maintained constant by regulating the air pressure *[26]*. A hydraulic system that applied the extension loads on the upper clamps was used in the LTRC testing equipment. Such a system offered the flexibility of applying higher loads to each loading frame independently. However, the equipment was costly as it required precision and maintenance to keep the applied loads constant within an acceptable range of accuracy during the testing period.

❒ **Clamping mechanism**: The design of the loading system permitted using different clamps according to the types of geosynthetics tested in order to prevent slippage or breakage of the specimens inside the clamps. Grip type clamps of model "Curtis Geo-Grip" were extensively used in the short-term extension tests at LTRC and

were also used in the long-term testing program.

❒ **Temperature control**: Creep tests in elevated temperatures were carried out with the specimens inside temperature controlled ovens. The ovens were constructed so that instrumentation and creep measuring devices are located outside the ovens. This configurations eliminated the possible effect of temperature on the instruments.

❒ **Response monitoring**: A data acquisition system was used for automatic monitoring of time, loads, temperature, and displacement of the specimens.

B. Creep Testing Equipment

The evaluation of temperature effects on the creep characteristics of geosynthetics required the development of testing equipment for testing geosynthetics in controlled temperatures. Two types of creep testing equipment were constructed to perform creep tests at room temperature and also in elevated temperature environments.

The first type of testing equipment consisted of four loading frames to test geosynthetic specimens at various loading levels at room temperature. The loading frames are shown in figure 9. The specimens were clamped to the loading frames using Curtis Geo-Grips. Loads were applied to each loading frame through a hydraulic cylinder mounted on the top plate.

A hydraulic loading system applied extension loads up to 4,500 kg (10,000 lb) to each loading frame independently. The loading system consisted mainly of a regulated air pressure source and an air driven hydraulic pump. The pump applied hydraulic pressure to the loading system. This pressure was regulated to the required load for each frame independently. Figure 10 shows a schematic of the hydraulic system for one frame.

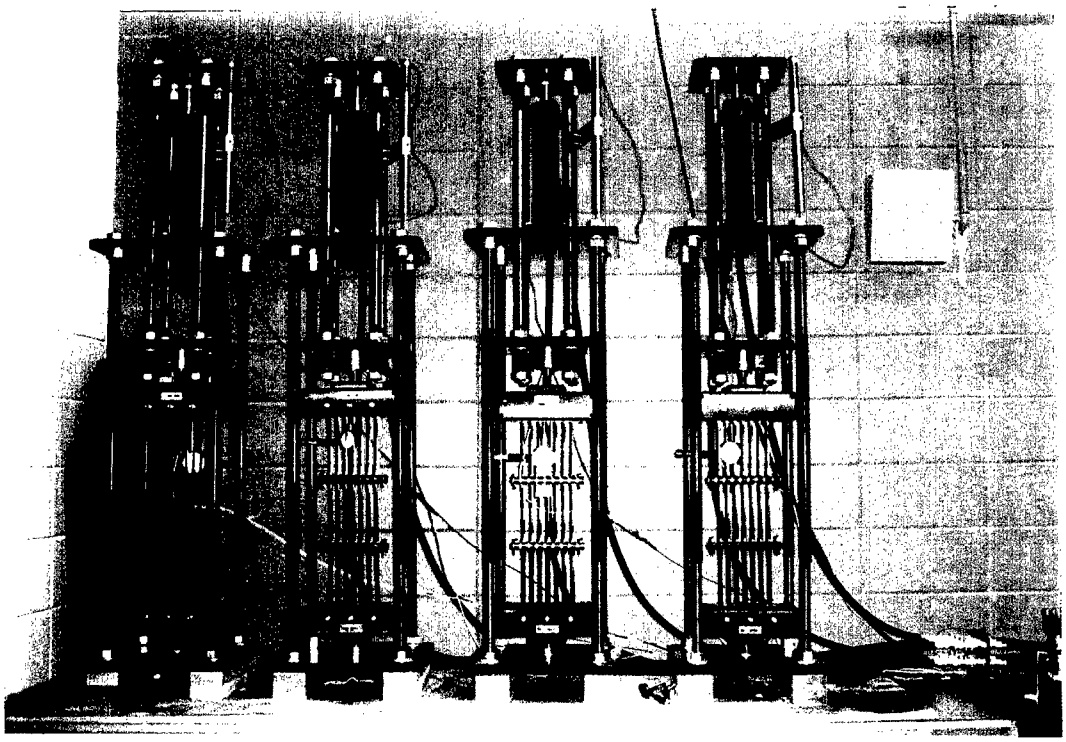

Figure 9

View of the loading frames for testing geogrids at room temperature

The applied load at each frame was monitored using a load cell mounted above the upper clamp. Displacement was monitored by a Linear Variable Differential Transformer (LVDT) mounted on the upper plate of the loading frame. The instruments were connected to a data acquisition system and a computer for response monitoring and recording at specific time intervals. Figure 11 shows a view of the testing equipment including the hydraulic loading system and the data acquisition system.

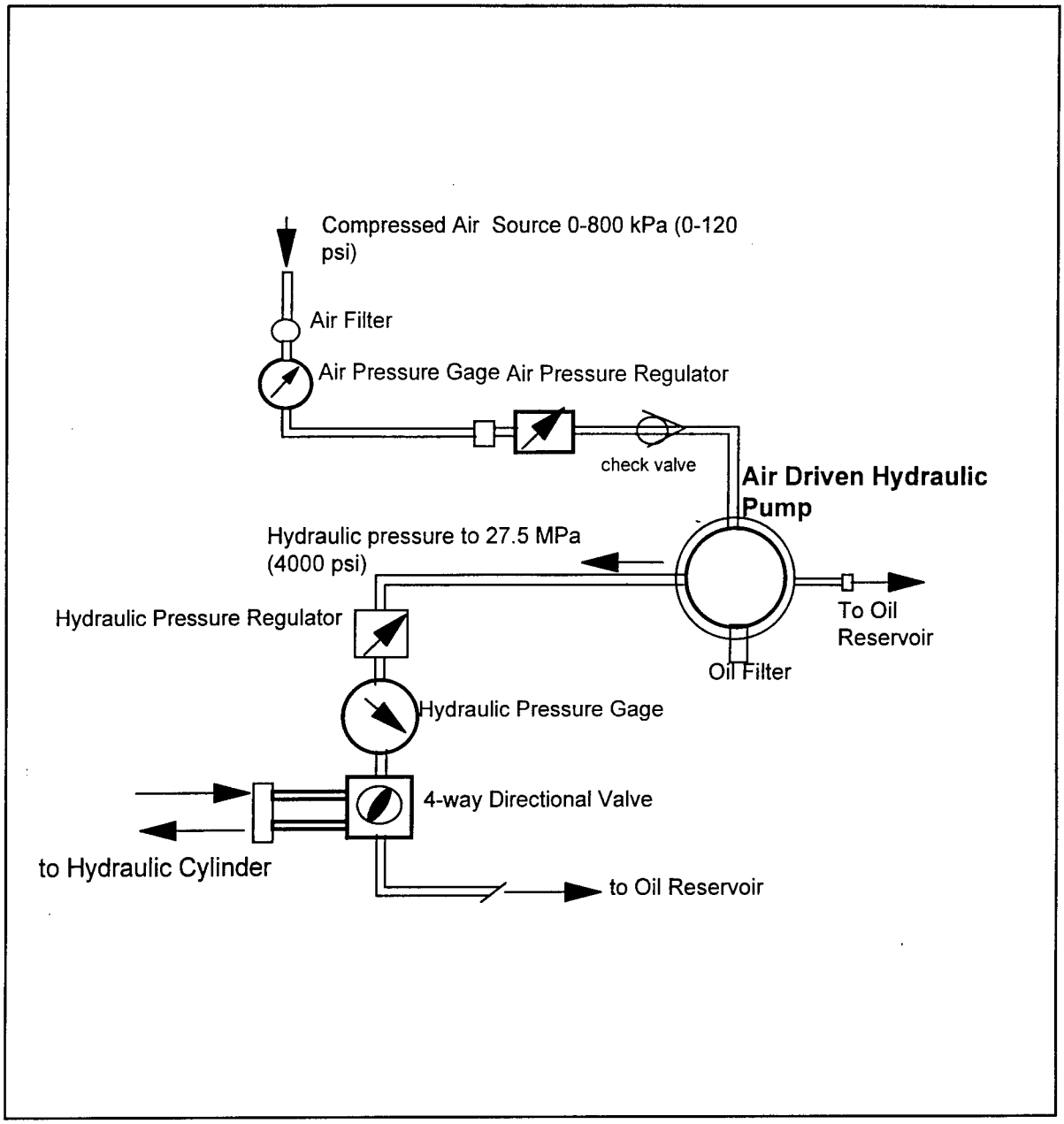

Figure 10

A schematic diagram of the hydraulic system for one loading frame

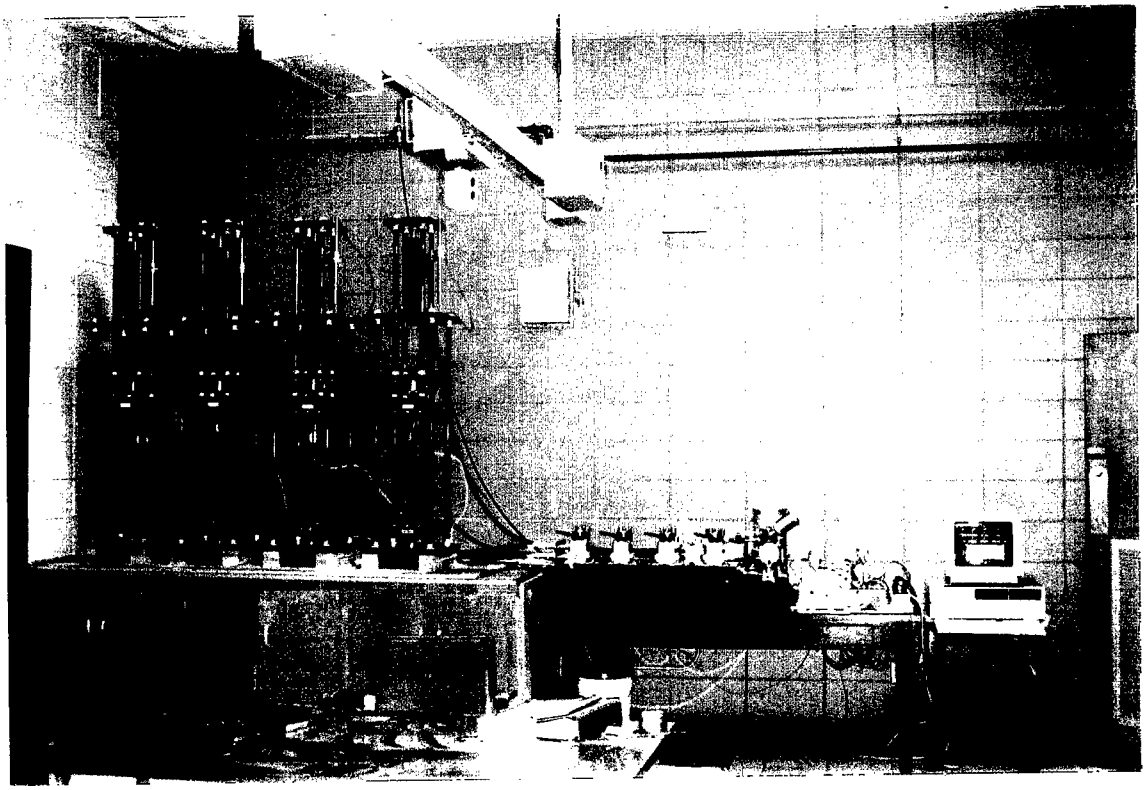

Figure 11

View of the creep testing equipment in room temperature

The second type of testing equipment was constructed to test the geogrids at elevated temperatures. It consisted of two testing frames that applied extension creep loads on specimens located inside the test ovens. Figure 12 shows a view of the loading frames and the specimens inside the ovens.

The ovens were made of stainless steel with block insulation. Temperature in each oven was controlled independently by a control box. The ovens could apply elevated temperatures from 32°C (90°F) to 150°C (300°F). The inside dimensions of the ovens are 50 cm (20 in) wide, 50 cm deep, and 76 cm (30 in) high. A schematic diagram of the ovens is shown in Figure 13. The hydraulic system of the second type was similar to the first type (figure 14).

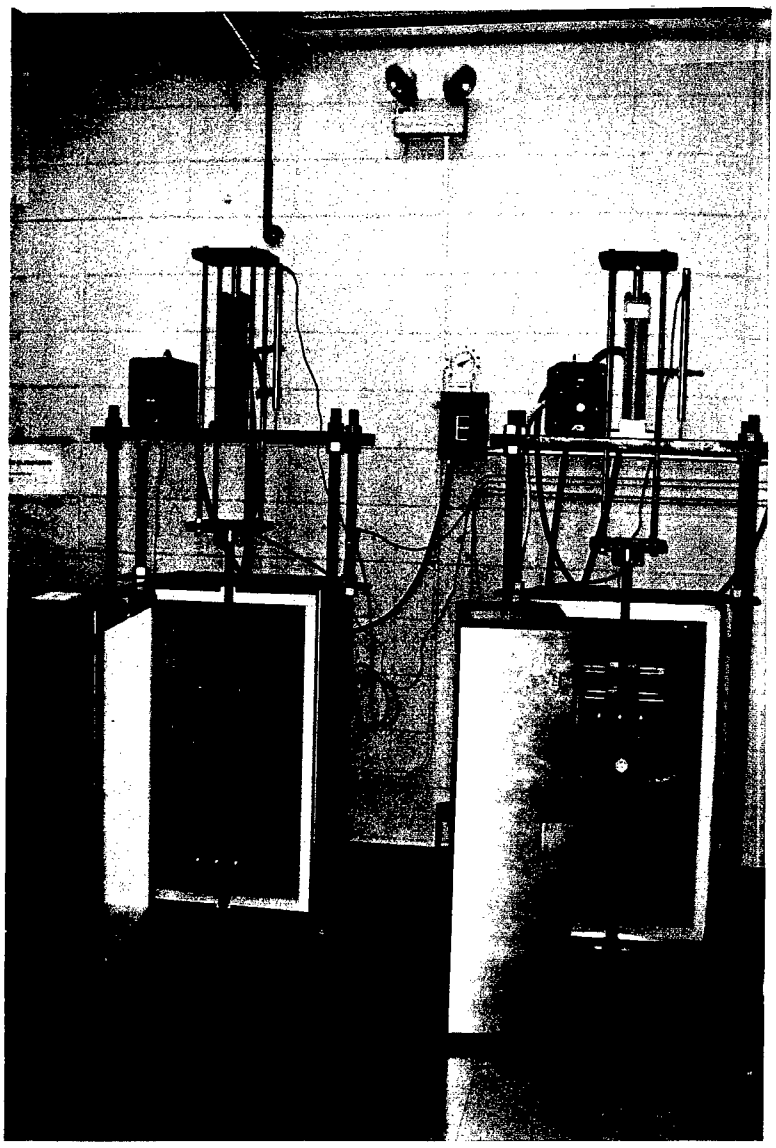

Figure 12

The geogrid specimens in the elevated temperature testing equipment

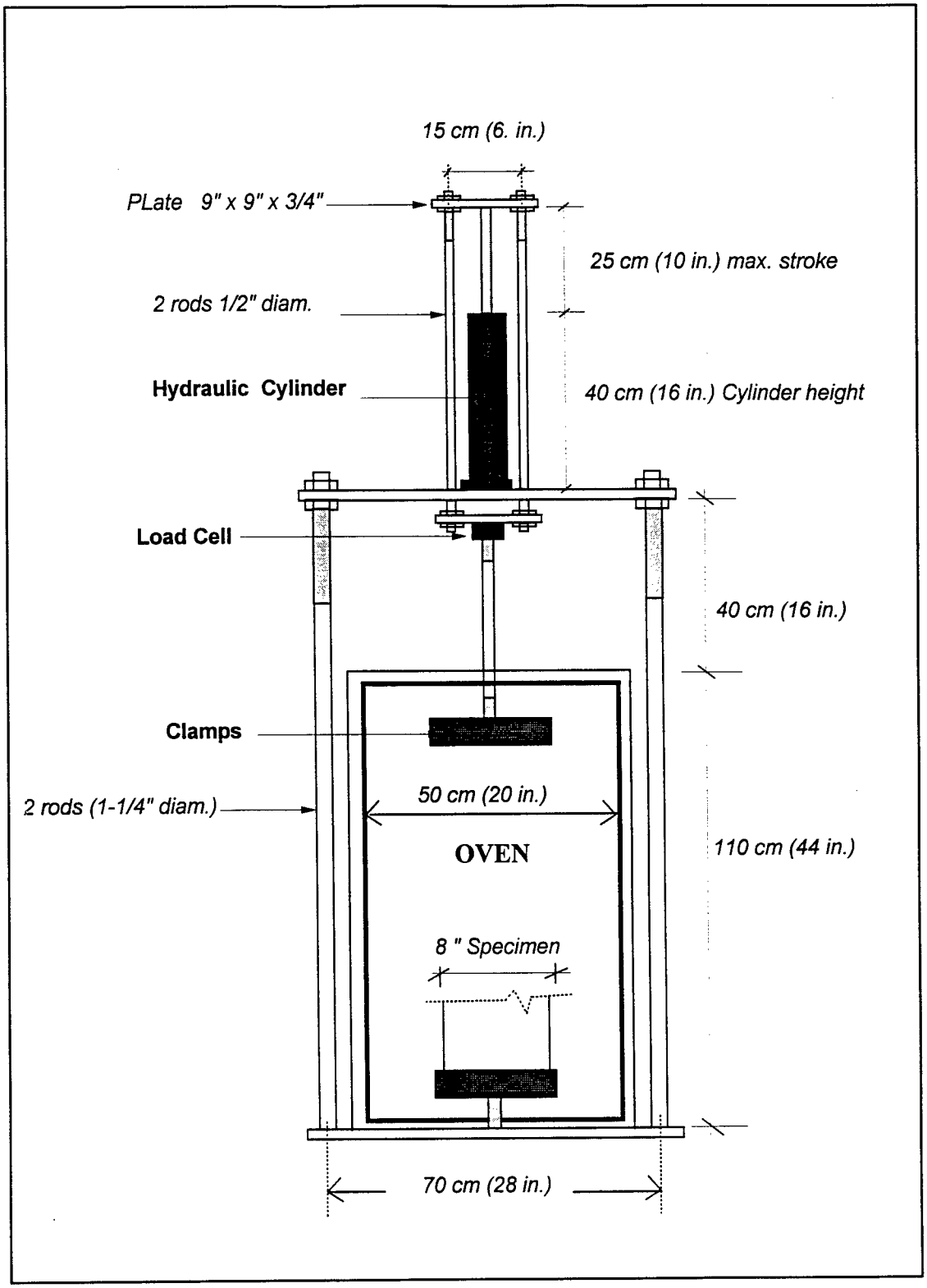

Figure 13

Schematic diagram of the elevated temperature testing equipment

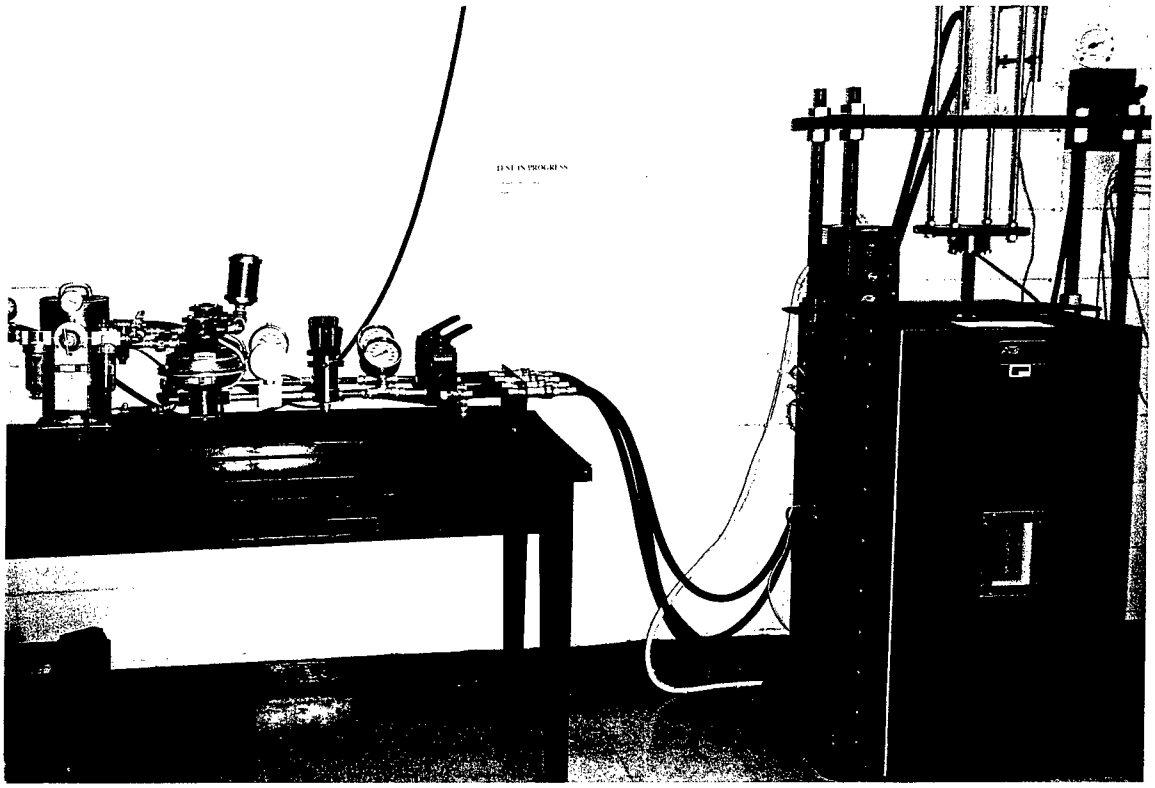

Figure 14

View of the hydraulic system in temperature-creep tests

C. Creep Testing Program

Objectives: The objectives of the testing program were to develop equipment and procedure for accelerated creep testing of geosynthetics, to evaluate this procedure through testing geogrids at various elevated temperatures and loading levels, to develop a data analysis methodology for extrapolating 1,000 hour creep strains at elevated temperatures to longer time intervals, and to evaluate this methodology through comparison with 10,000 hour creep strains at room temperature. Accordingly, the testing program was conducted to accomplish the following tasks:

1. Determine the creep strains of geogrids in 10,000 hour tests at room temperature. These tests were performed at loading levels ranging from about 15 percent to 40 percent of the short-term tensile strength of the geogrids. The tests served as an evaluation of the testing procedure and equipment. The results were used in evaluating the analytical procedure used in extrapolating creep strains from the 1,000 hour tests to longer time periods.

2. Evaluate the effect of temperature on the creep behavior (i.e strain and elasticity modulus) of geogrids. These tests were performed at elevated temperatures ranging from 24°C (75°F) to 72°C (160°F) and the same loading levels as in room temperature tests. The results were used in evaluating the temperature dependency of the geogrids, in investigating the applicability of the methods of extrapolating creep test results, and in determining the shift factors for the time-temperature superposition.

Geogrid Properties: Two types of geogrids commonly used in soil reinforcement were tested in order to establish the applicability of time-temperature equivalency. The first type of geogrid was Tensar UX1500, which is a punched sheet drawn HDPE geogrid *[28]* . This geogrid was selected because PE polymers usually demonstrate measurable creep deformations and temperature dependency. The

second type of geogrid was Stratagrid 500, which is a PET geogrid with PVC coating. This geogrid was selected in order to investigate the applicability of time-temperature relationships on a PET geogrid, which is less sensitive to long-term loading and temperature.

Table 2 shows the geometrical and physical properties of both geogrids *[29]*. Modified wide width tensile tests were performed on both geogrids to determine their maximum short-term tensile strength (T_{max}). These tests were performed on specimens approximately 15 cm (6 in) wide for both geogrids. The results of these tests are shown in figures 15 and 16 for the Tensar and the Stratagrid, respectively. The results showed an average T_{max} of 76 kN/m (5.2 Kips/ft) for the Tensar UX1500 geogrid, and an average T_{max} of 68 kN/m (4.7 Kips/ft) for the Stratagrid 500 geogrid. These values were used in determining the loading levels in creep tests.

Table 2

Properties of the geogrids in the testing program *[29]*

Product type	**Mass/unit area** *(ASTM D5261)* *gm/m² oz/yd²)*	**Aperture Size** *mm (in)* *MD*	*XD*	**Strength at 5% Strain** (ASTM D 4595) kN/m (lb/ft)	**Ultim. Strength** *(ASTM D 4595)* *kN/m (lb/ft)*	**Creep Strength** *(ASTM D 5262)* *kN/m (lb/ft)*
TensarUX1500	338.5 (10)	NA	NA	53.0 (3,640)	N/A	32.0 (2,190)
Stratagrid 500	838.5 (10.0)	25.4 (1.00)	58.4 (2.30)	15.9 (1,100)	61.0 (4200)	30.8 (2,120)

Notes:

(1) MD : Machine Direction; XD: Cross Direction

(2) Strength values are in Machine Direction

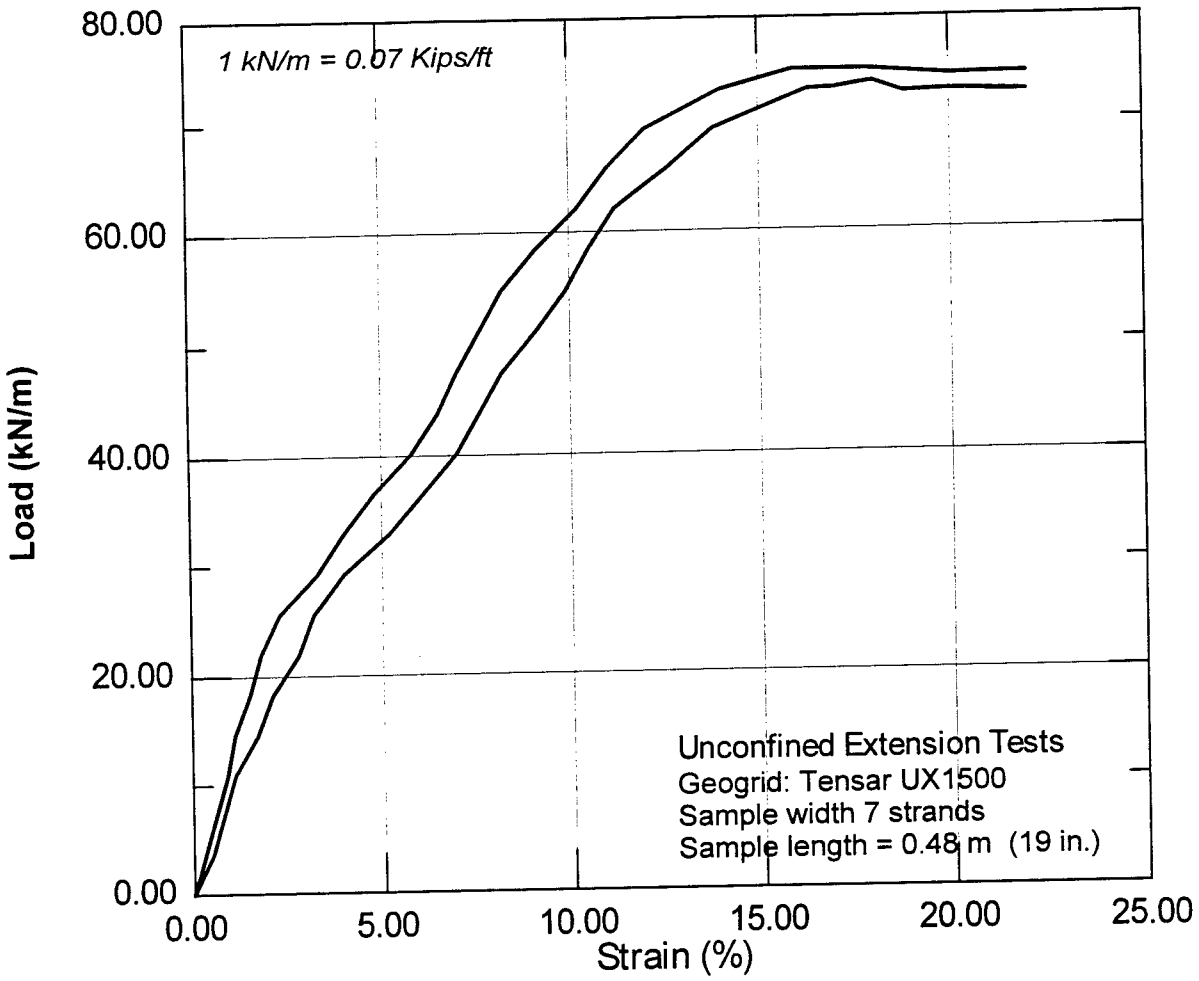

Figure 15

Unconfined extension tests on Tensar UX1500 geogrid

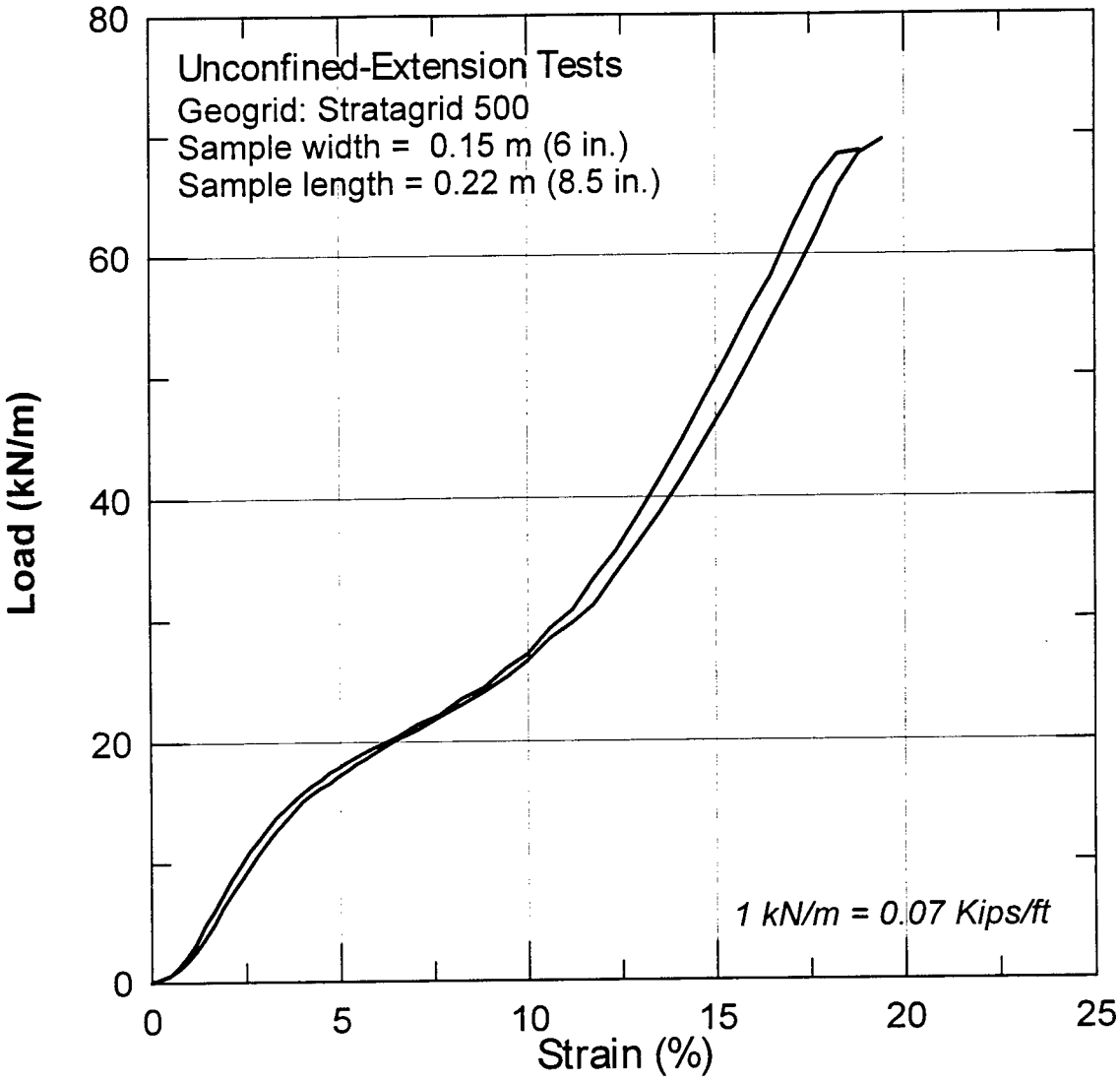

Figure 16

Unconfined extension tests on Stratagrid 500 Geogrid

Testing Program: The testing program consisted of the following testing sets:

- Test Set No. 1: Creep tests of a duration of 10,000 hours were conducted on the Tensar UX1500 geogrid in room temperature. The specimens were 7 strands wide (15 cm), 48 cm (19 in) long, and were subjected to loads ranging from 17percent to 38 percent of the maximum tensile strength of the geogrid.

- Test Set No. 2: Creep tests were conducted on the Tensar UX1500 geogrid at room temperature and at the same loading levels as in set no. 1. The durations of these tests were 1,000 hours. Tests were performed twice at the same testing conditions to evaluate the accuracy of the results.

- Test Sets No. 3 to 6 : These tests were conducted on the Tensar geogrids at various temperatures from 38° C (100° F) to 72° C (160° F). These tests were conducted for duration of 1,000 hours with the same dimensions of the specimens and loading levels as the previous test sets.

- Test Set No. 7: These tests were conducted on the Tensar geogrid. Each test was performed at a constant loading level, and temperatures were increased incrementally every 20 hours.

- Test set No. 8. : These tests were performed on the Stratagrid 500 geogrid at a constant loading level 44 percent of the tensile strength of the geogrid. The specimens were 5 strands wide and 46 cm (18 in) long. These tests were conducted at temperatures varying from room temperature to a temperature of 72° C (160° F) for duration of 1,000 hours.

Temperature ranges in these tests were below the melting temperatures of geogrids in order not to affect the physical properties of the material. The testing program is shown in tables 3 and 4 for the Tensar and Stratagrid geogrids, respectively.

Table 3

Creep testing program on the Tensar UX1500 geogrid

Test Sets	Duration (Hour)	Extension Load kN/m (kips/ft)	%Tmax	Temperature °C (°F)	Notes
Set No.1					Specimens 7 strands,
1. Test: Creep-All-0.9	10,000	13 (0.9)	17	24 (75)	48 cm (19 in.) long
2. Test: Creep-All-1.1	10,000	16 (1.1)	22	24 (75)	
3. Test: Creep-All-1.5	10,000	22 (1.5)	30	24 (75)	
4. Test: Creep-All-1.9	10,000	28 (1.9)	38	24 (75)	<= failed at 7,000 Hour
Set No. 2					
1. Test :T-075-A-0.9	1,000	13 (0.9)	17	24 (75)	
2. Test: T-075-A-1.1	1,000	16 (1.1)	22	24 (75)	
3. Test: T-075-B-1.1	1,000	16 (1.1)	22	24 (75)	
4. Test: T-075-A-1.5	1,000	22 (1.5)	30	24 (75)	
5. Test :T-075-A-1.9	1,000	28 (1.9)	38	24 (75)	
6. Test: T-075-B-1.9	1,000	28 (1.9)	38	24 (75)	
Set No. 3					
1. Test: T-100A-0.9	1,000	13 (0.9)	17	38 (100)	
2. Test: T-100A-1.1	1,000	16 (1.1)	22	38 (100)	
3. Test: T-100A-1.5	1,000	22 (1.5)	30	38 (100)	
4. Test: T-100A-1.9	1,000	28 (1.9)	38	38 (100)	
Set No. 4					
1. Test: T-120A-0.9	1,000	13 (0.9)	17	49 (120)	
2. Test: T-120A-1.1	1,000	16 (1.1)	22	49 (120)	
3. Test: T-120A-1.5	1,000	22 (1.5)	30	49 (120)	
4. Test: T-120A-1.0	1,000	28 (1.9)	38	49 (120)	
Set No. 5					
1. Test: T-140A-1.1	1,000	16 (1.1)	22	60 (140)	
2. Test: T-140A-1.5	1,000	22 (1.5)	30	60 (140)	
3. Test: T-140A-1.0	1,000	28 (1.9)	38	60 (140)	

Table 3

Creep testing program on the Tensar UX1500 geogrid [*continued*]

Test Sets	Duration (Hour)	Extension Load kN/m (Kips/ft)	%Tmax	Temperature °C (°F)	Notes
Set No. 6					
1. Test: T-160-A-0.9	1,000	13 (0.9)	17	72 (160)	
2. Test: T-160-B-1.1	1,000	22 (1.5)	30	72 (160)	
3. Test: T-160-A-1.5	1,000	28 (1.9)	38	72 (160)	<= Failed at 300 Hour
Set No. 7				(°F)	For each test,
1. Test: VarT-01A	200	1.5 (0.1)	-	90 to 140	Temp. increased
2. Test: VarT-11A	100	16 (1.1)	22	75 to 140	incrementally every
3. Test: VarT-15A1	60	22 (1.5)	30	120-160-140	20 hours at constant
4. Test: VarT-15A2	60	22 (1.5)	30	120-160-140	load.
5. Test: VarT-15B1	100	22 (1.5)	30	75 to 140	
6. Test: VarT-15B2	100	22 (1.5)	30	75 to 140	
7. Test: VarT-19A1	100	28 (1.9)	38	75 to 140	
8. Test: VarT-19A2	100	28 (1.9)	38	75 to 140	

Table 4

Creep testing program on the Stratagrid-500

Test Sets	Duration (Hour)	Extension Load kN/m (Kips/ft)	%Tmax	Temperature °C (°F)	Notes
Set No. 8					Specimens 5 strands
1. Test: Str-1k-0A	1,000	29 (2)	44	24 (75)	wide, 46 cm
2. Test: Str-1k-0B	1,000	29 (2)	44	24 (75)	(18 in.) long
3. Test: Str-1k-A1	1,000	29 (2)	44	38 (100)	
4. Test: Str-1k-A2	1,000	29 (2)	44	49 (120)	
5. Test: Str-1k-B1	1,000	29 (2)	44	60 (140)	
6. Test: Str-1k-B2	1,000	29 (2)	44	72 (160)	

CHAPTER III
CREEP TEST RESULTS

A. Creep Test Results on the HDPE Geogrid

The results of the first set of 10,000 hour creep tests on the HDPE geogrid at room temperature are shown in figure 17. Strain measurements are plotted versus time for various loading levels in Figure 17-a, while the elasticity moduli E(t) are plotted versus time in Figure 17-b.

Long-term stress-strain relationships of geosynthetics can also be presented to focus the output information on a particular response, such as in the plots of the logarithm strain rate versus strain (Sherby-Dorn curves) in figure 18. These plots facilitate the determination of the creep load which corresponds to a specified strain limit.

The second set of results of 1,000 hour creep tests at room temperature are shown in figure 19. Creep tests at loading levels 16 kN/m (1.1 kips/ft) and 28 kN/m (1.9 Kips/ft) were repeated to evaluate the testing procedure and the repeatability of the results. The results of these tests are shown in figures 20. The results in these figures showed similar strains at the same loading levels. Overall, they demonstrated consistency under the same testing conditions.

Figures 21, 22, 23, and 24 show the results of 1,000 hour creep tests at controlled temperatures of 38^{o}C (100 ^{o} F), 49 ^{o}C (120 ^{o} F), 60 ^{o}C (140 ^{o} F), and 72 ^{o}C (160 ^{o} F), respectively (test sets No. 3, 4, 5 and 6). These tests were performed at loading levels ranging from 17 percent to 38 percent of the maximum tensile strength of the geogrid. The results in these figures show an increase in creep strains at elevated temperature.

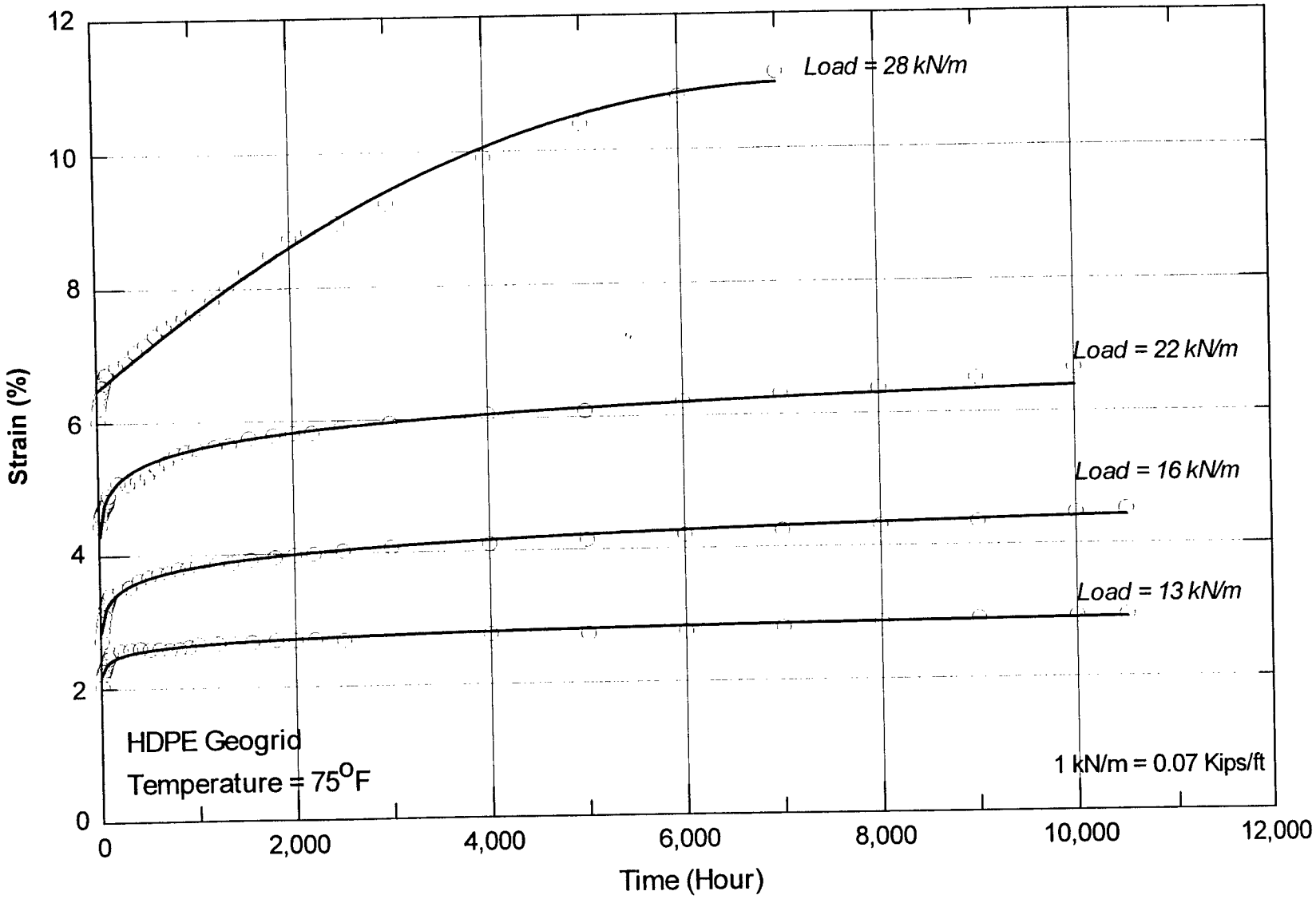

Figure 17 (a)

10,000 hour creep test results at room temperature

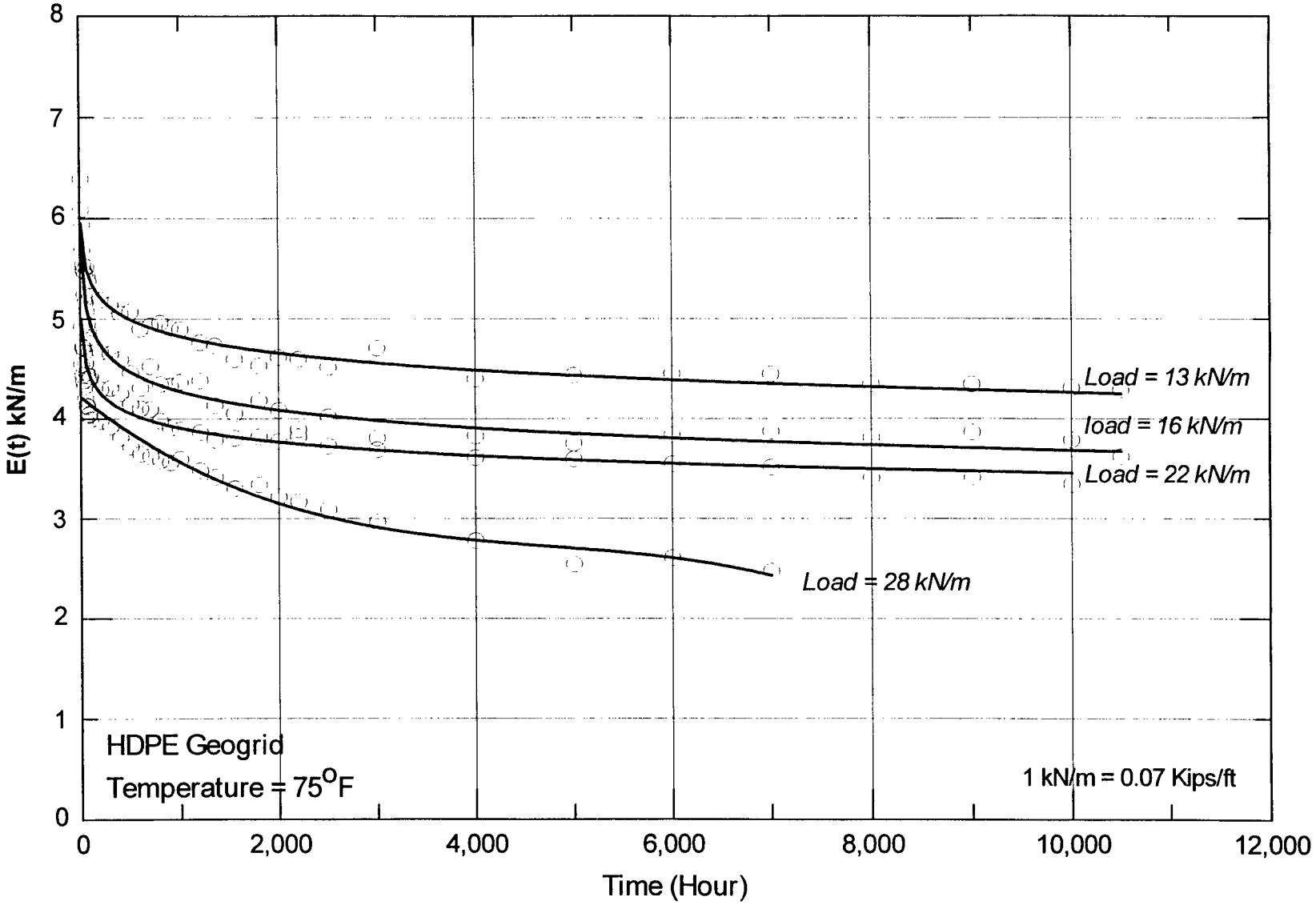

Figure 17 (b)

10,000 hour creep test results at room temperature (Test set #1)

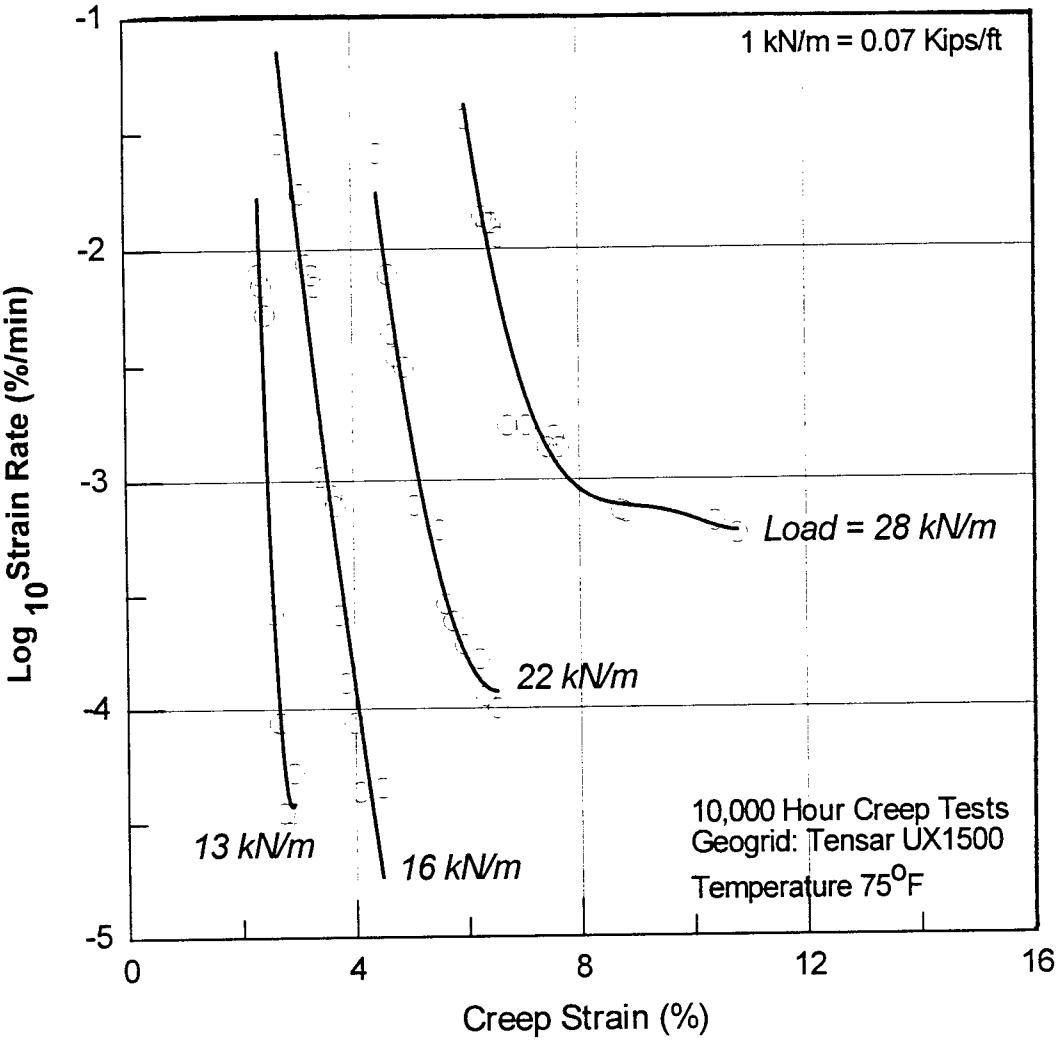

Figure 18

Determination of creep loads at specified creep strains

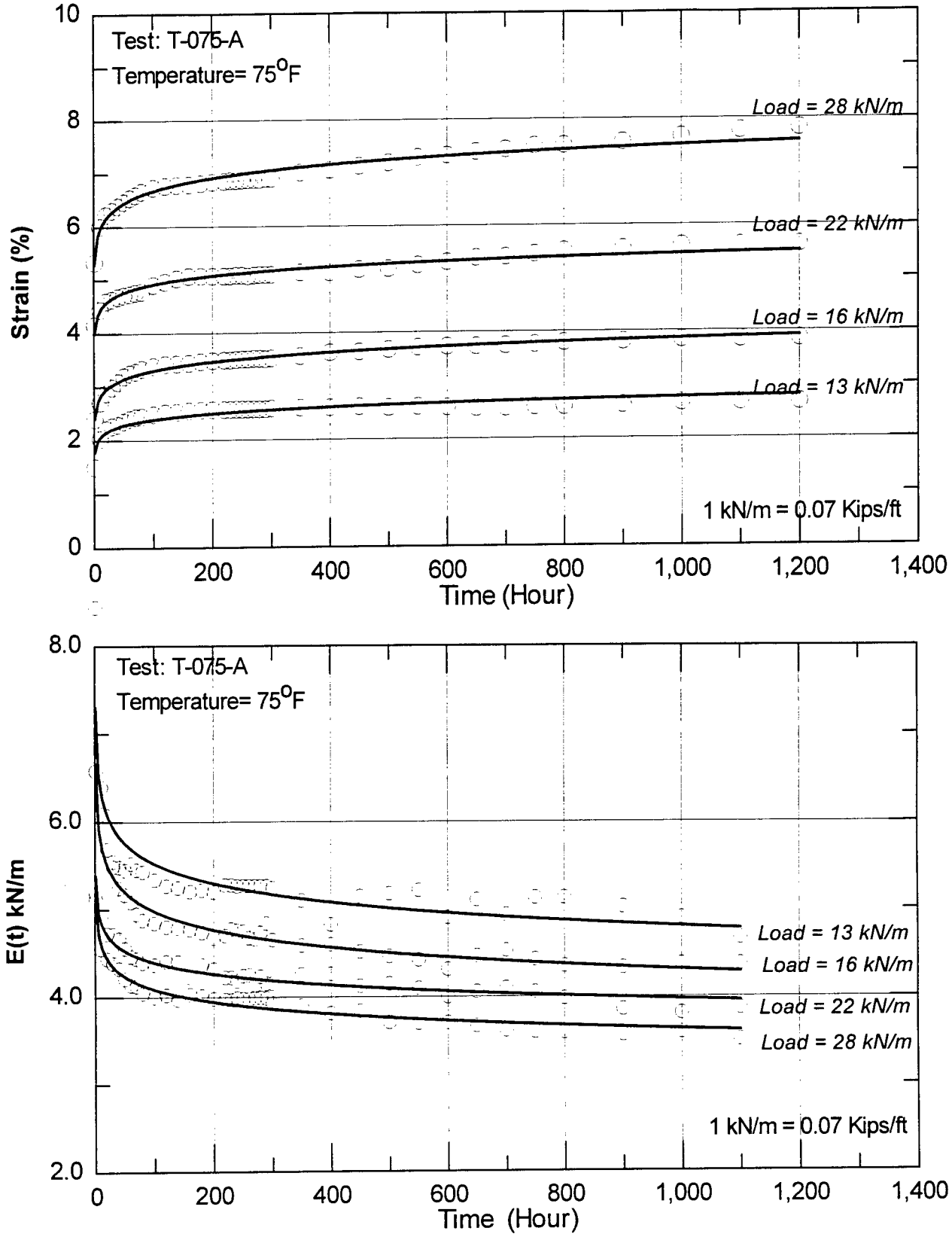

Figure 19

Creep test results in room temperature (Test Set No. 2)

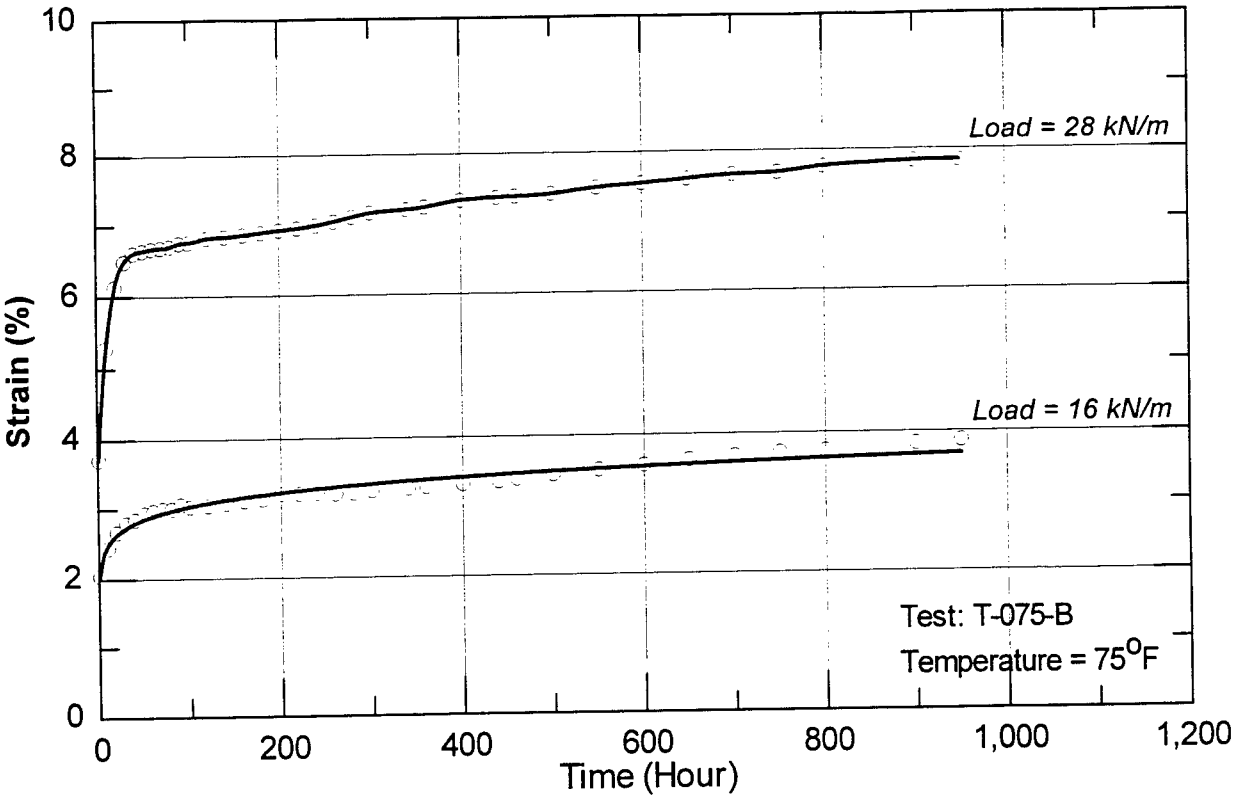

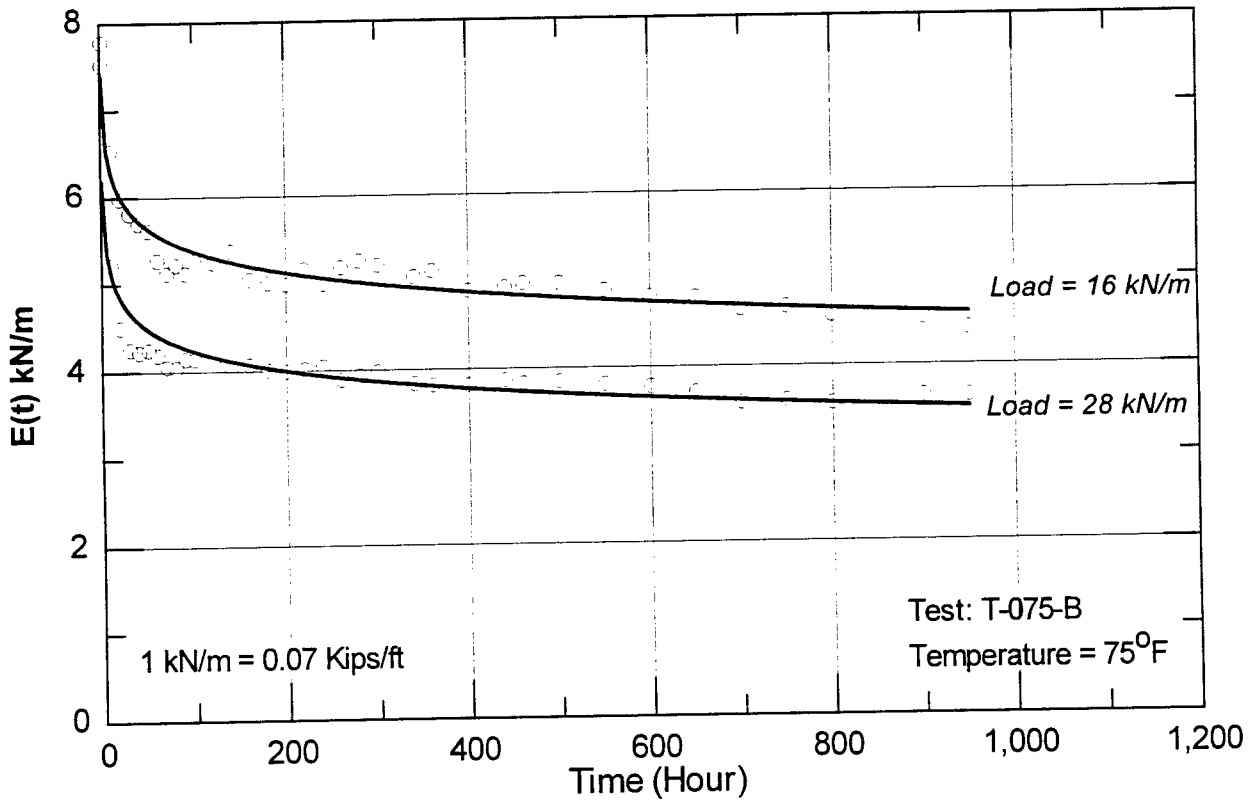

Figure 20

Creep test results in room temperature (Test Set No. 2)

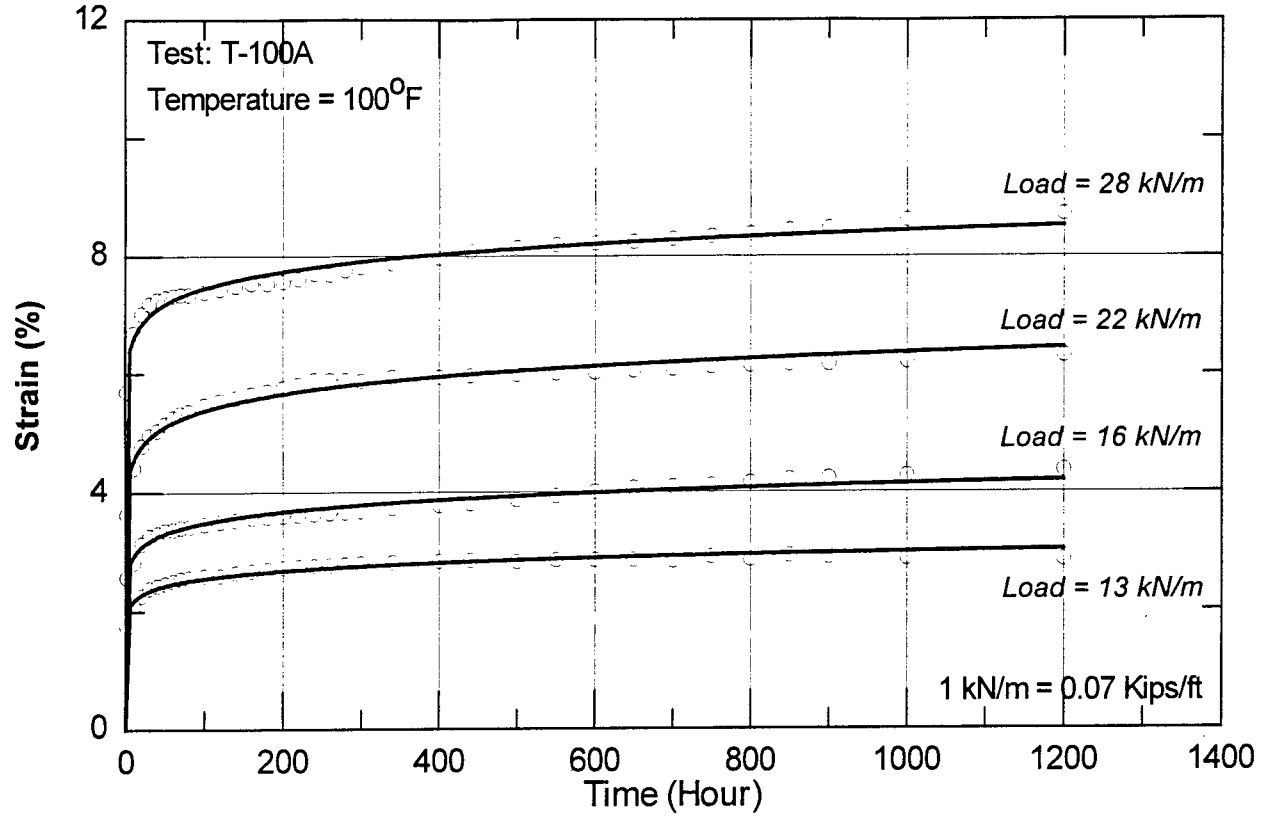

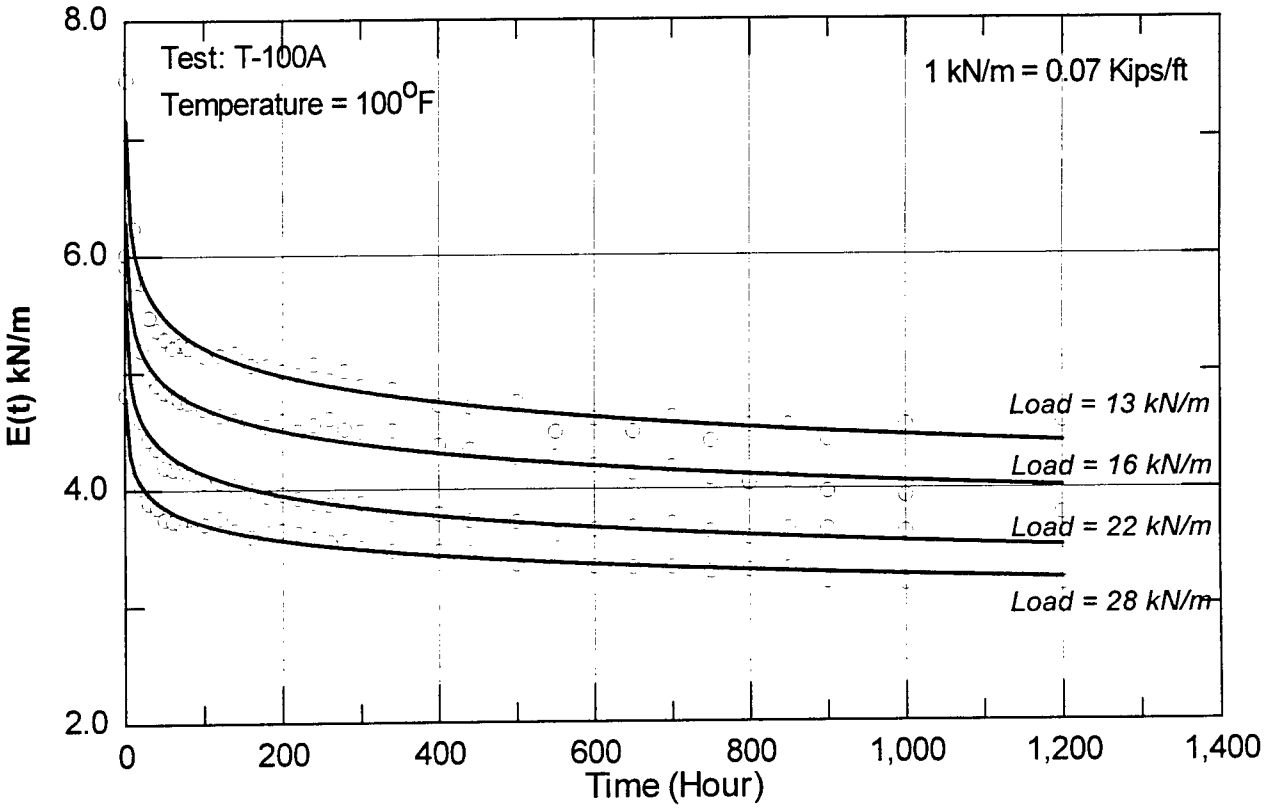

Figure 21

Creep test results in temperature 38°C (100° F) (Set No. 3)

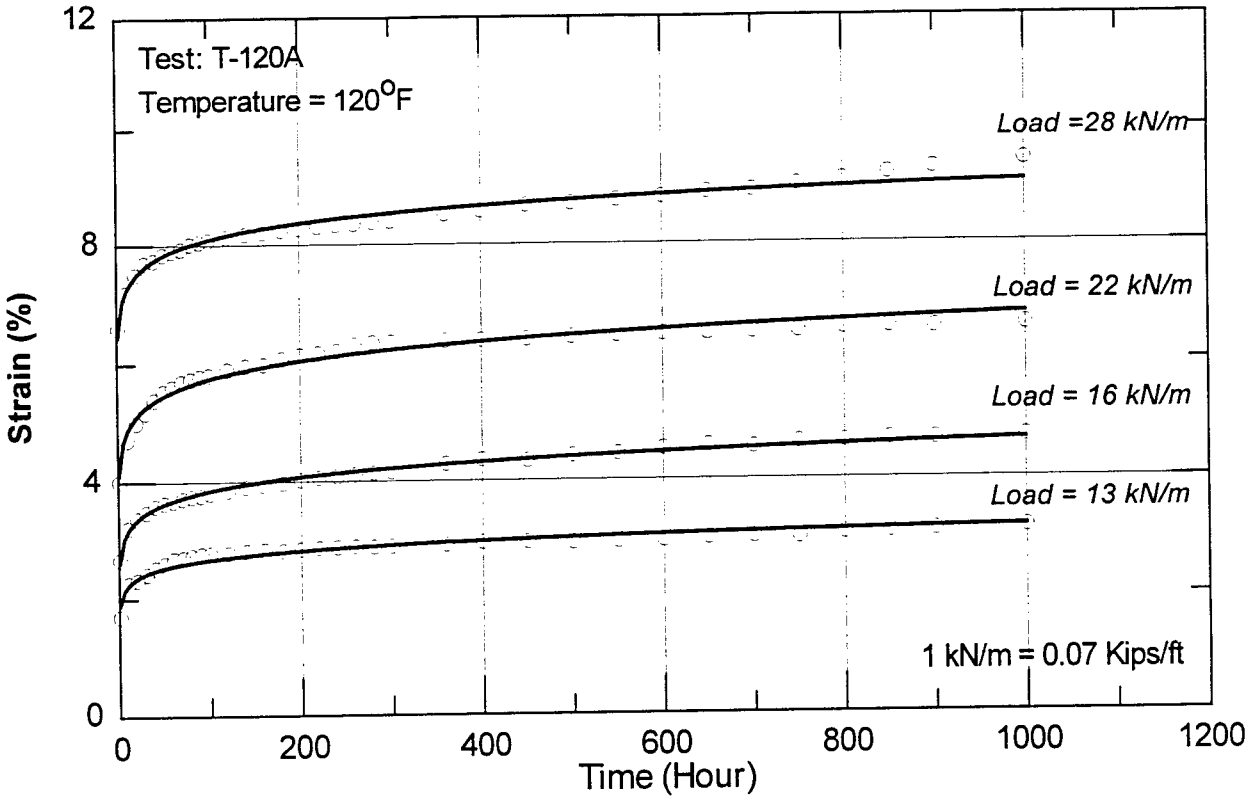

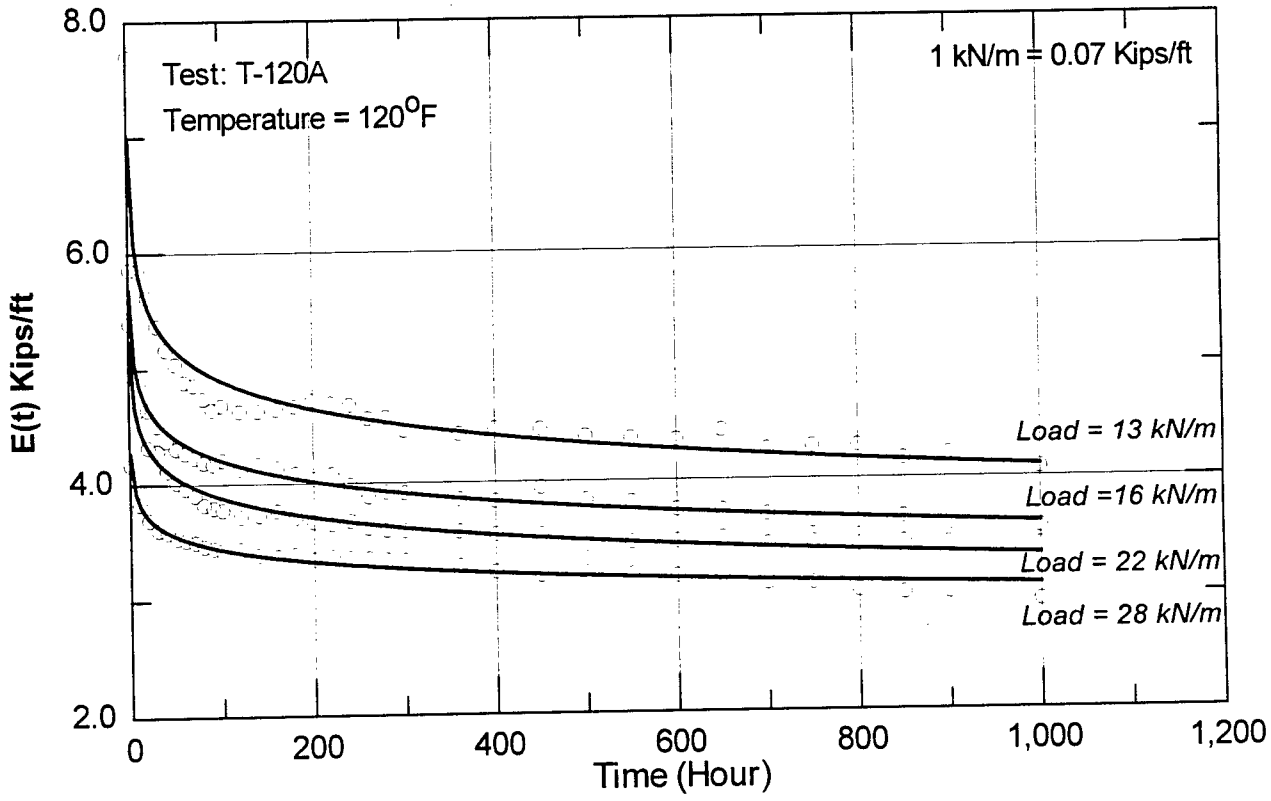

Figure 22

Creep test results in temperature 49°C (120° F) (Set No. 4)

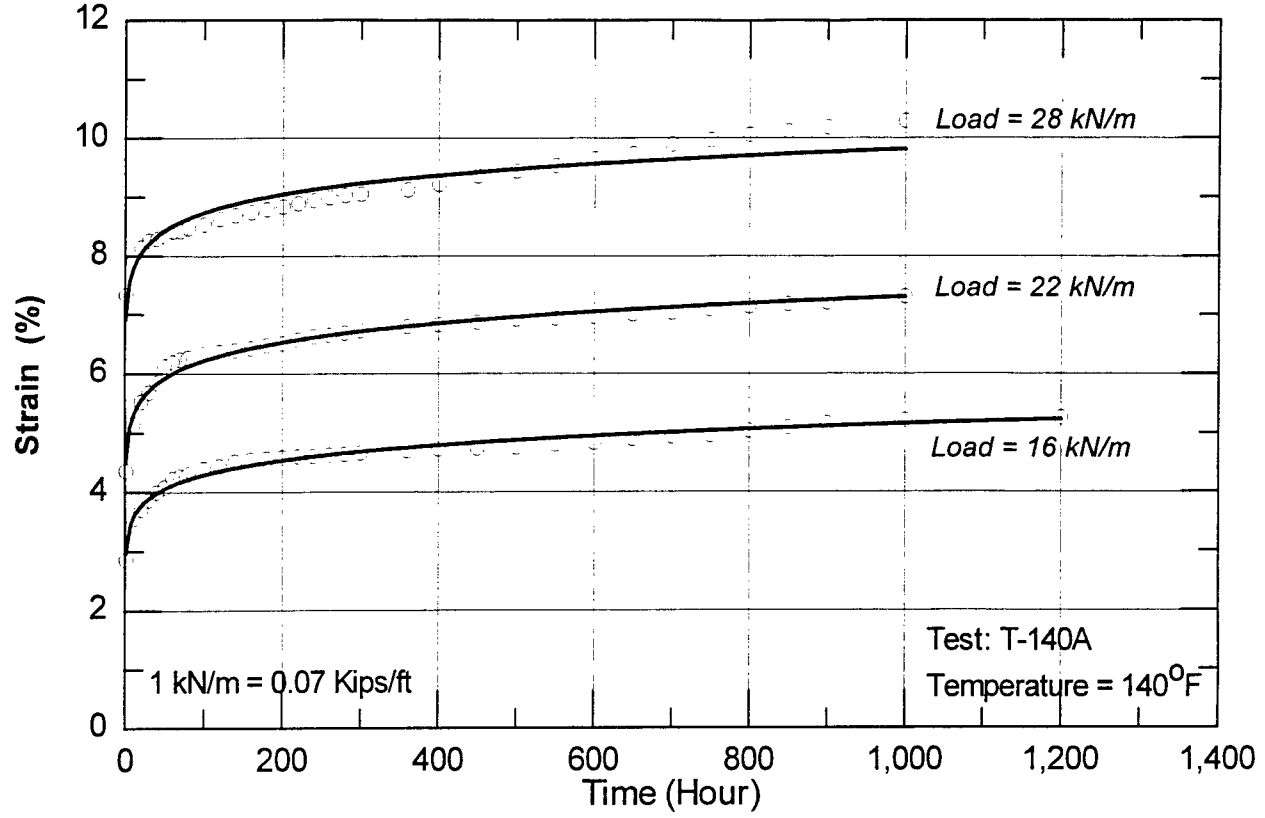

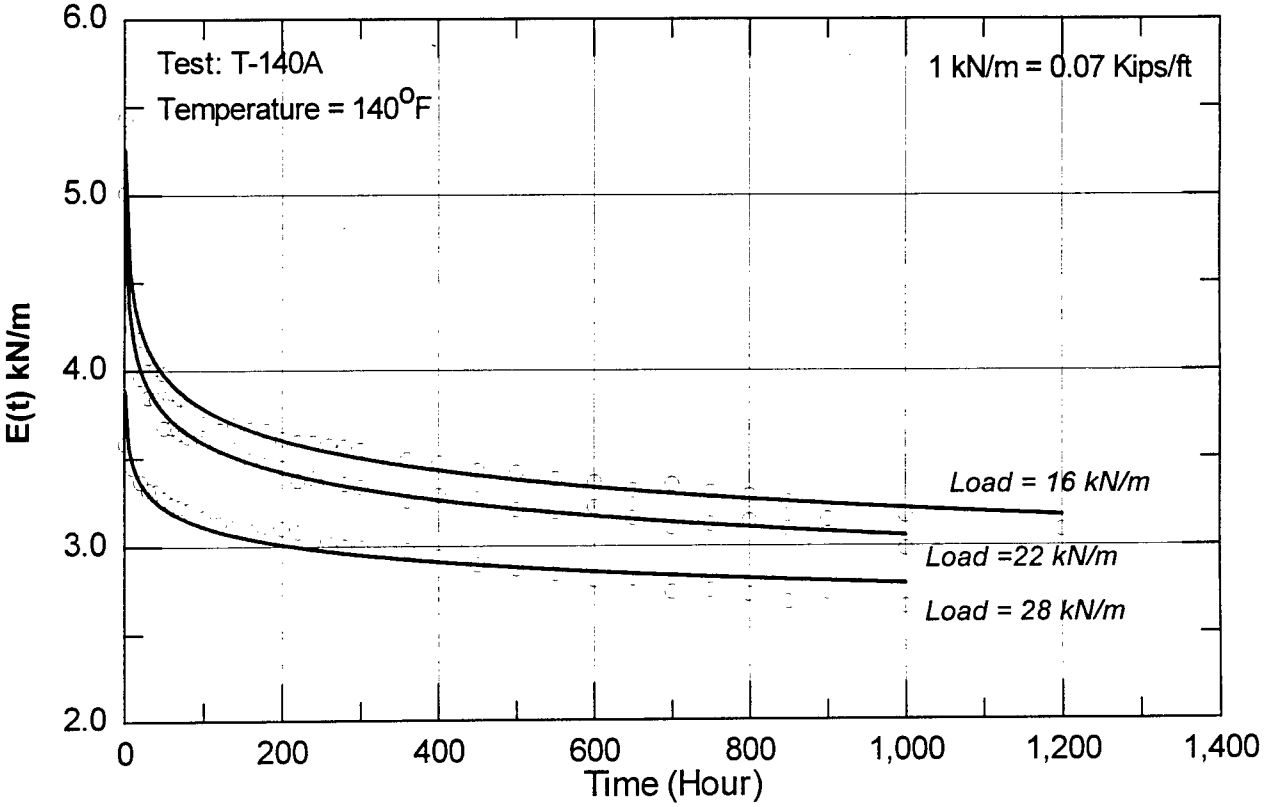

Figure 23

Creep test results in temperature 60°C (140° F) (Set No. 5)

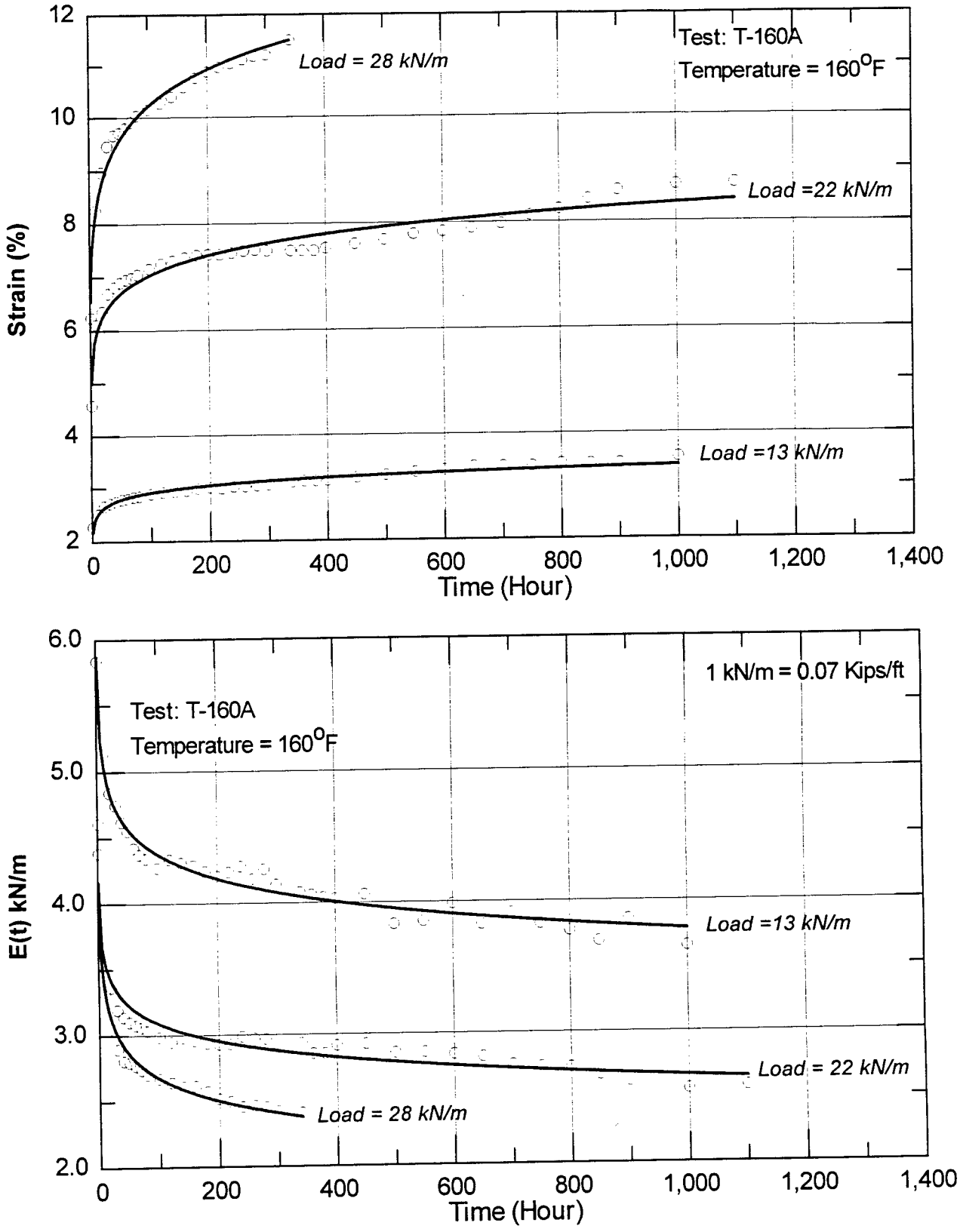

Figure 24

Creep test results in temperature 72°C (160° F) (Set No. 6)

The results of the creep tests showed that creep strains increased with temperature elevation. Temperature effect is summarized in figure 25 where creep strains after one hour and 1,000 hours of loading are plotted versus temperature. Strains after one hour of loading showed a slight increase at elevated temperature, while an accelerated increase at the 1,000 hour creep strains occurred as the temperature elevated to 72°C (160°F).

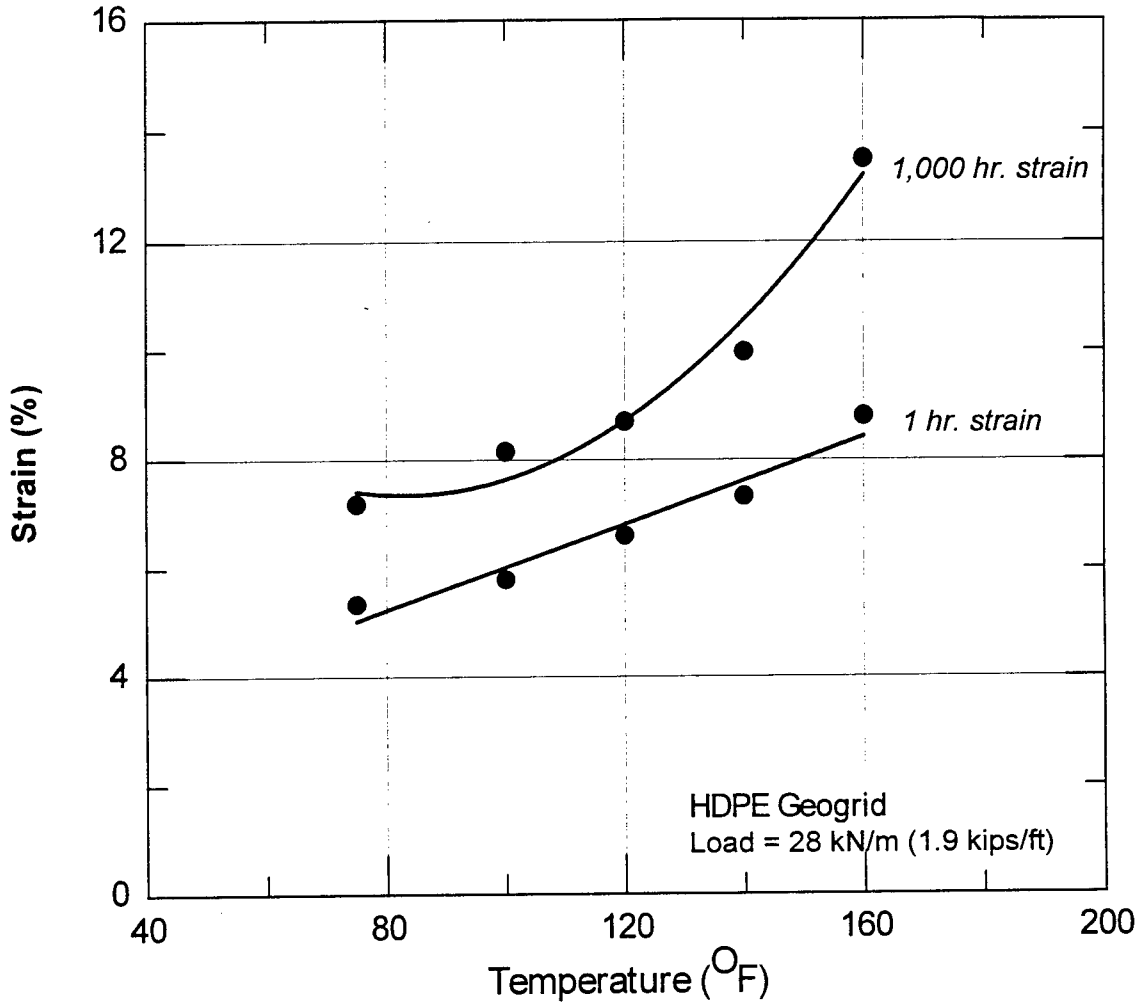

Figure 25

Effect of temperature on creep strains of the HDPE geogrid

B. Creep Test Results on PET Geogrid

The results from 1,000 hour creep tests on the PET geogrids are shown in figure 26. The tests were performed on geogrid specimens of 5 strands wide and 46 cm (18 in.) long. The creep load was about 45 percent T_{max} of this geogrid. Tests were performed at controlled temperatures ranging from temperature of 24°C (75°F) to 72°C (160°F). Creep strains after one hour and 1,000 hours of loading are plotted versus temperature in figure 27. The results in the figure show that short term (one hour) exposure to higher temperatures did not affect the strains in the PET geogrid. However, creep strains increased at higher temperatures after 1,000 hours of creep loading.

The load-strain-temperature relationships of both geogrids show that the PET geogrid demonstrated higher short-term strains than the HDPE grid when loaded at approximately similar loading levels (figure 27). However, the HDPE geogrid showed a higher increase in strain levels in long-term loading due to temperature increase. Creep strains in the PET geogrid increased from around 11.5 percent at room temperature to about 15% percent at 72°C (160°F) (an increase of approximately 30 percent); while strains in the HDPE geogrid increased from about 7.8 percent at room temperature to 13 percent at 72°C (an increase of approximately 50 percent).

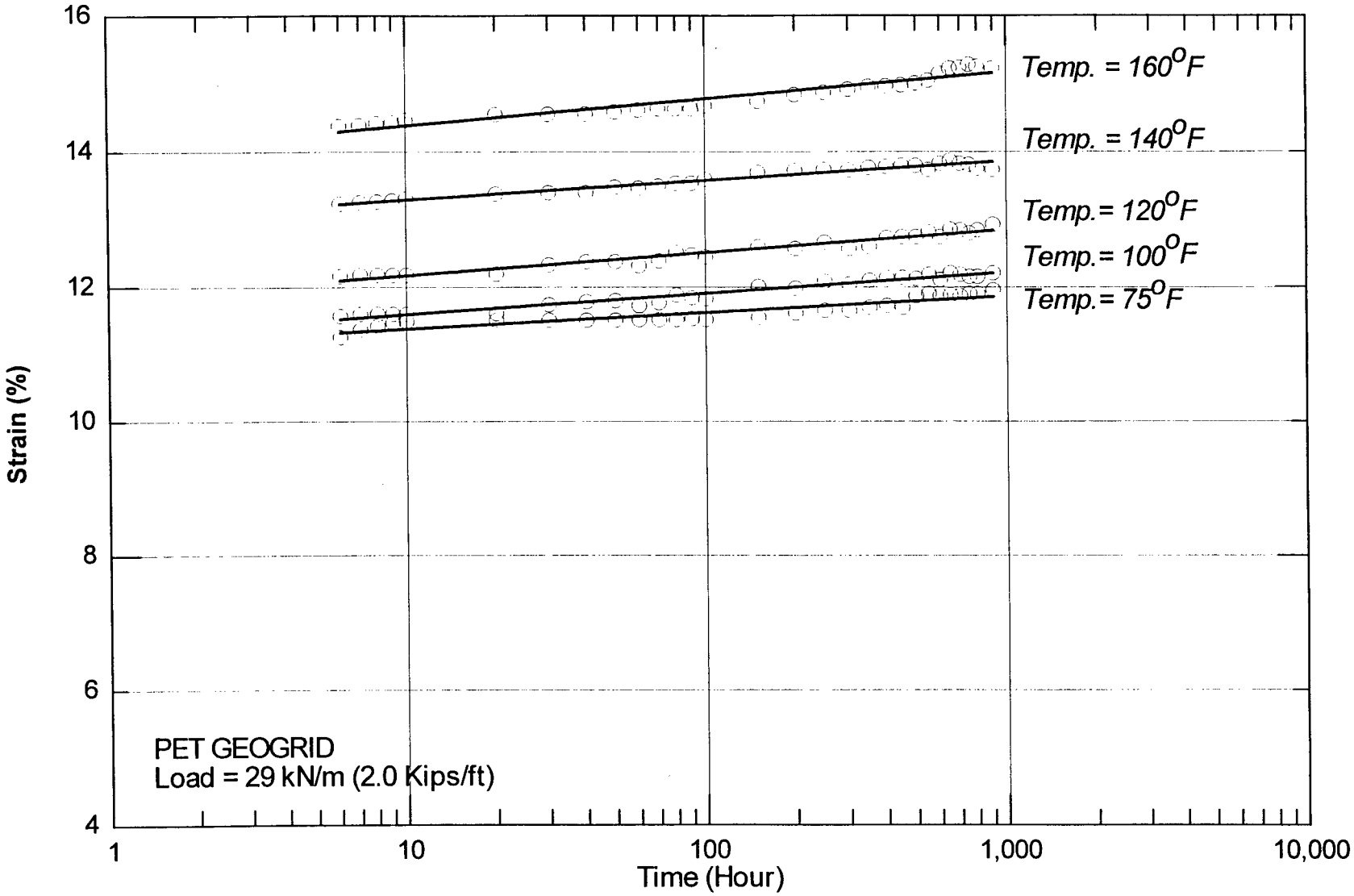

Figure 26-a

Creep test results on the PET geogrid (Test set #8)

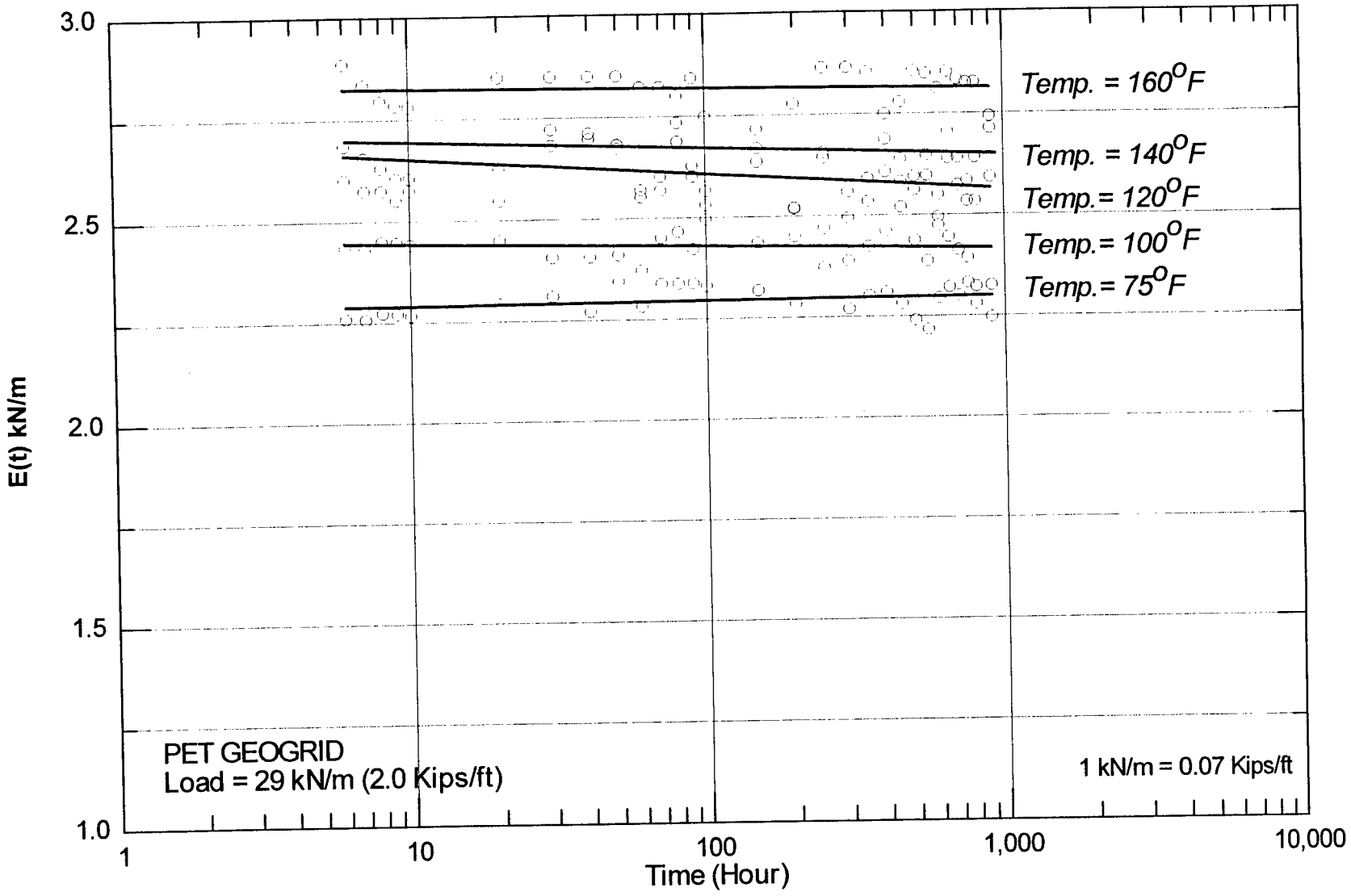

Figure 26-b

Creep test results on the PET geogrid (Test set #8)

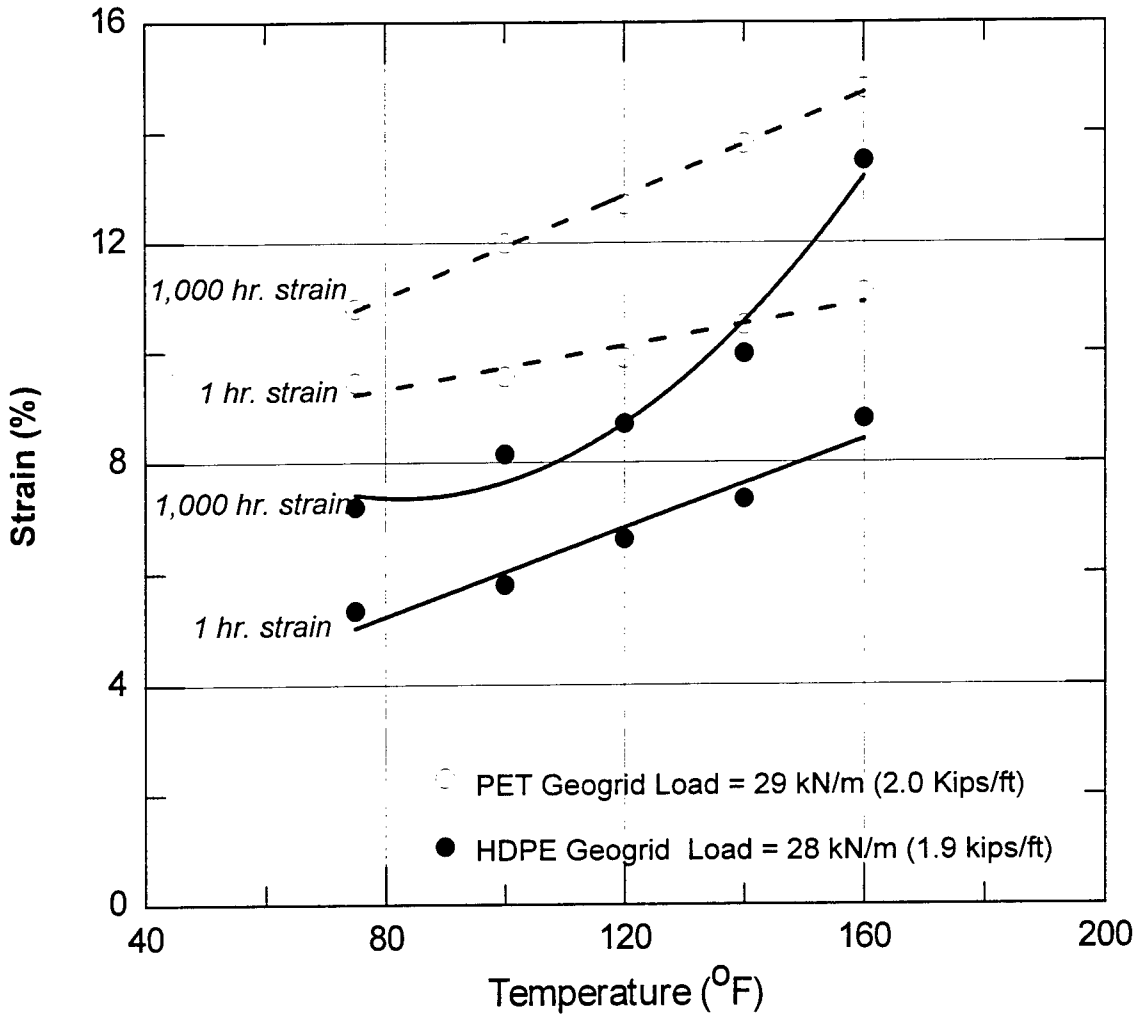

Figure 27

Effect of temperature on the long-term strains of the geogrids

CHAPTER IV

EVALUATION OF CREEP STRAIN-RATES USING ARRHENIUS EQUATION

A. Introduction

The relation between temperature (T) and creep strain-rate ($\dot{\varepsilon}$) can be expressed by the Arrhenius Equation as follows *[18], [19]*:

$$\dot{\varepsilon} = A\, e^{-\frac{E}{R\,T}} \tag{4}$$

where, $\dot{\varepsilon}$ = creep strain-rate,

A = a kinetic rate constant,

E = experimental activation energy (cal/mol),

R = universal gas constant (= 1.987 cal/mol-K),

and T = absolute temperature (K).

Equation 4 shows that creep strain-rate increases with temperature and with the decrease in the activation energy, providing that all other factors affecting creep are kept constant. Equation 4 is usually used in predicting creep strain-rates for longer time intervals. Although time *t* is not an explicit parameter in the equation, the ratio between $\dot{\varepsilon}_1$ at temperature T_1 and $\dot{\varepsilon}_2$ at temperature T_2 presents a multiplier coefficient of the kinetics μ that can be used in shifting strain-rates along the time axis. This relationship is expressed in the form *[19]*:

$$Ln\ \mu = Ln\ (\dot{\varepsilon}_1 / \dot{\varepsilon}_2) = \frac{E}{R}\left(\frac{1}{T_2} - \frac{1}{T_1}\right) \tag{5}$$

One of the inherit problems in the use of Arrhenius equation arises from the difficulty in determining the activation energy E from creep tests as the strain-rate is constantly changing throughout the test. However, a common and simple technique for the estimation of E consists of applying rapid change in temperature during creep under a

constant load *[30]*. Creep strain rates $\dot{\varepsilon}_1$ and $\dot{\varepsilon}_2$ are measured before and after the change in temperature from T_1 to T_2, respectively, and E is determined from equation 5.

The evaluation of E at various creep loads was assessed in test set No. 7 through testing the HDPE geogrid at various temperatures and creep loads. The results of test set No. 7 are presented in this chapter. The estimation of the parameters associated with the Arrhenius Equation and the significance of applying this equation to predicting creep strain-rates at longer times are also evaluated.

B. Estimation of the Activation Energy From Test Results

The testing procedure of set No. 7 consisted of increasing the temperature incrementally every 20 hours while maintaining constant loads. The results of these tests are shown in figure 28 for creep load 16 kN/m (1.1 Kips/ft), figures 29 and 30 for load 22 kN/m (1.5 Kips/ft), and figure 31 for load 28 kN/m (1.9 Kips/ft). In these figures, the slopes of strains before and after the change in temperature represent creep strain-rates at these temperatures and loading levels. Substituting the values of the strain-rates into equation 5 resulted in an estimation of the activation energy at each temperature change and loading level.

The estimated values of the activation energy at various loads and temperatures are shown in figure 32. The figure shows that an increase in the applied loads results in a linear decrease in the activation energy. The results also show that the activation energy was sensitive to the changes in temperature levels. Since E is assumed to remain constant over the time and temperature range for extrapolation of creep rates *[18]*, the application of equation 4 in predicting strain-rates would only be valid within the temperature range where E is calculated. The change of the activation energy with temperature raises difficulty in estimating its proper value for predicting strain-rates at room temperature from tests at higher temperature levels.

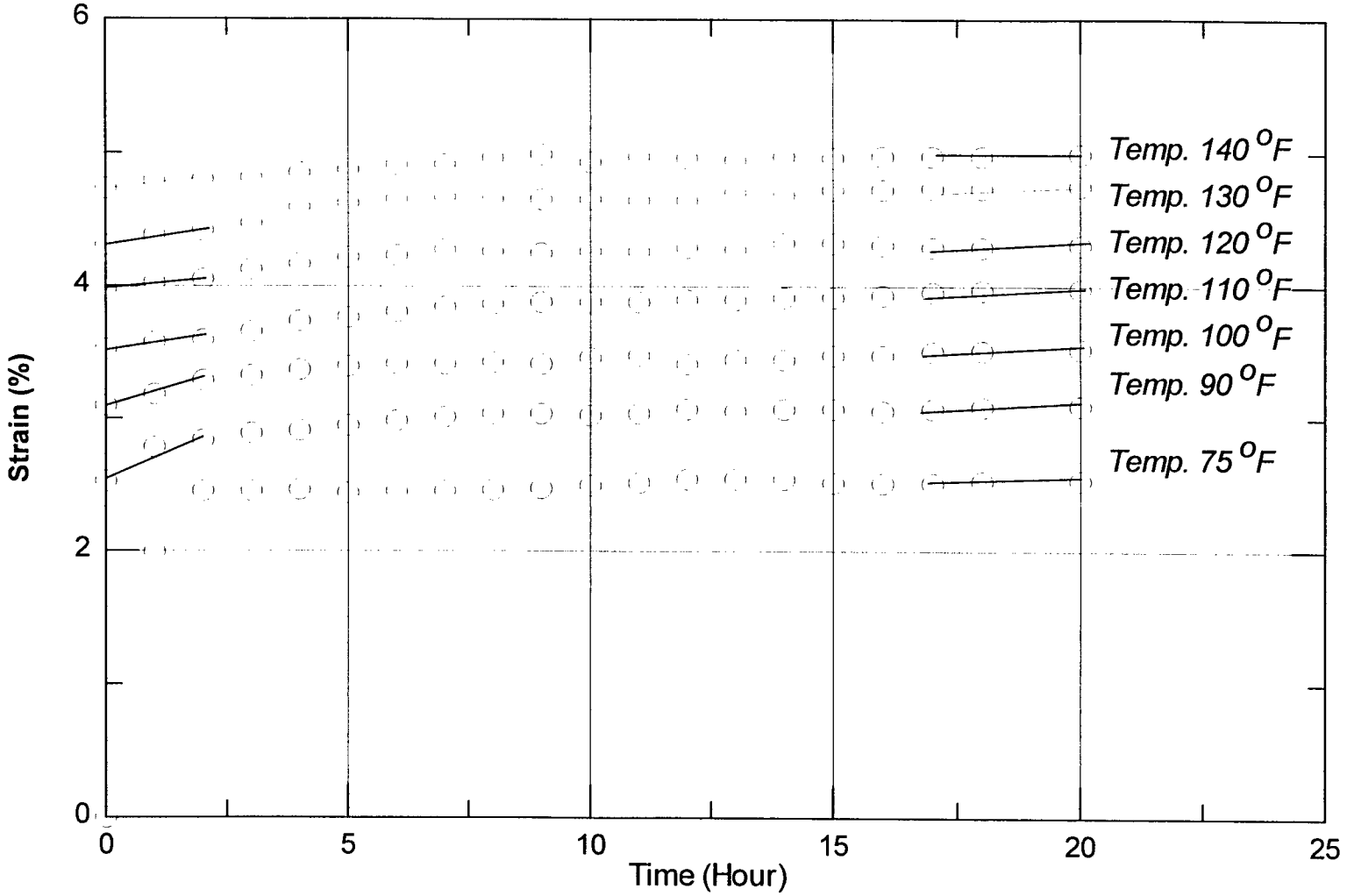

Figure 28

Estimation of creep strain-rate with temperature at load 16 kN/m

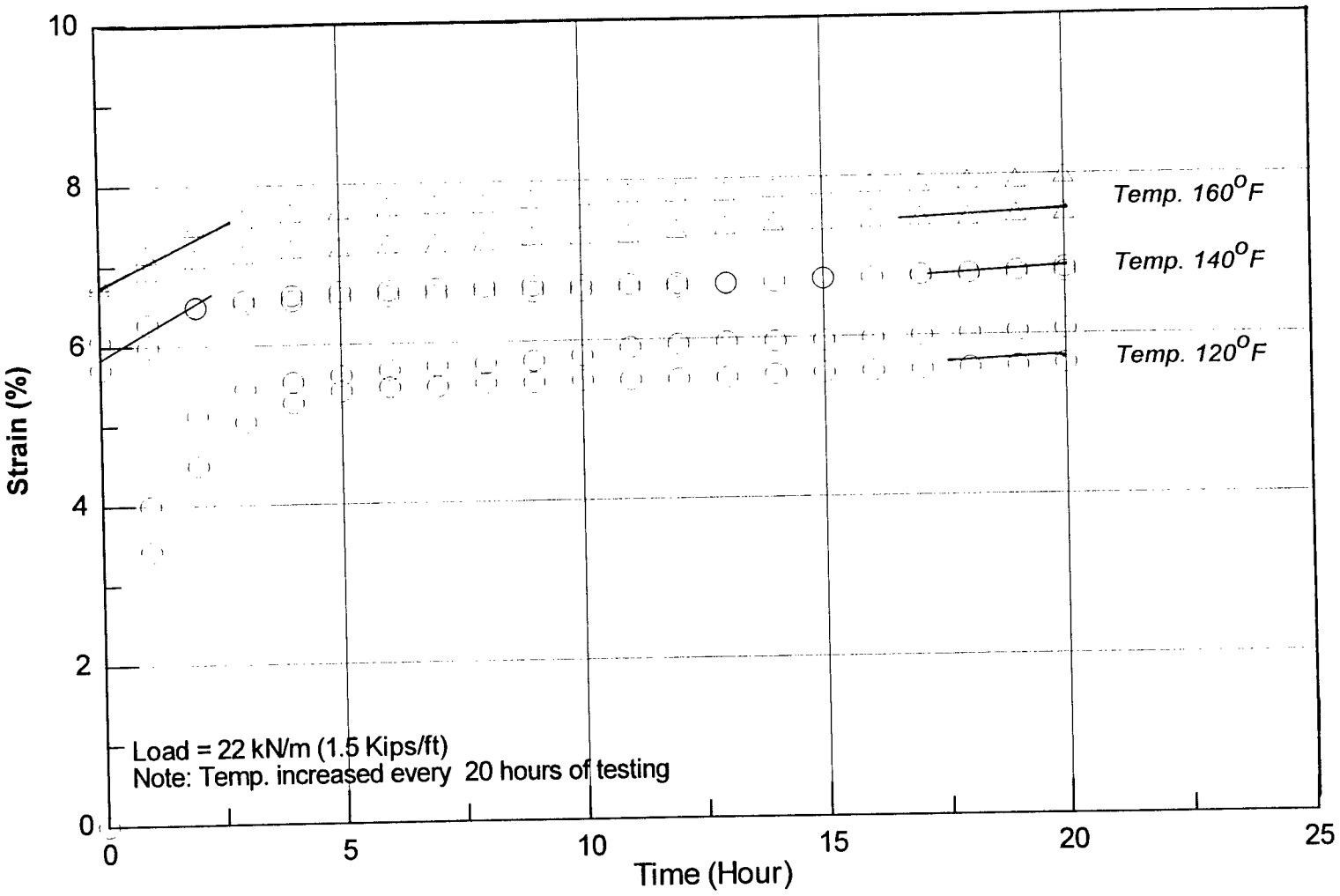

Figure 29

Estimation of creep strain-rate with temperature at load 22 kN/m

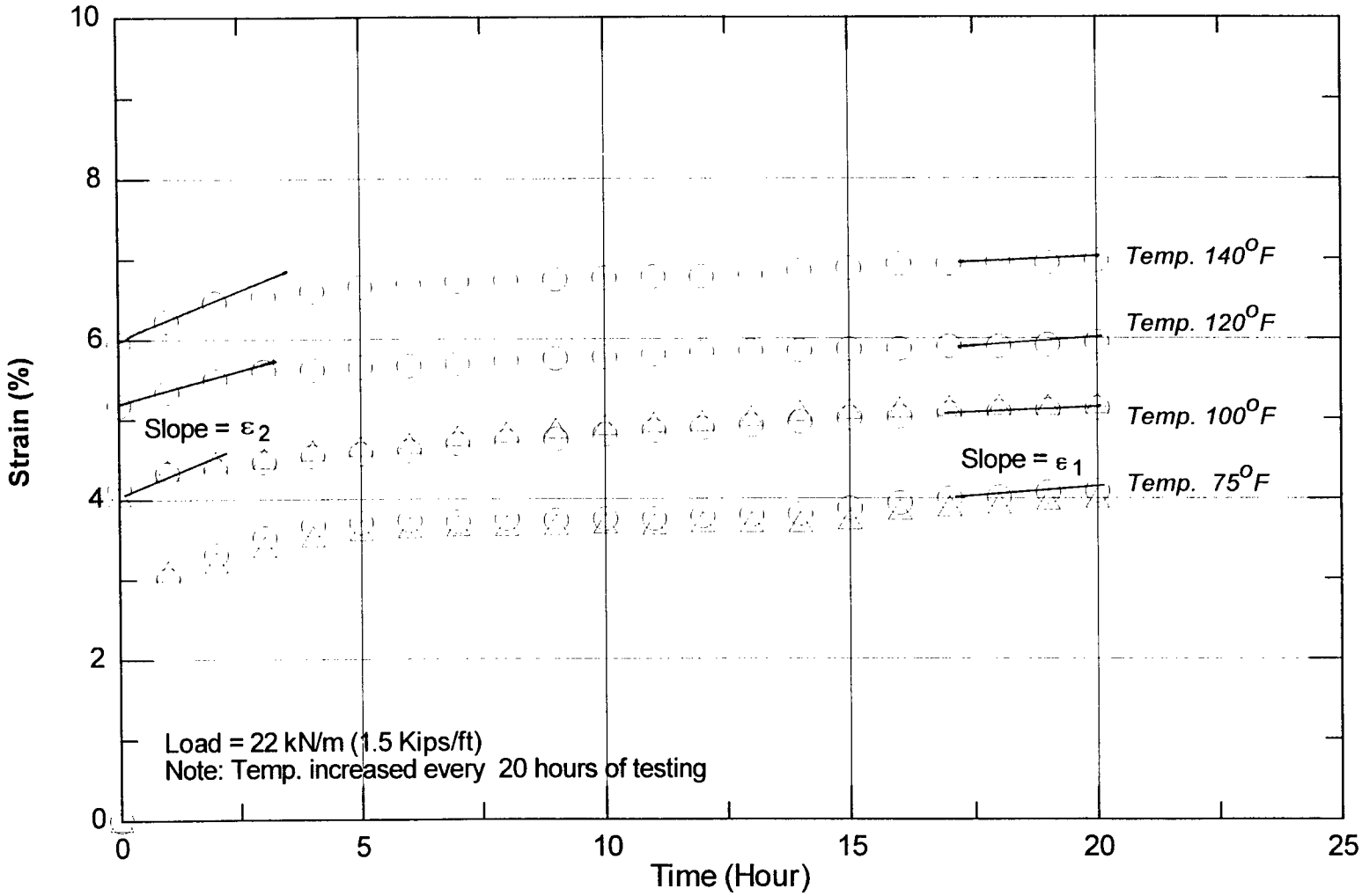

Figure 30

Estimation of Creep strain-rate with temperature at load 22 kN/m

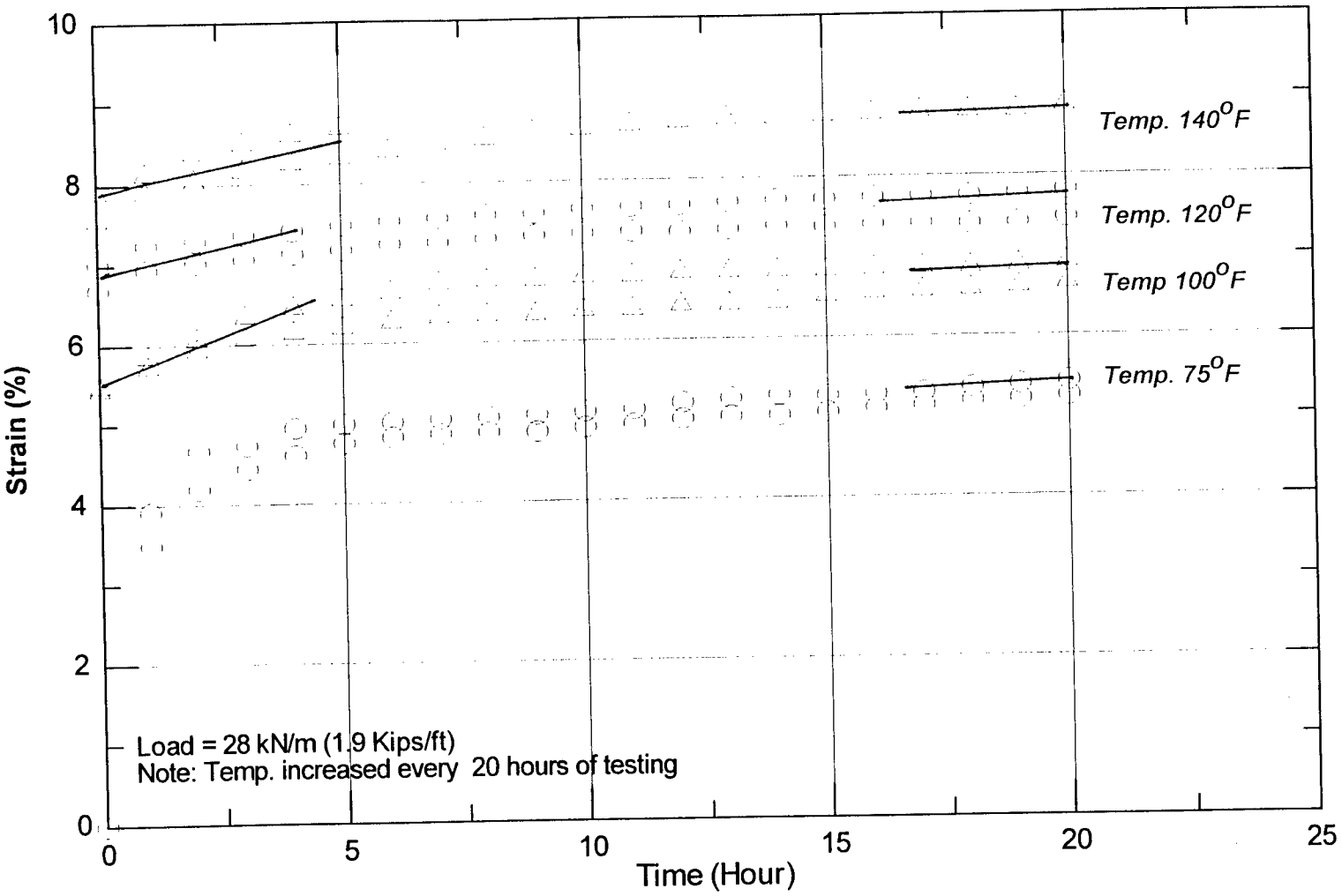

Figure 31

Estimation of creep strain-rate with temperature at load 28 kN/m

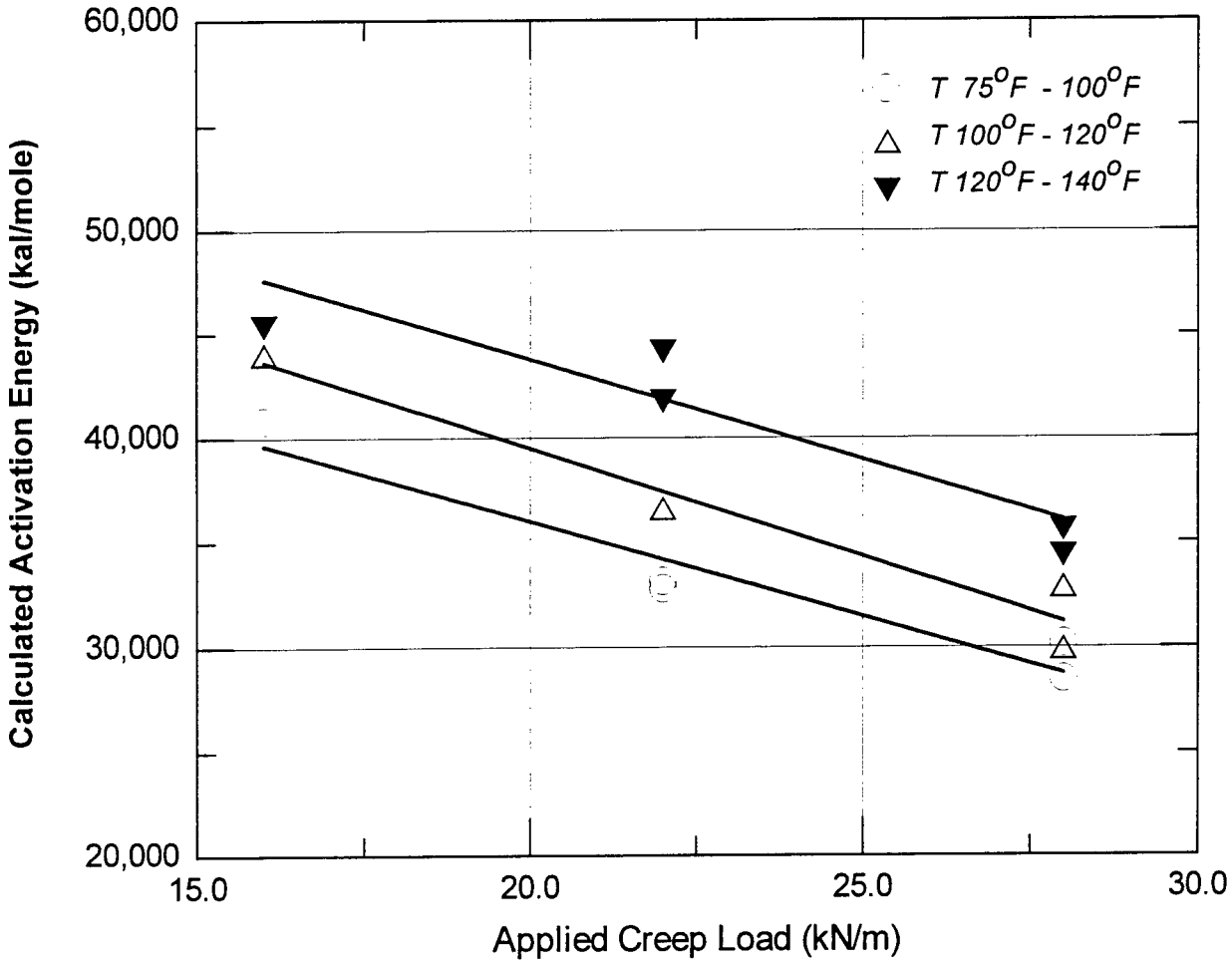

Figure 32

Estimation of E at various creep loads

The results of 1,000 hour tests at various temperatures are shown in figure 33. The figure shows that the multiplier coefficient (μ) is not constant along the temperature ranges in the figure. The calculation of μ from equation 5 would require the correct estimation of E that corresponds to each temperature increase.

Although the Arrhenius equation is a useful tool in estimating creep strain-rates, the analysis showed difficulties associated with the estimation of the equation parameters. As a results, a different procedure was used to directly estimate creep strains, rather than strain-rates,. This procedure was based on the temperature shift principals formerly presented in chapter I and it is discussed in detail in the following chapter.

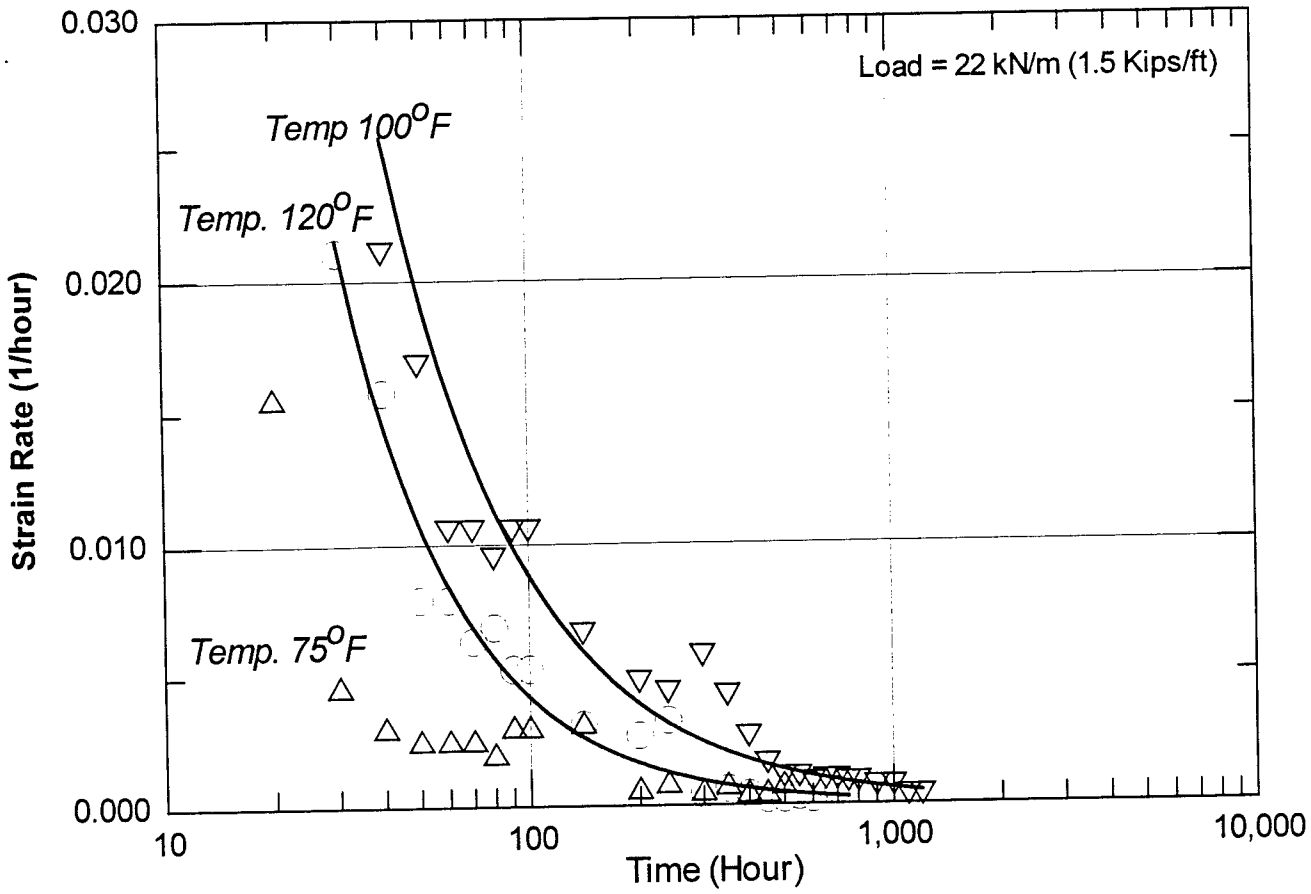

Figure 33

Change of creep rates in 1,000 hour tests at various temperatures

CHAPTER V

APPLICATION OF THE TIME-TEMPERATURE SHIFT PRINCIPALS

A. Background

The principals of strain-time-temperature relationships in polymers were briefly introduced in chapter I. The discussion showed that the results of creep tests at elevated temperatures could be shifted by certain shift factors to predict creep strains at longer time durations.

The principal of shifting creep strains (or other visco-elastic function) against the logarithm of time (or frequency) is known as the time-temperature superposition and it was first developed for amorphous polymers above their glass transition temperature *[21]*. The empirical equation for the temperature dependency of the shift factor a_T could be written in the form :

$$Log\ a_T = \frac{-C_1\ (\ T - T_g\ )}{(C_2 + T - T_g)} \qquad (6)$$

where C_1 and C_2 are constants that change slightly according to the polymer type; and T_g is the glass-transition temperature of the polymer. Typical Values of T_g for different geosynthetics were shown in table 1 while values of C_1 and C_2 are shown in table 5. The dependency of a_T on temperature T is illustrated in figure 34 for Polystyrene polymer using equation 6 and the parameters in table 5.

Equation 6 was based on empirical relationships between the viscosity of liquids and their free volume at different temperatures. The theoretical considerations for the development of equation 6 are not in the scope of this report as they are discussed in detail in reference *[22]*.

TABLE 5

Parameters C_1 and C_2 in WLF Equation *[16]*

Polymer	C_1	C_2	Glass-transition T_g	
			°C	°K
Natural rubber	16.7	53.6	-73	200
Polystyrene	14.5	50.4	100	373
Universal Constants	17.4	51.6	---	

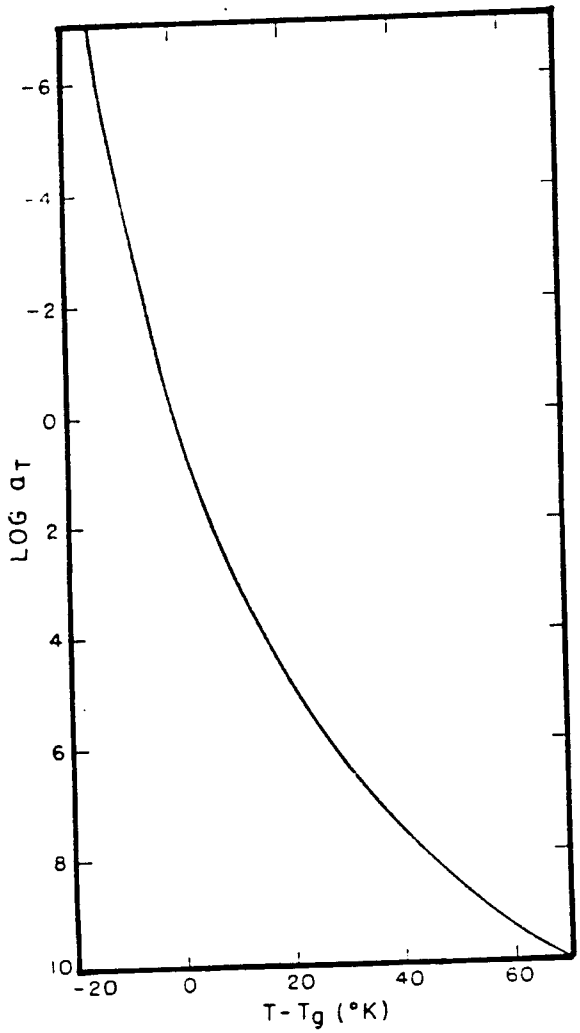

Figure 34

Theoretical values of the shift factor in WLF equation *[16]*

Procedures for time-temperature superposition were established for plastic pipes tested at higher temperatures *[20]*. Figure 35 shows the creep stress data for HDPE plastic pipes at two temperatures *[31]*. Research has also been conducted to establish the time shift factors a_T for geotextile yarns. The time shift factors for different geotextiles are presented in table 6 *[5]*. The shift factors give the multiples of time which should be applied to extrapolate the isochronous curves. For example, for a shift factor of 11, the 100 hour isochronous curve at 20°C creep tests for drawn polyethylene grids may be treated as 1100 hour curve at temperature 10°C. However, these shift factors were based on limited data available. Moreover, the change of shift factors with temperature need to be established in a similar fashion for a wider temperature range for shifting creep response to longer time intervals.

The application of the time-temperature shift principals in geogrids are presented in this chapter. The results of the creep testing program were analyzed and implemented in a procedure for applying the shift factors to predict creep strains at longer time intervals.

Table 6

Time-temperature shift factors for different polymers [5]

Material	Temperature Range (°C)	Multiple of time for every +10 °C
Polyester yarn	20-60	6
Polypropylene yarn	20-10	4
	28-40	4
	40-60	6
Polyethylene grid	10-20	11

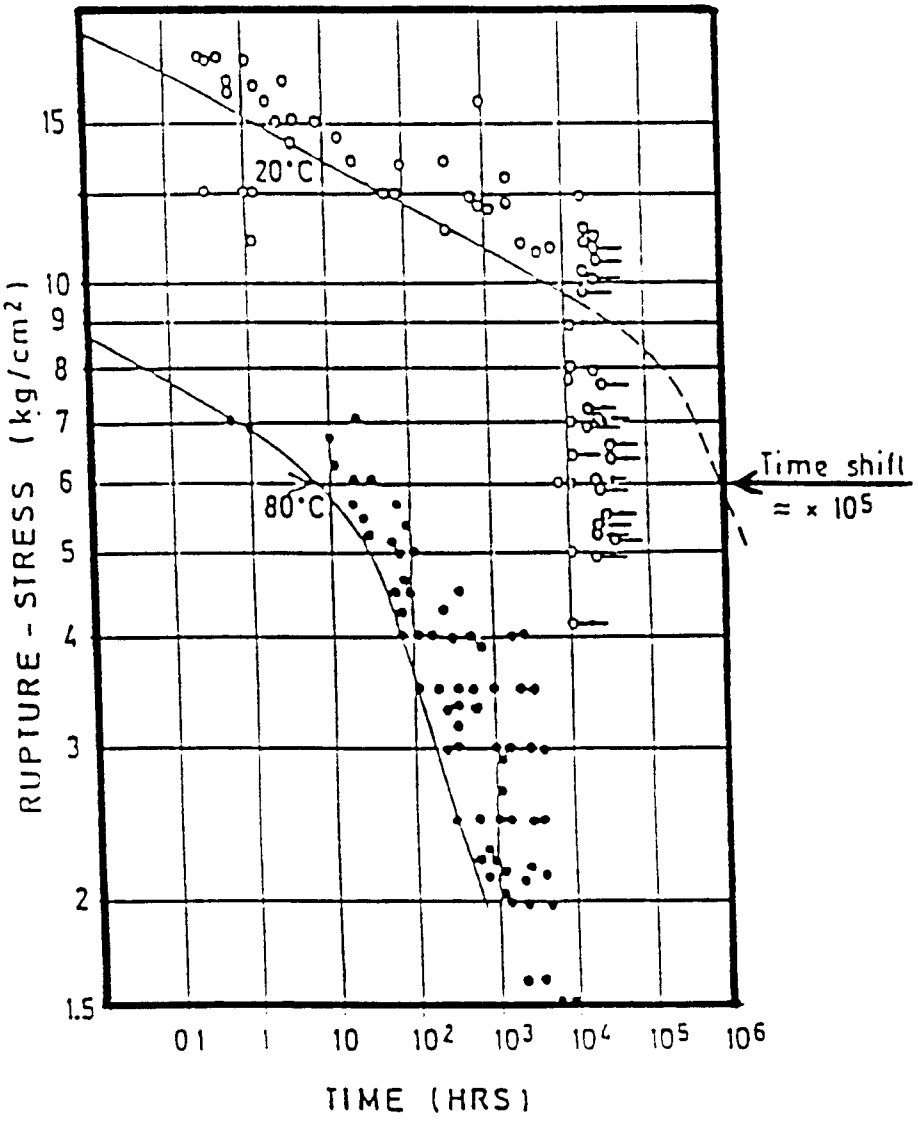

Figure 35

Creep stress data for HDPE pipes *[31]*

B. Application of Time-Shift Principals on Creep Test Results

The application of the time-temperature shift factors on the creep test results should satisfy several criteria which are summarized as *[22]* :

(a) The exact matching of the shapes of adjacent curves of the visco-elastic function versus log time at various temperatures.

(b) The calculated values of the shift factors a_T must superpose all the visco-elastic functions.

(c) The temperature dependence of a_T must have a reasonable form consistent with experience.

These criteria were observed when establishing shift factors from the results. This procedure was applied to the test results of the Tensar UX1500 as follows:

1. Plot the logarithm of the visco-elastic function (strain, elasticity modulus, or creep compliance) against log-time:

The results of the testing program were shown in the previous chapters as creep strains and elasticity moduli verses time at various temperatures and creep loads. Test results of the HDPE geogrid were plotted in figures 36, 37, 38, and 39 as log-strains verses log-time at loading levels 13 kN/m (0.9 Kips/ft), 16 kN/m (1.1 Kips/ft), 22 kN/m (1.5 Kips/ft), and 28 kN/m (1.9 Kips/ft), respectively. In order to evaluate the consistency of the shift factors a_T with other response functions, the results of the elasticity moduli were similarly plotted versus log-time in figures 40, 41, 42, and 43 .

Regression analysis was conducted to obtain the best fitting curve of linear functions on the logarithmic scale. These functions are shown in tables 7 and 8 for the strain and elasticity modulus curves, respectively. The analysis shows that the linear regression fitted the results with coefficients of determination well above 0.9.

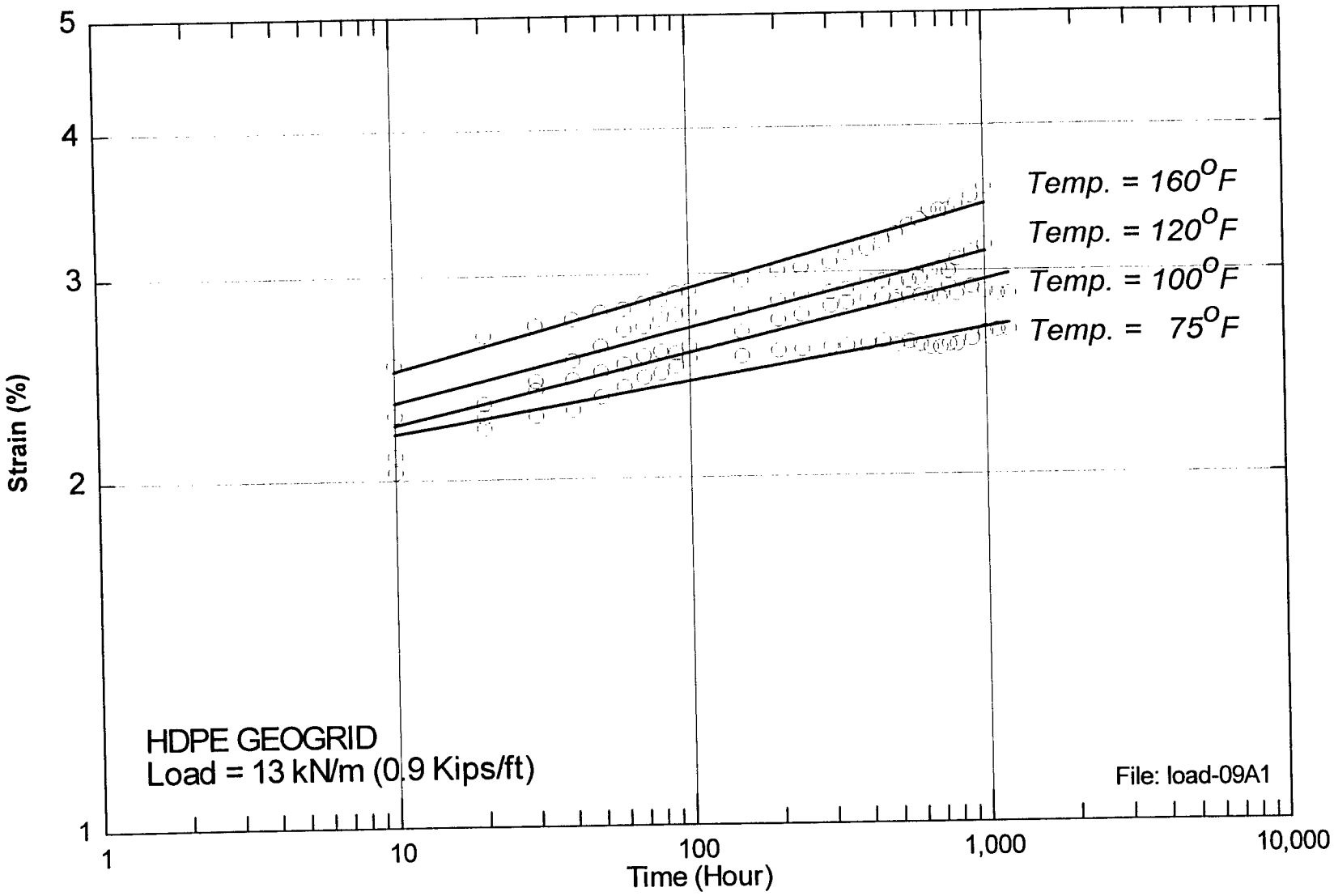

Figure 36

Creep Strain vs. Log-time at creep load 13 kN/m

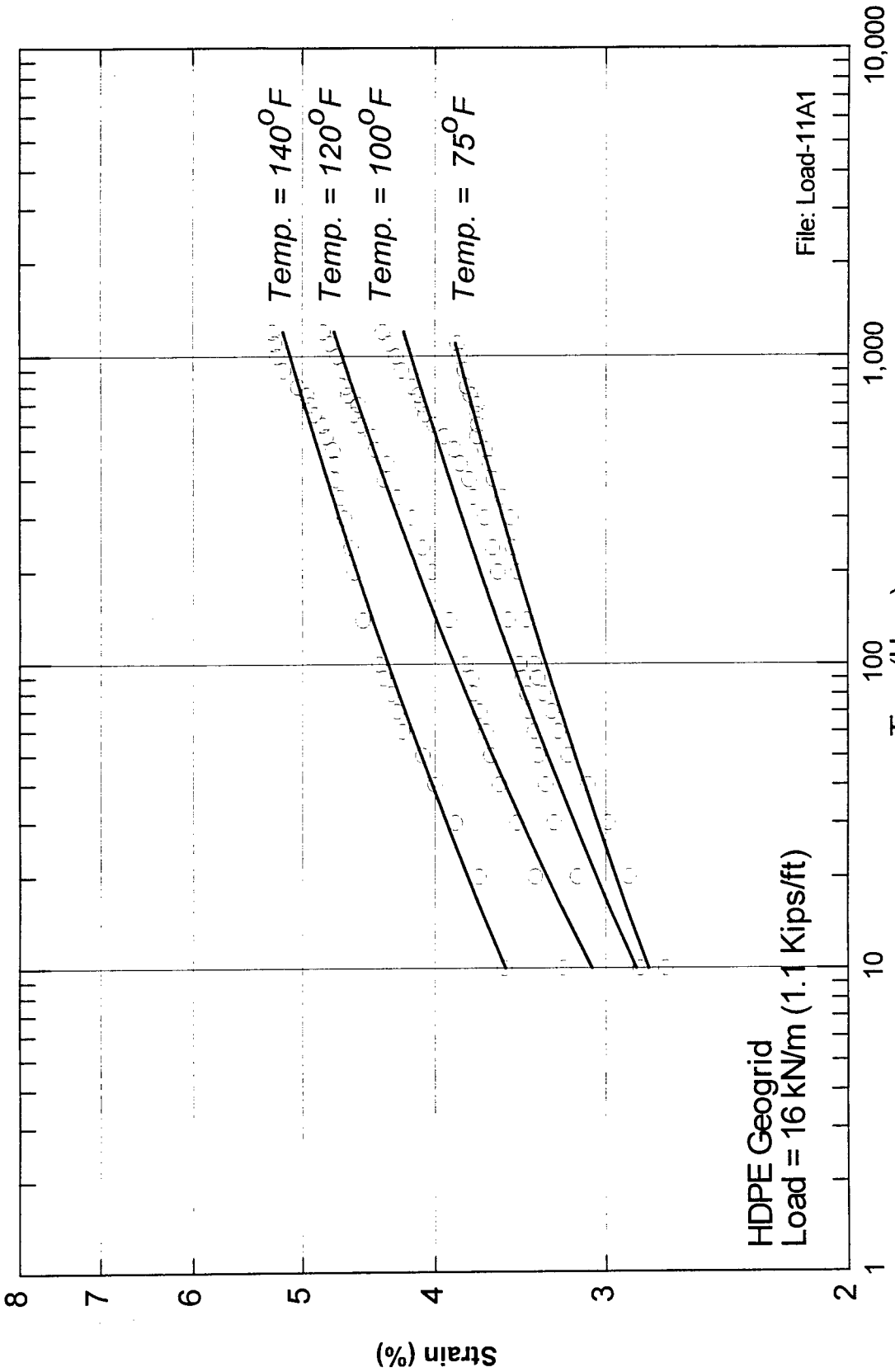

Figure 37

Creep strains vs. Log-time at creep load 16 kN/m

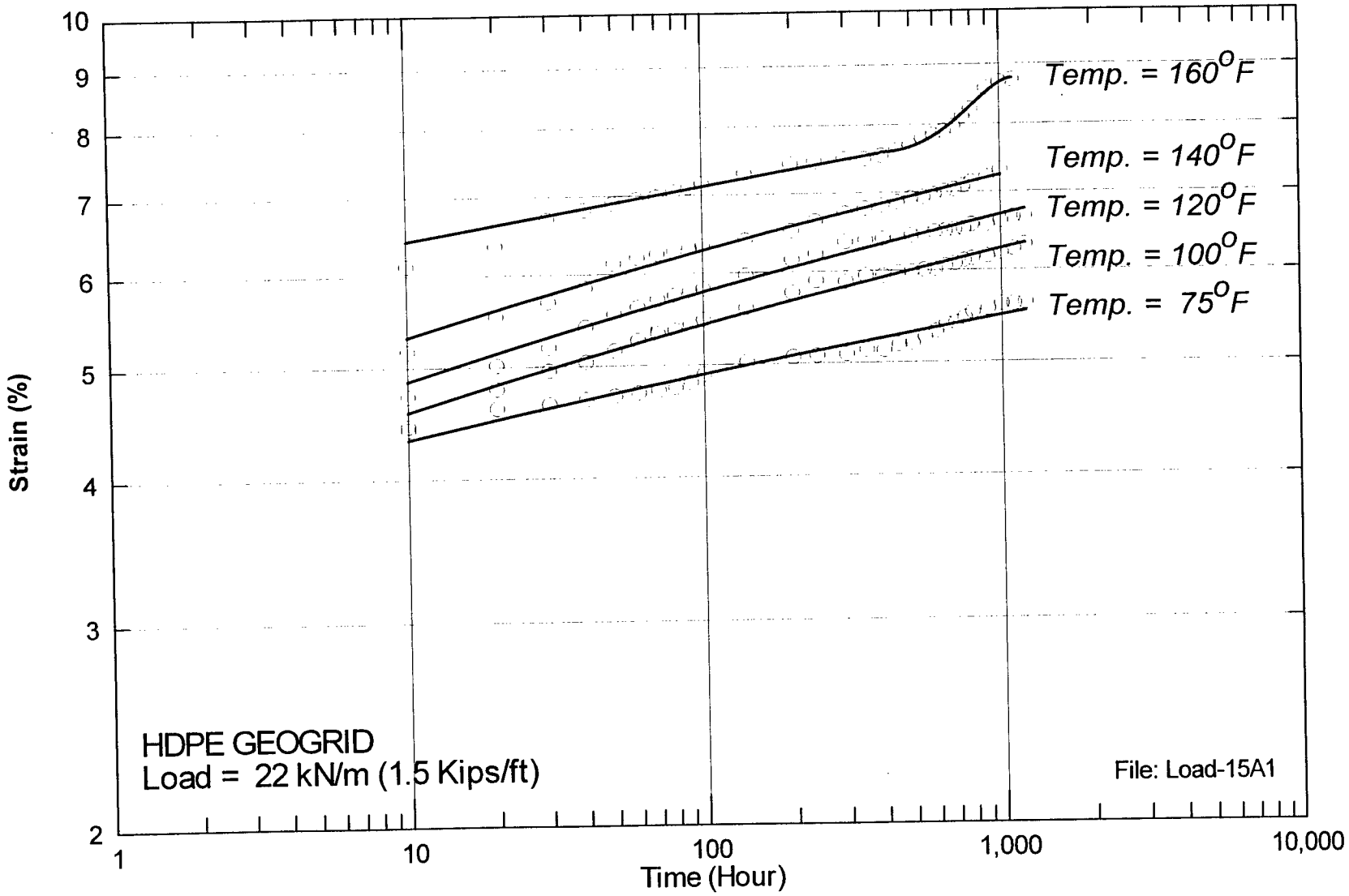

Figure 38

Creep strains vs. Log-time at creep load 22 kN/m

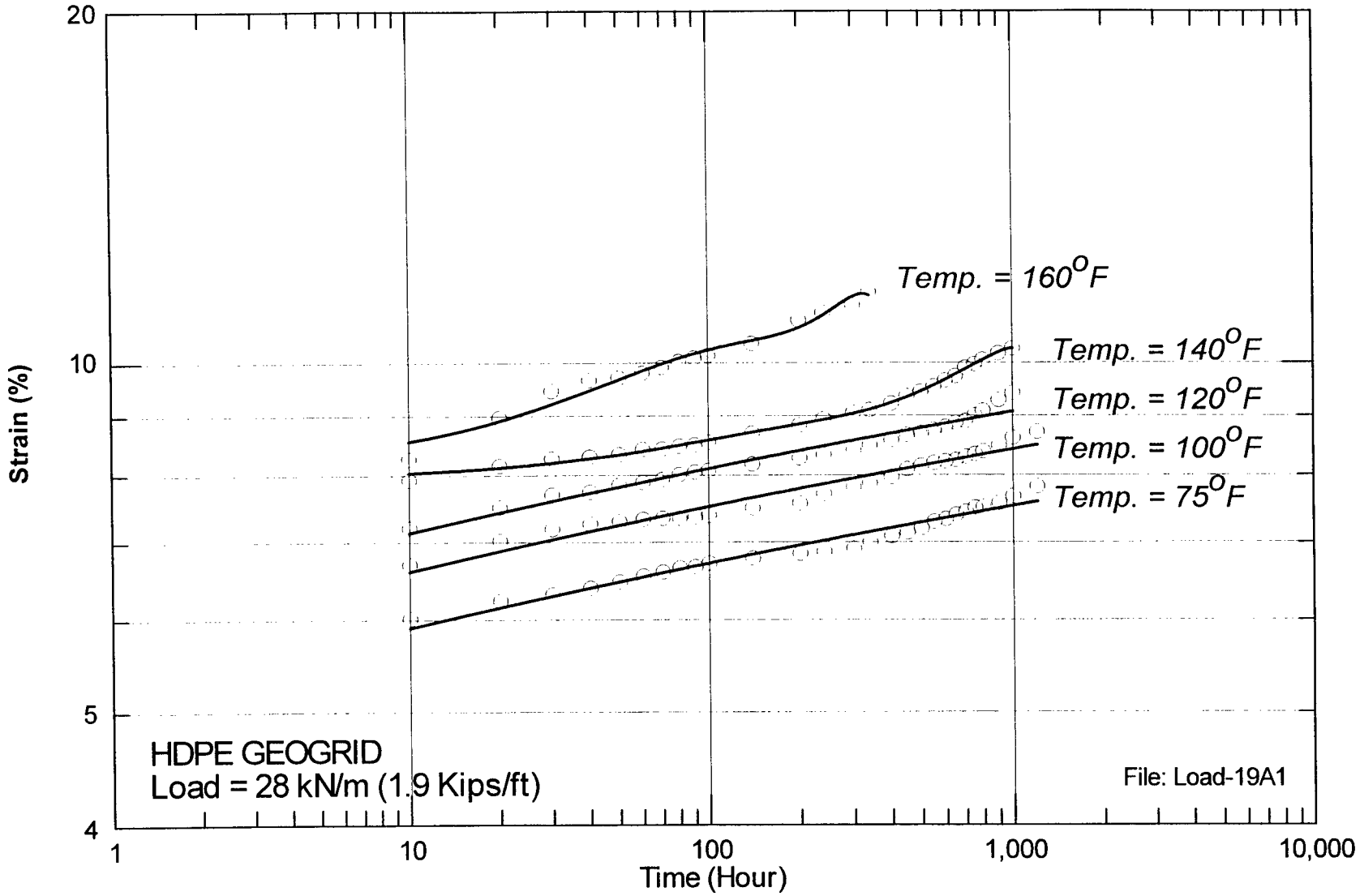

Figure 39

Creep strains vs. Log-time at creep load 28 kN/m

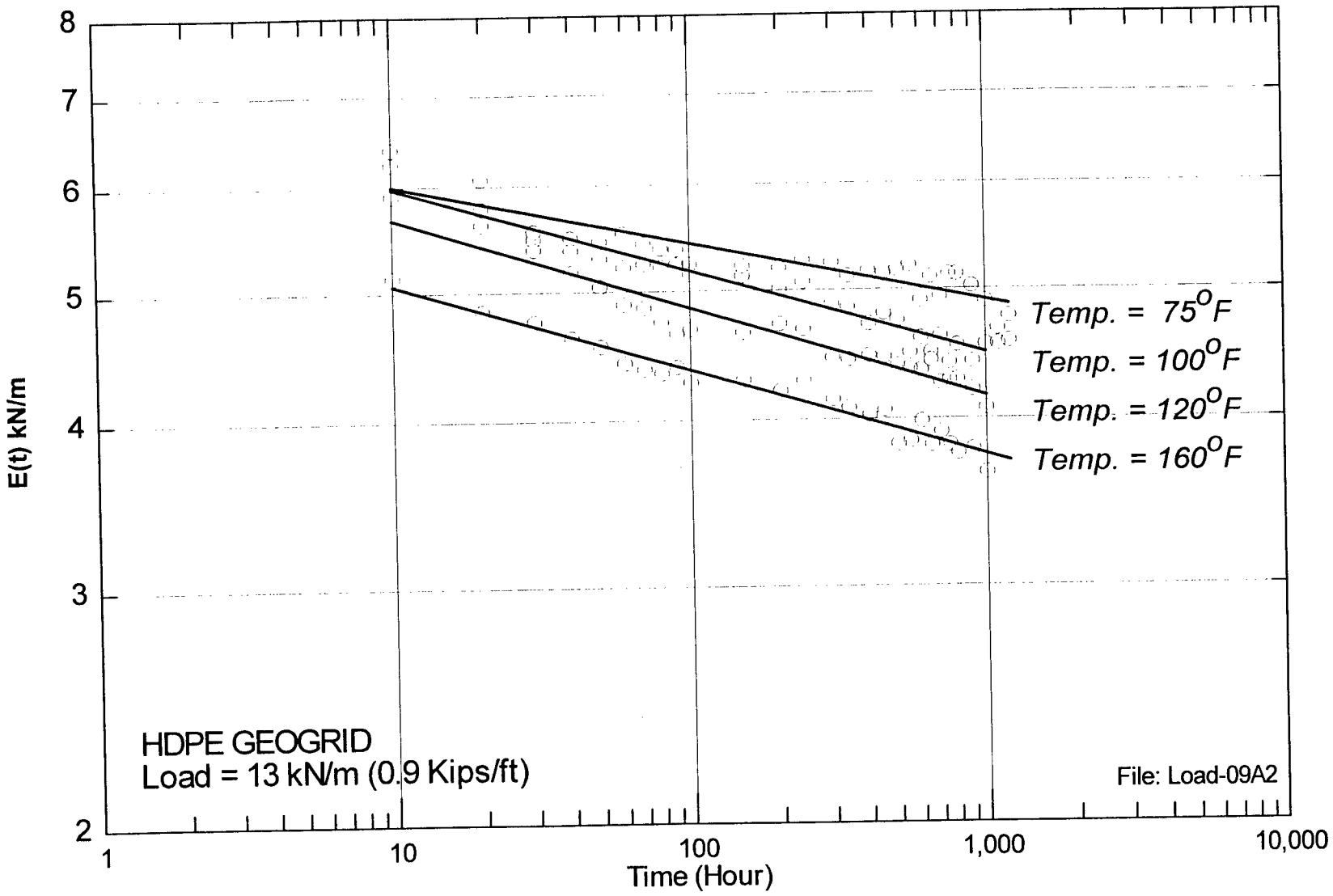

Figure 40

Creep elasticity modulus vs. Log-time at load 13 kN/m

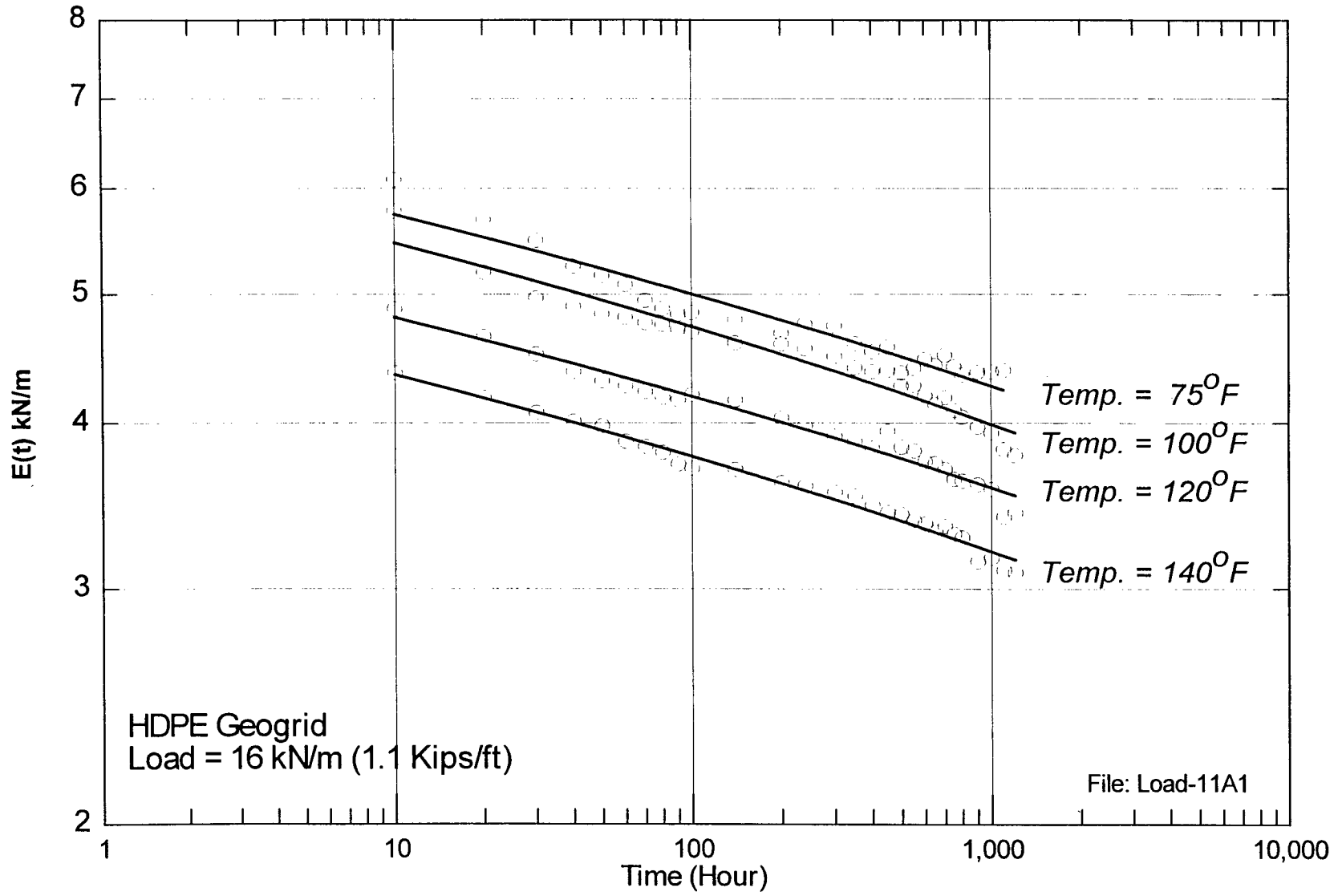

Figure 40

Creep elasticity modulus vs. Log-time at Load 16 kN/m

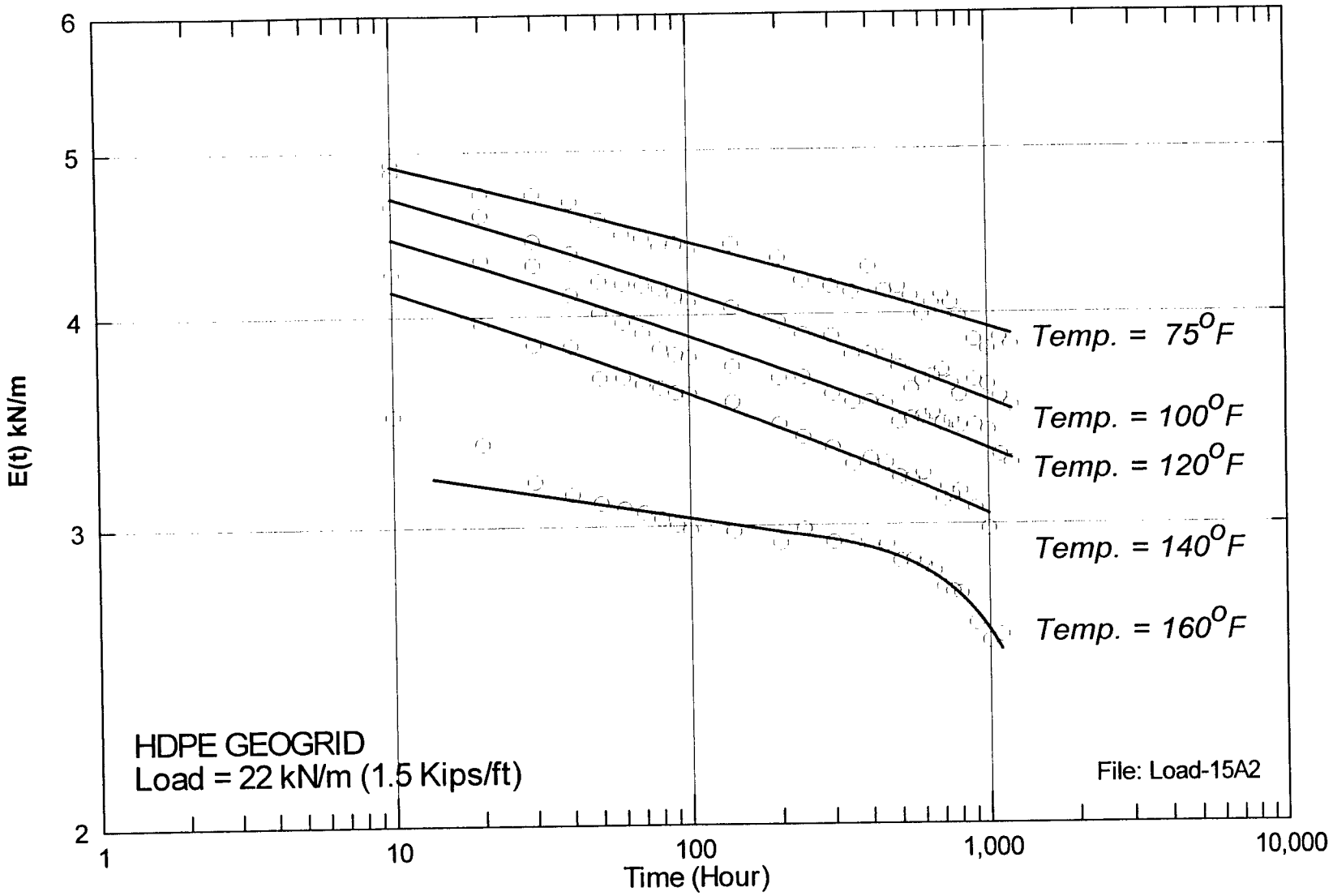

Figure 42

Creep elasticity modulus vs. Log-time at load 22 kN/m

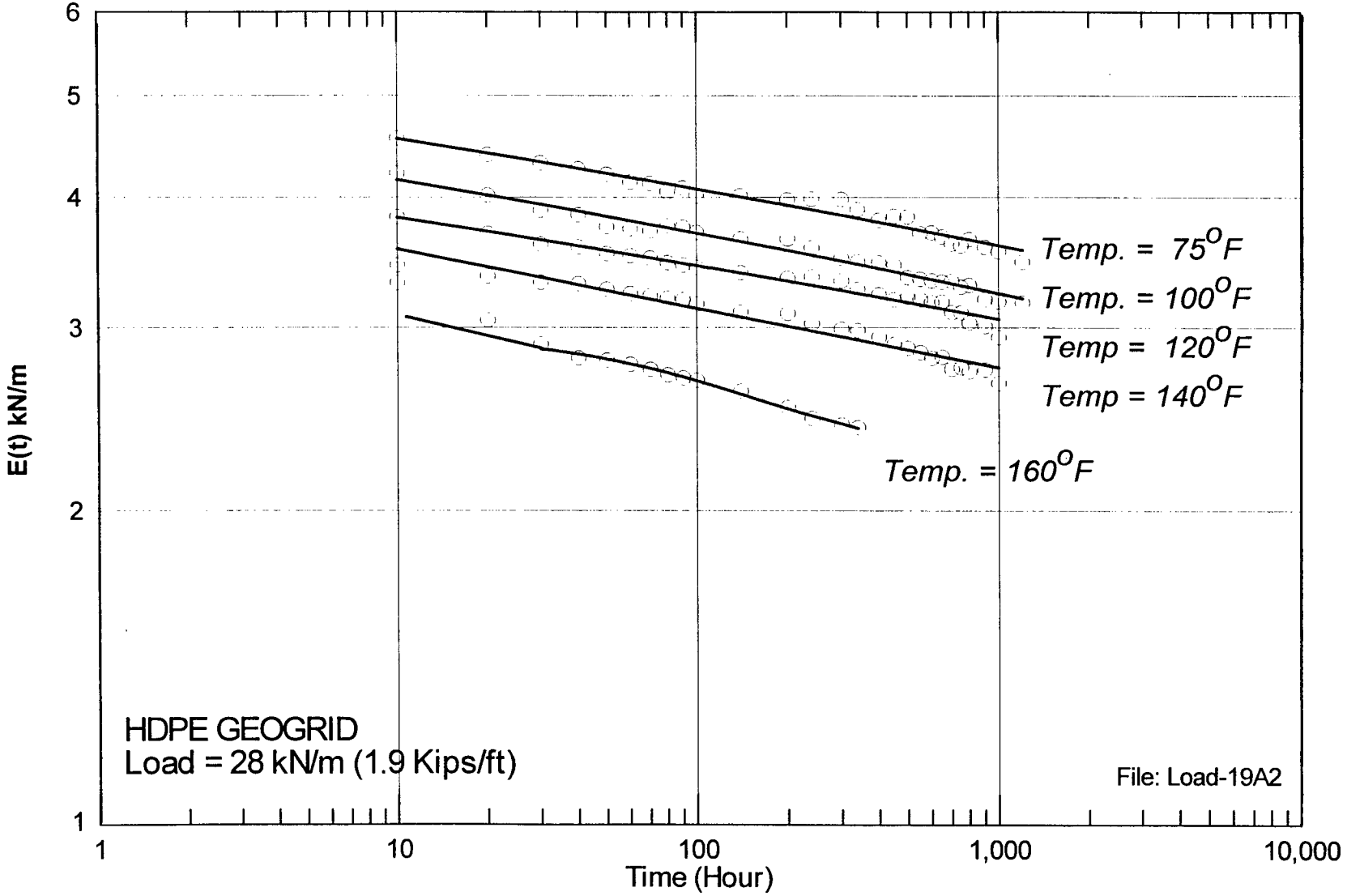

Figure 43

Creep elasticity modulusvs. Log-time at load 28 kN/m

The fitted response curves at various temperatures showed similarity of shapes with increase in slope as temperature and loads increase. However, the curves did not show exact match of shape at higher temperatures and loading levels, specifically at temperature 72°C (160°F) and at creep loads of 22 kN/m (1.5 Kips/ft) and 28 kN/m (1.9 Kips/ft). Polynomial functions best matched creep response at these higher temperatures and loading levels.

Table 7 .

Linear correlation of creep strain (y) with log-time

Geogrid Type	Load (Kips/ft)	Temperature °F	(Y) Intercept	Slope of (Y)	r^2 (*)
HDPE	0.9	75	1.966	0.242	0.81
		100	1.823	0.381	0.96
		120	1.942	0.385	0.95
		160	1.955	0.474	0.94
	1.1	75	2.271	0.524	0.98
		100	2.188	0.650	0.94
		120	2.253	0.801	0.98
		140	2.798	0.766	0.97
	1.5	75	3.927	0.501	0.93
		100	3.705	0.862	0.98
		120	3.971	0.915	0.98
		140	4.347	0.960	0.99
		160	(**)	(**)	--
	1.9	75	5.448	0.610	0.98
		100	6.127	0.650	0.95
		120	6.494	0.780	0.99
		140	7.060	0.777	0.97
		160	(***)	(***)	--

(*) r^2 = coefficient of determination

(**) Best fitted polynomial function $y = 0.763 + 8.601 (\log x) - 4.106 (\log x)^2 + 0.7 (\log x)^3$

(***) Best fitted polynomial function $y = 1.811 + 10.751 (\log x) - 5.313 (\log x)^2 + 1.016 (\log x)^3$

Table 8

Linear correlation of creep elasticity modulus (y) with log-time

Geogrid Type	Load (Kips/ft)	Temperature °F	(Y) Intercept	Slope of (Y)	r^2 (*)
HDPE	0.9	75	0.44	-0.034	0.76
		100	0.46	-0.052	0.93
		120	0.43	-0.050	0.89
		160	0.39	-0.043	0.95
	1.1	75	0.44	-0.050	0.91
		100	0.42	-0.049	0.94
		120	0.37	-0.041	0.97
		140	0.34	-0.039	0.98
	1.5	75	0.364	-0.031	0.95
		100	0.377	-0.046	0.95
		120	0.351	-0.042	0.94
		140	0.330	-0.041	0.98
		160	(**)	(**)	--
					0.92
	1.9	75	0.33	-0.026	0.93
		100	0.31	-0.028	0.97
		120	0.28	-0.022	0.98
		140	0.26	-0.021	0.97
		160	(***)	(***)	--

(*) r^2 = coefficient of determination

(**) Best polynomial fitted function $y = 0.42 - 0.287 (\log x) + 0.132 (\log x)^2 - 0.21 (\log x)^2$

(***) Best polynomial fitted function $y = 0.397 - 0.279 (\log x) + 0.131 (\log x)^2 - 0.023 (\log x)^3$

2. **A reference temperature T_O is arbitrary chosen within the applied range of temperatures:**

The constants C_1 and C_2 of the WLF equation (shown in table 5 for different polymers) corresponded to their glass-transition temperatures T_g as their reference temperatures. The values of these constants can be converted to correspond to other reference temperature T_0 by the following relationships *[32]*:

$$C_1^g = C_1 C_2 / (C_2 + T_g - T_0)$$
$$C_2^g = C_2 + T_g - T_0 \qquad (7)$$

where C_1^g and C_2^g are the constants corresponding to the glass-transition temperature.

HDPE polymer has a glass-transition temperature of about -80°C (-112°F). At this temperature, the values of the universal constants C_1 and C_2 are 17.4 and 51.6, respectively. Equation 7 was used to calculate the constants at reference temperature of 24°C (75°F). The substitution of these relationships resulted in constants C_1 and C_2 of 5.77 and 155.6, respectively. The values of C_1 and C_2 at room temperature were utilized in equation 6 to obtain the values of a_T at different temperatures for the geogrid. The analytical values of a_T are shown in figure 44.

It should be noted that the selection of the reference temperature as the room temperature is arbitrary. However, such selection facilitated comparing the results of the analytical procedure with the experimental values of a_T. It should also be noted that the values of T_g used in these calculations are approximate values and they may differ according to the manufacturing process of each specific product. Accordingly, figure 44 may slightly differ with different values of T_g.

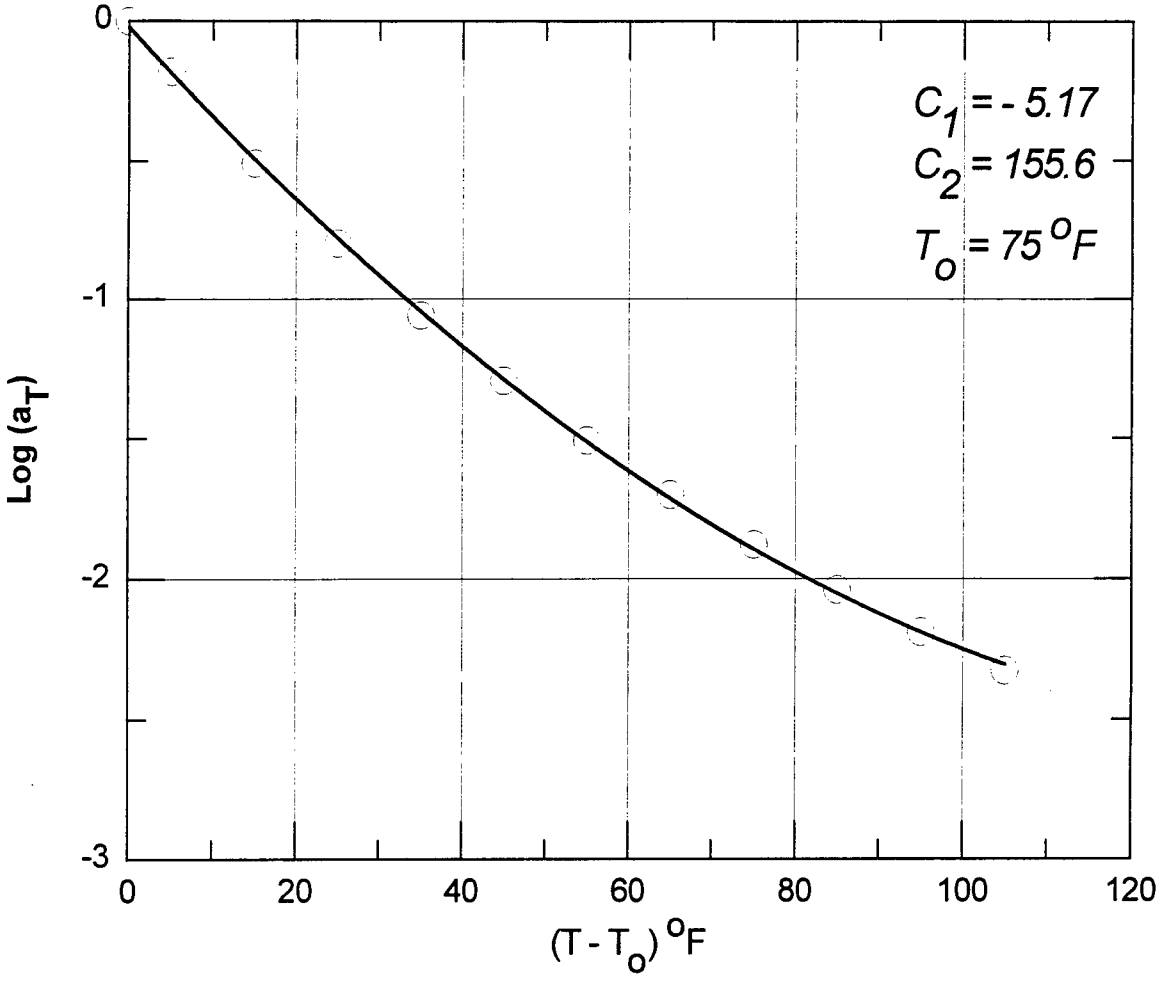

Figure 44

Analytical values of a_T for the HDPE geogrid

3. **The adjacent response curves are shifted to obtain the 10,000 hour master curve:**

The adjacent response curves for each loading level were shifted on the log-time scale. The curves were shifted first to obtain the 10,000 hour master curves. The parameters of the master curves equations were then compared with those of the 10,000 hour creep test results. The results of the 10,000 hours tests are shown in figures 45 and 46 for creep strains and creep elasticity moduli, respectively. Table 9 shows the parameters of the best fitting curves of the 10,000 creep tests.

In establishing the 10,000 hour master curves, the shift factors were measured graphically to obtain best fits of one curve. Response curves of temperatures 20°C (75°F), 38°C (100°F), and 49°C (120°F) were used to establish the master curves up to 10,000 hours. Figures 47 to 54 show the comparison between the master curves and the 10,000 hour test results for the loads: 13 kN/m (0.9 Kips/ft), 16 kN/m (1.1 Kips/ft), 22 kN/m (1.5 Kips/ft), and 28 kN/m (1.9 Kips/ft). The best fits of the linear functions of the master curves are shown in Table 10 along with the corresponding shift factors.

The comparison between the established master curves and the 10,000 hours experimental results showed that:

- The shift factors were practically the same for the temperature shift of both creep responses: strain and elasticity modulus.

- Shift factors could successfully predict the 10,000 hour creep response from the 1,000 hour tests at elevated temperatures. Table 10 showed that the master curves were almost identical to the 10,000 hour test results at loading levels up to 1.5 kips/ft. However, the shift factors could not successfully predict creep strains at loading level 1.9 kips/ft. Figures 53 and 54 show that shift factors did not successfully predict the accelerated creep failure at this loading level.

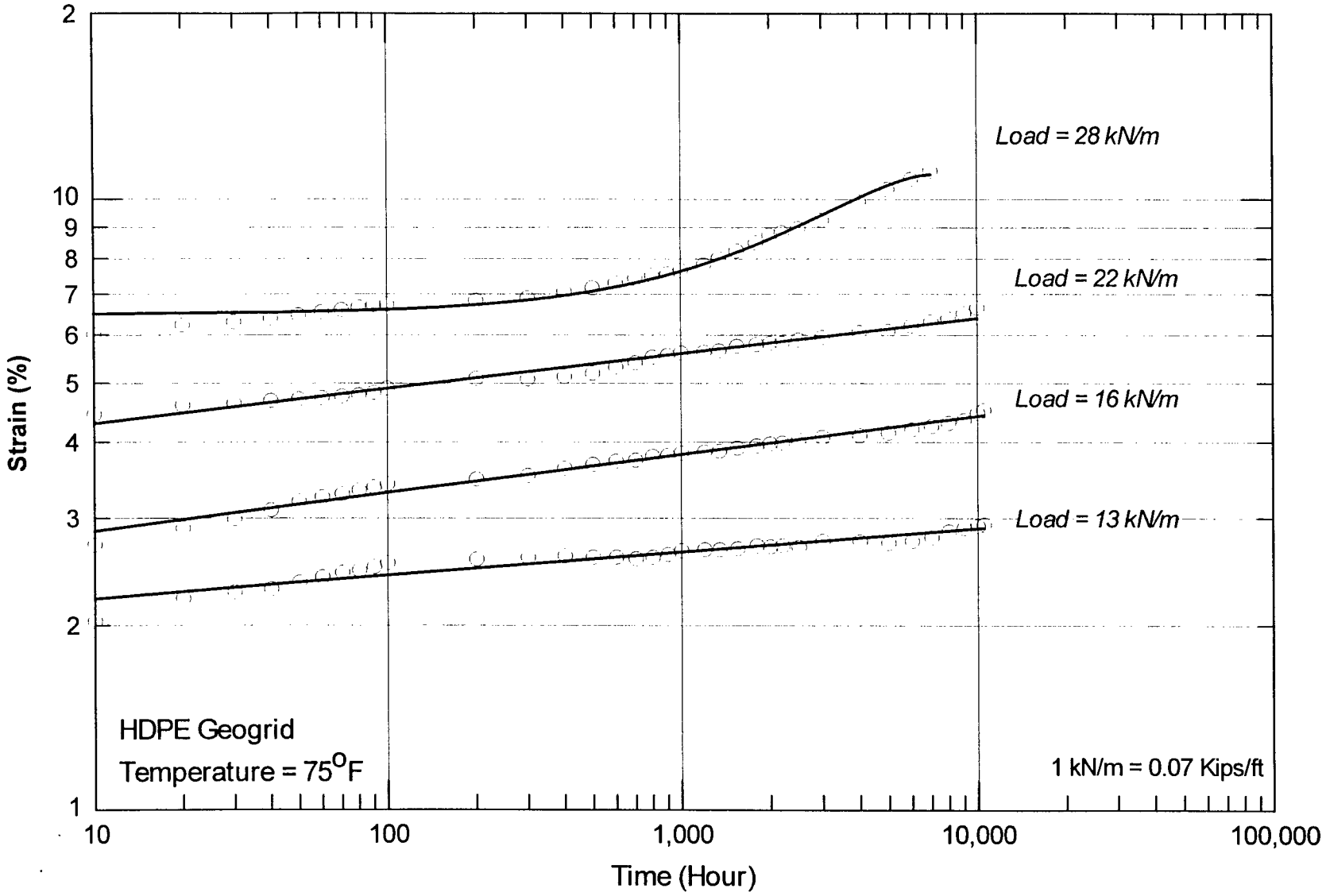

Figure 45

10,000 hour creep strains vs. Log-time in room temperature

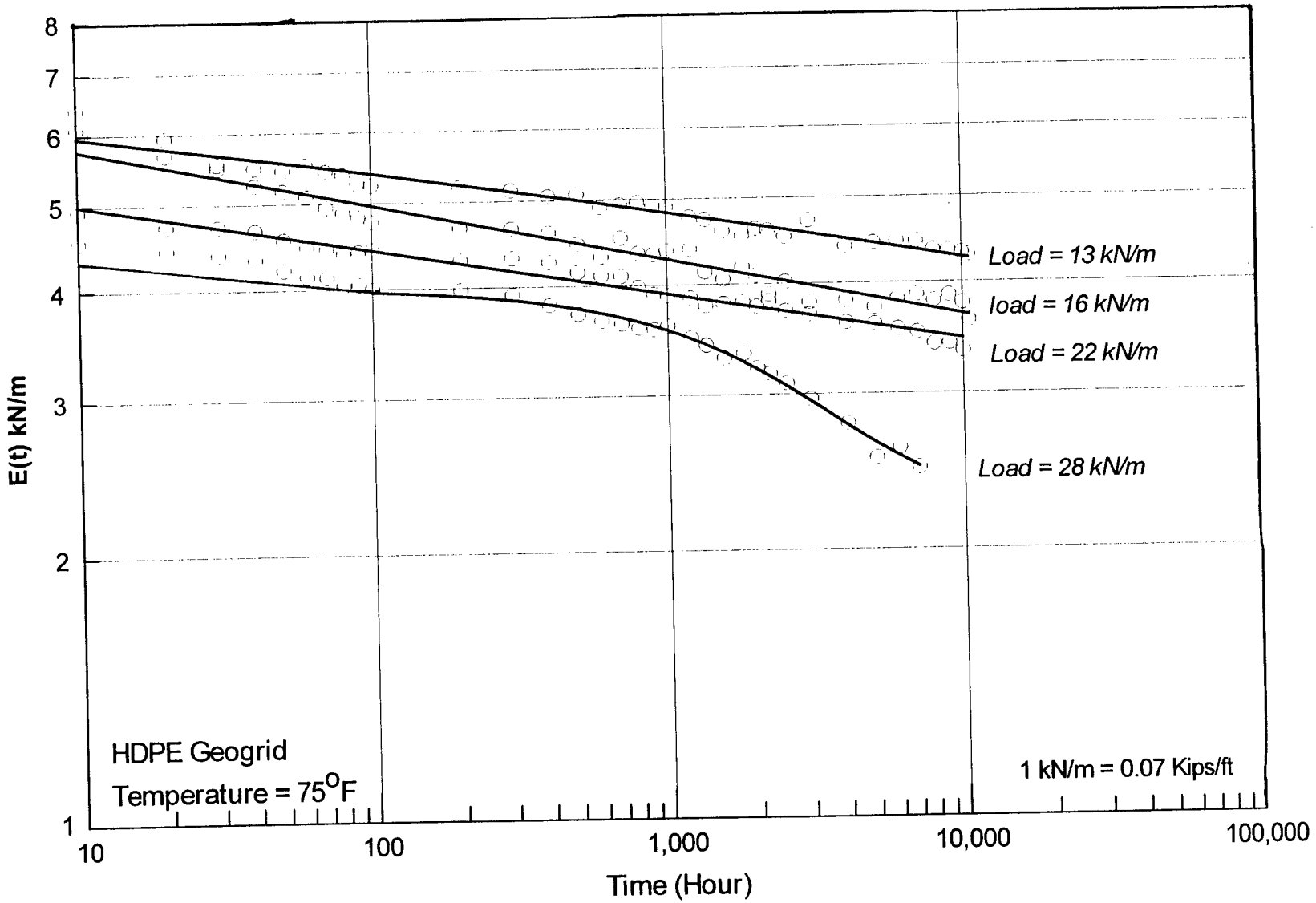

Figure 46

10,000 hour creep elasticity modulus at room temperature

Table 9

Parameters of the best fit equations of the 10,000 hour creep tests

Load (Kips/ft)	Response Function (Y)	Linear fit parameters [$Y = a + b\ Log\ (t)$] (a)	(b)	r^2
0.9	Strain	1.973	0.224	0.93
	E(t)	0.44	-0.038	0.95
1.1	Strain	2.26	0.524	0.99
	E(t)	0.435	-0.047	0.95
1.5	Strain	3.475	0.716	0.96
	E(t)	0.372	-0.034	0.98
1.9	Strain	(*)	(*)	-
	E(t)	(**)	(**)	-

(*) Best fitted polynomial function: $y = 5.231 + 2.19\ (Log\ t) - 1.412\ (Log\ t)^2 - 0.322\ (Log\ t)^3$

(**) Best fitted polynomial function : $y = 0.348 - 0.06\ Log(t) + 0.024\ (Log\ t)^2 - 0.005\ (Log\ t)^3$

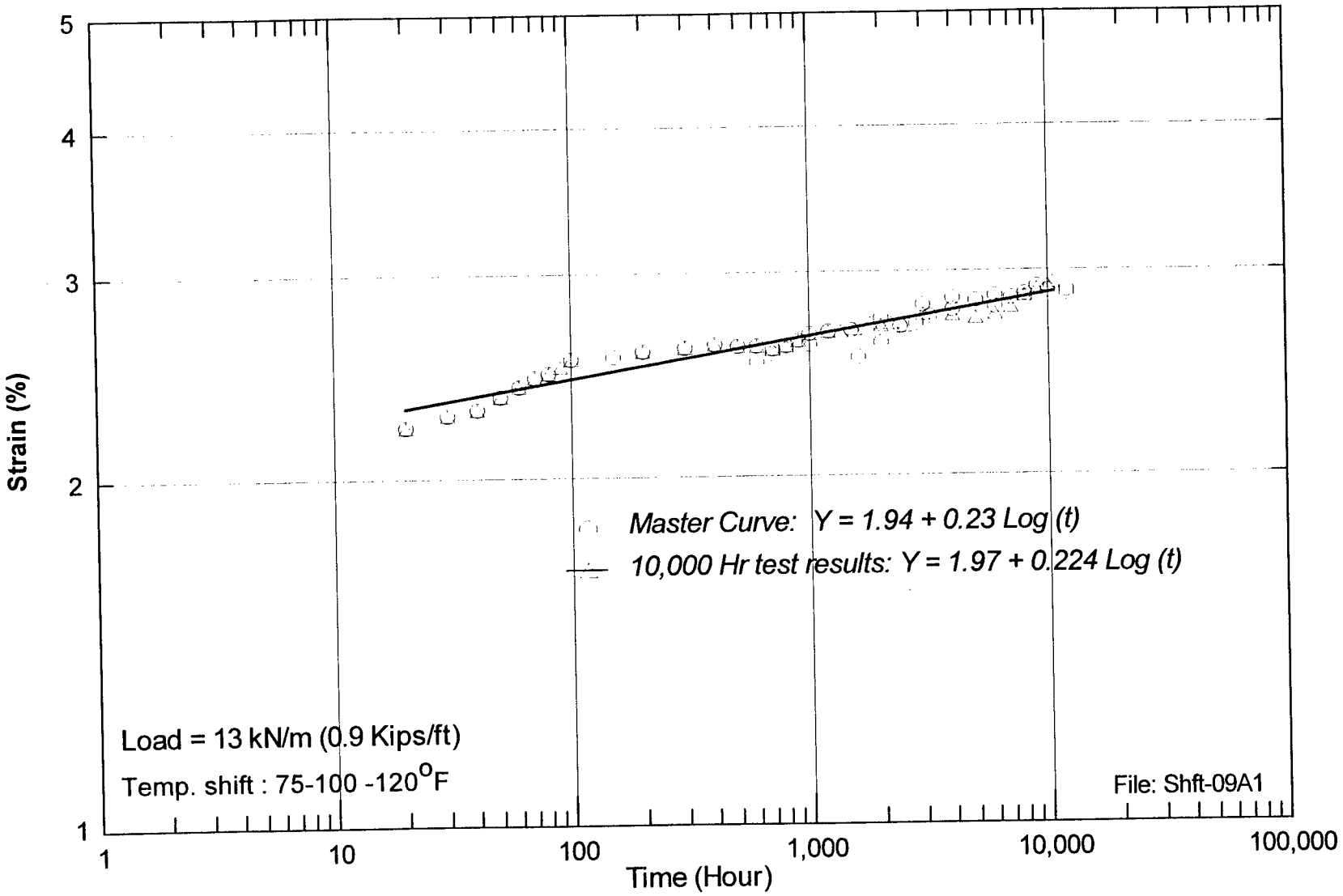

Figre 47

Master curve and 10,000 hour test results for strains at load 13 kN/m

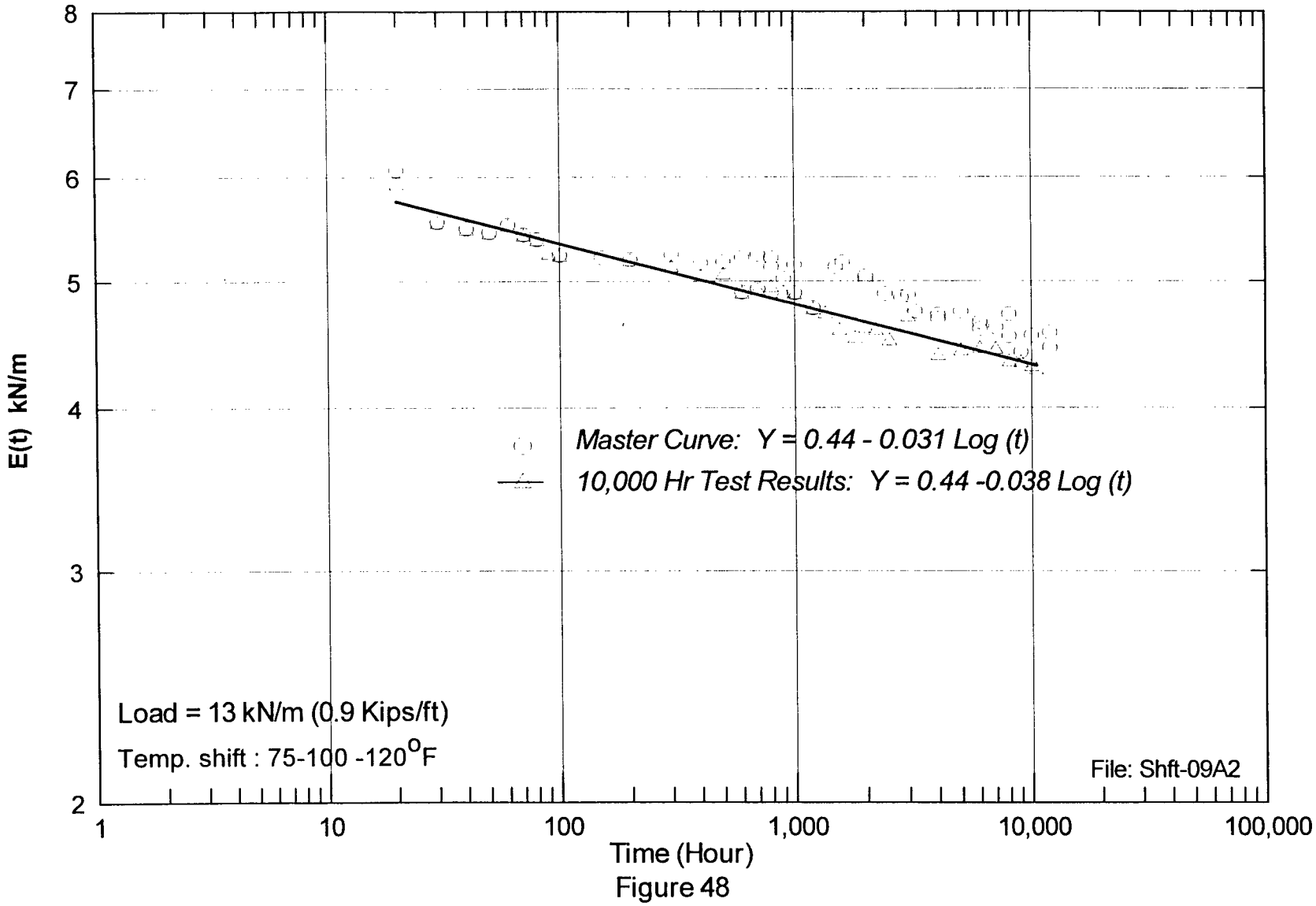

Figure 48

Master curve and 10,000 hour test results for elasticity modulus at load 13 kN/m

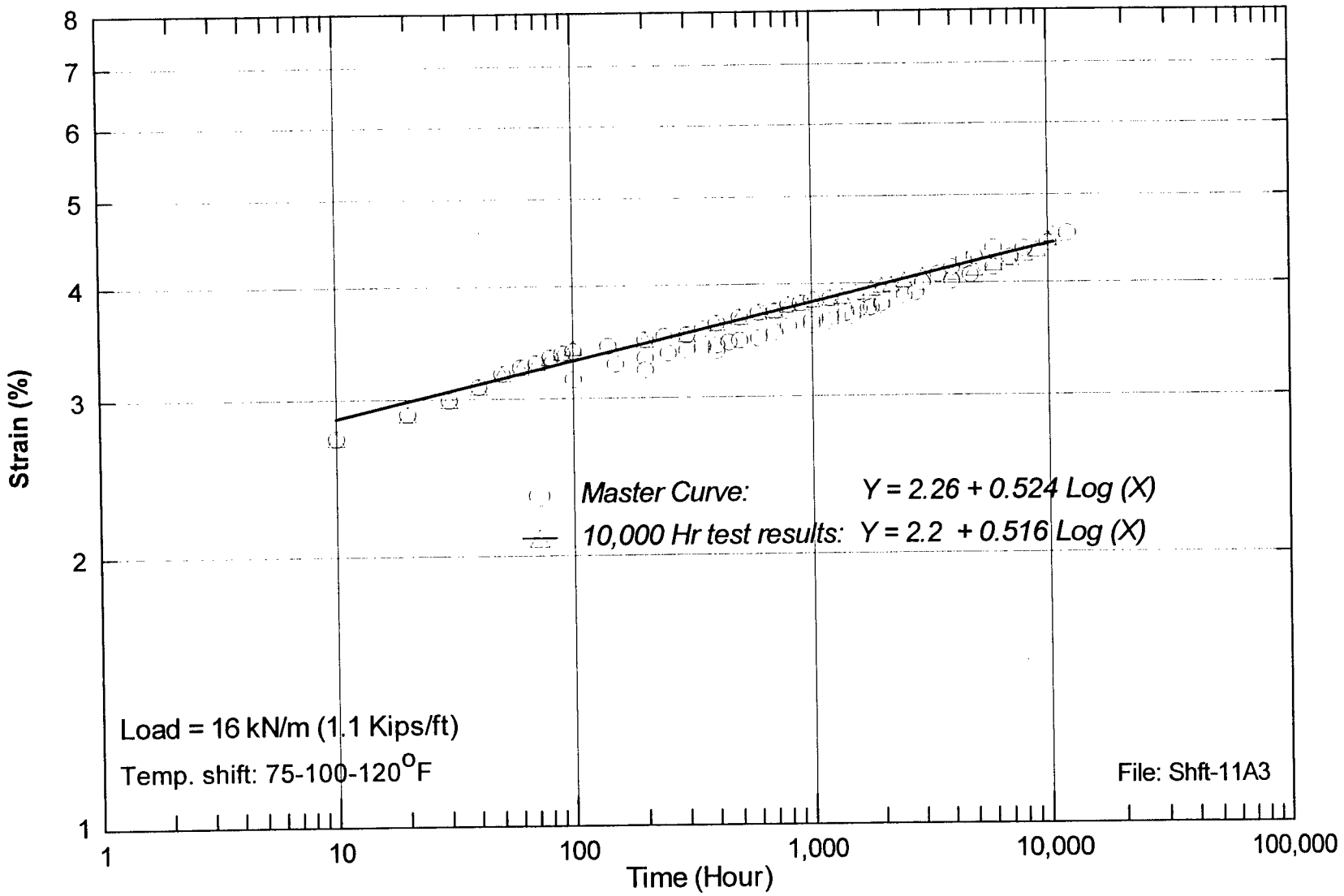

Figure 49

Master curve and 10,000 hour test results for strain at load 16 kN/m

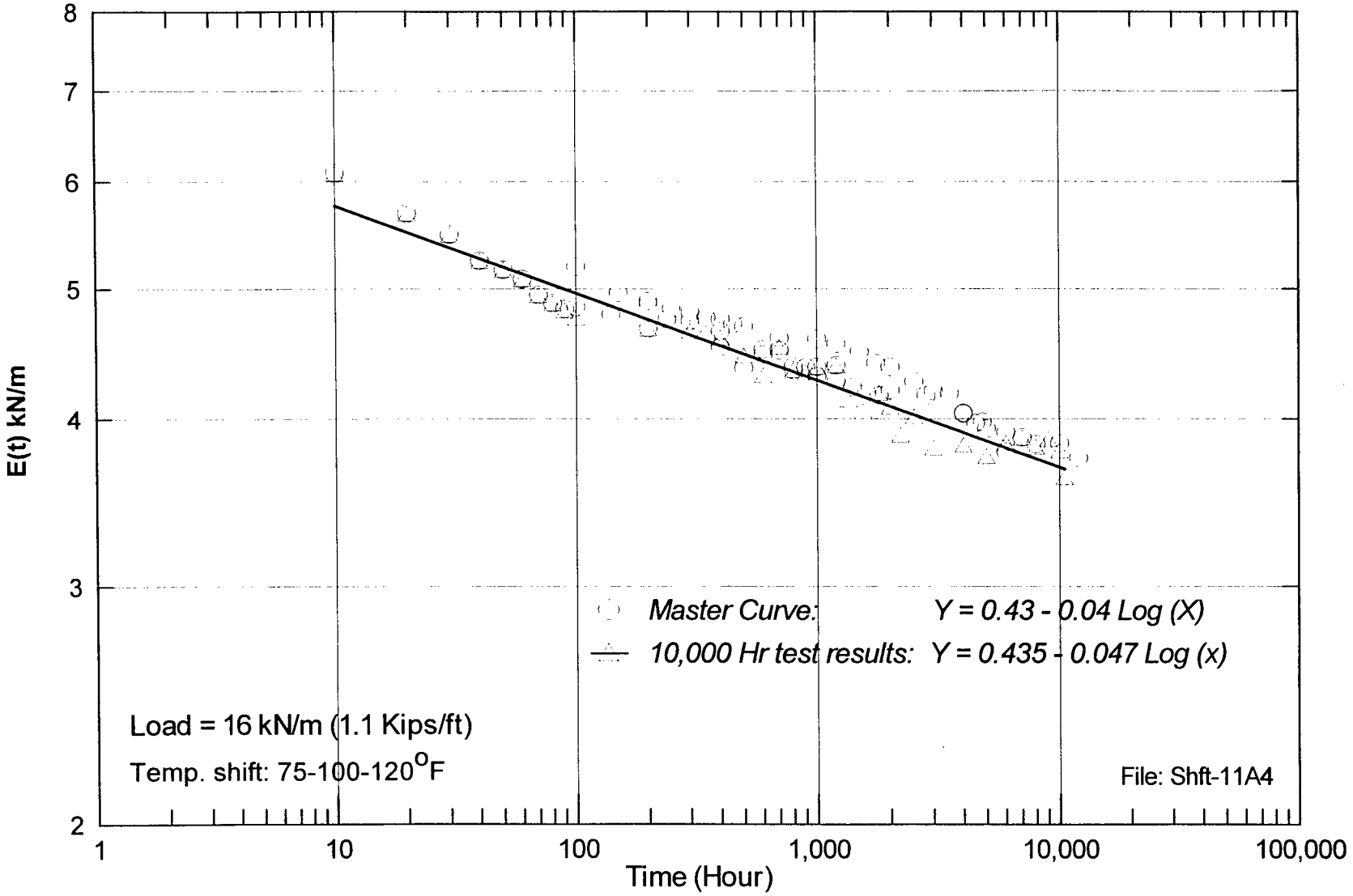

Figure 50

Master curve and 10,000 hour test results for elasticity modulus at load 16 kN/m

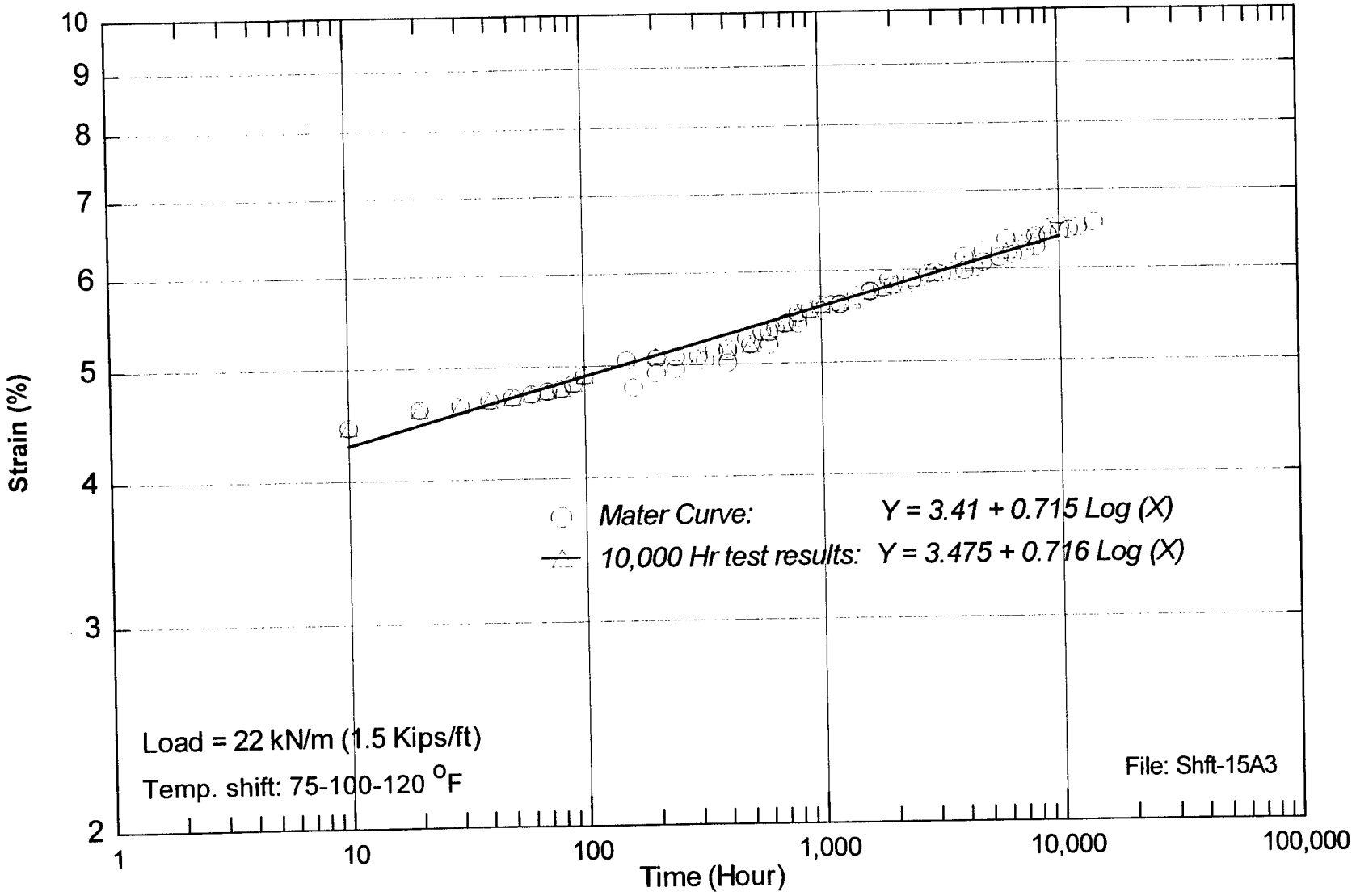

Figure 51

Master curve and 10,000 hour test results for strain at load 22 kN/m

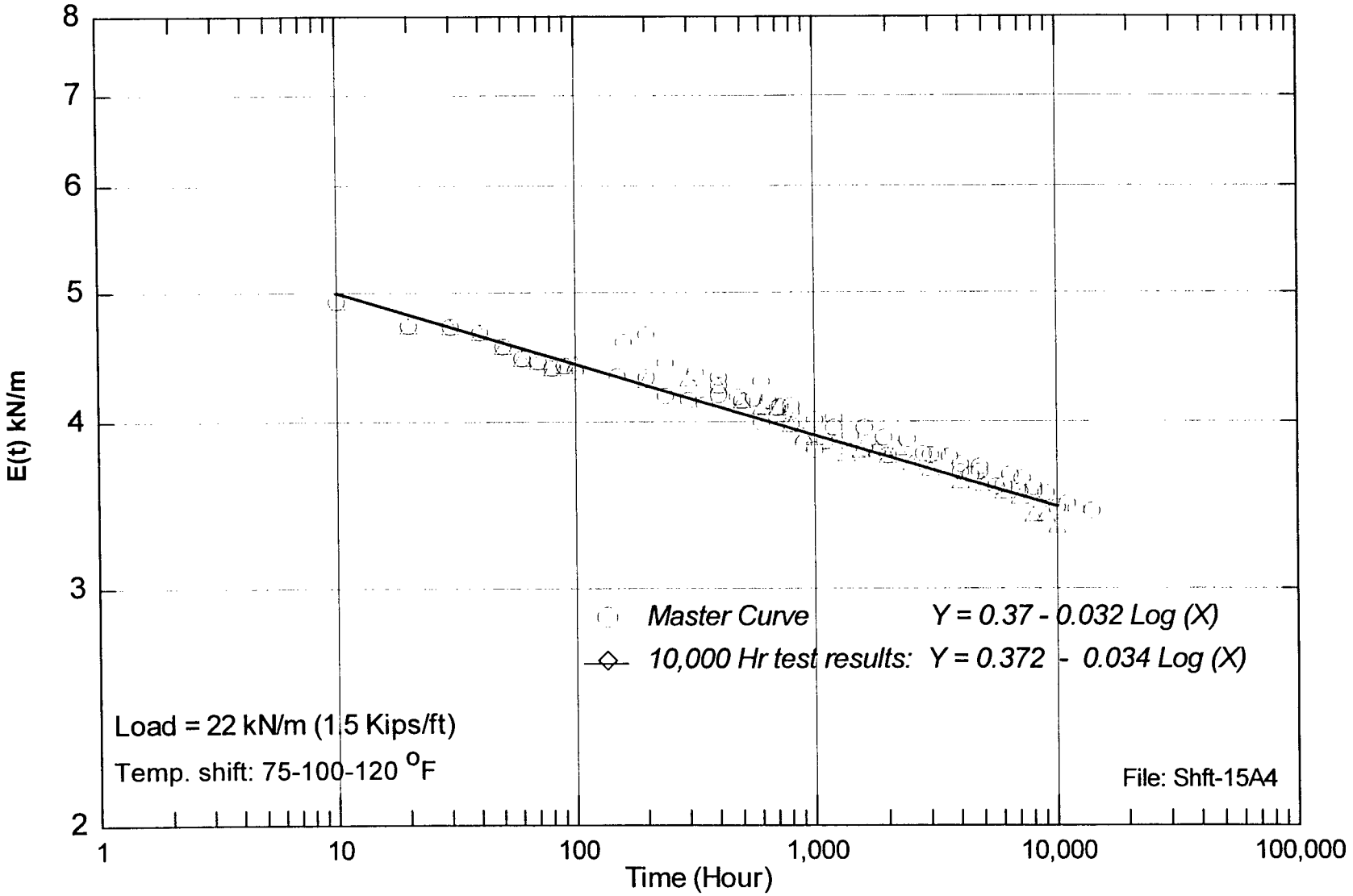

Figure 52

Master curve and 10,000 test results for elasticity modulus at load 22 kN/m

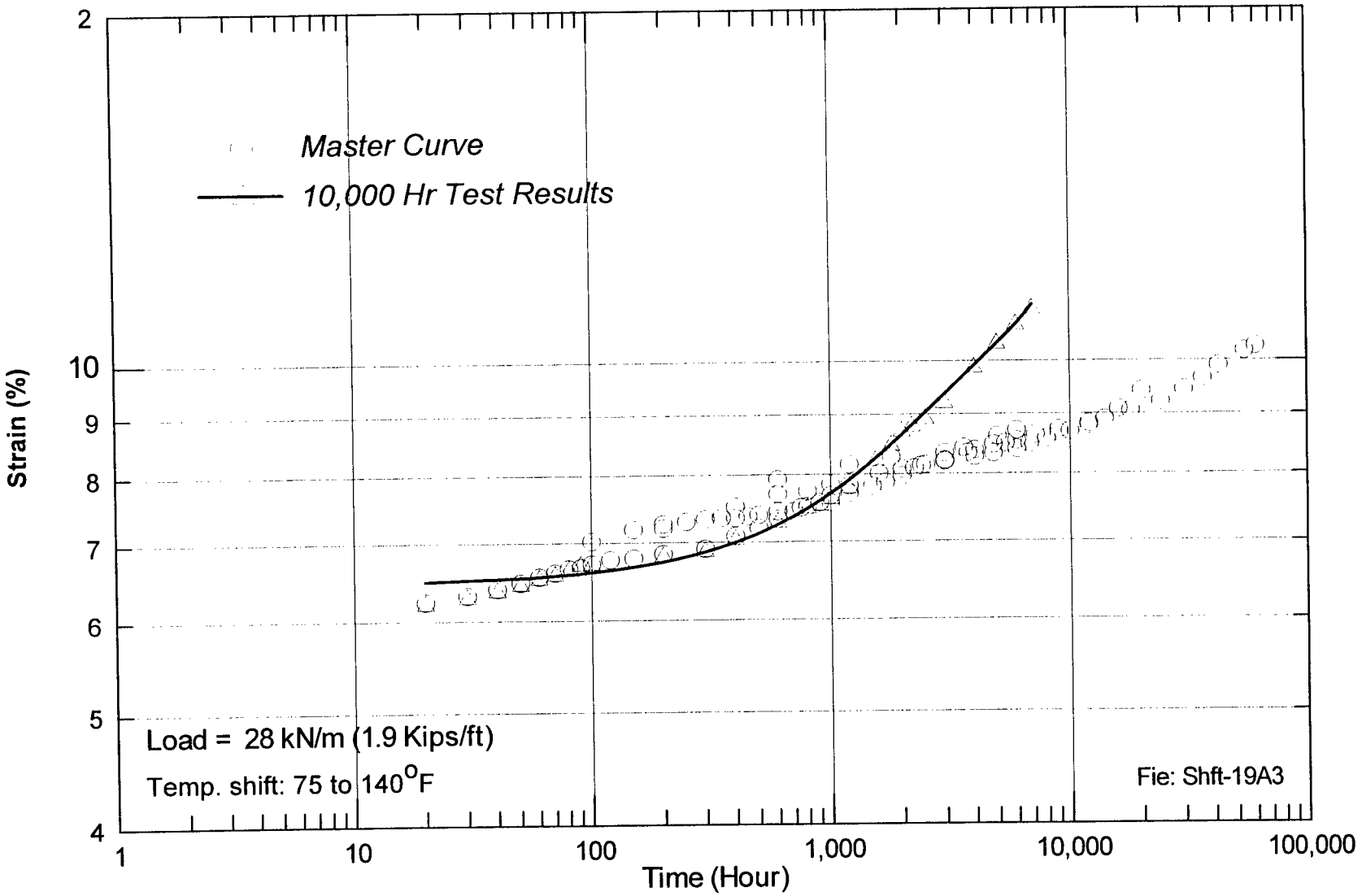

Figure 53

Master curve and 10,000 hour test results for strain at load 28 kN/m

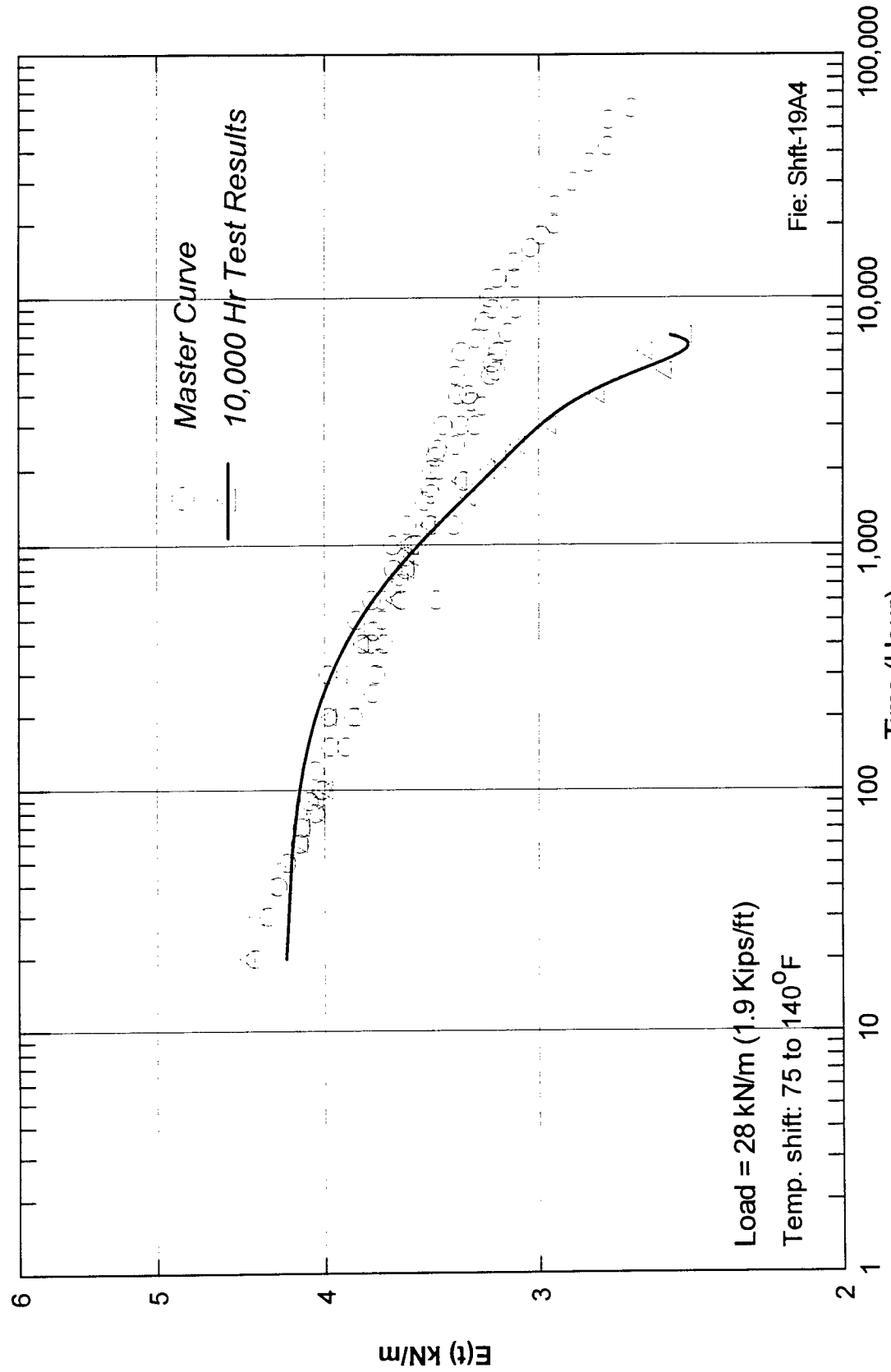

Figure 54

Master curve and 10,000 hour test results for elasticity modulus at load 28 kN/m

Table 10

Parameters of the best fit equations of the shift curves

Load (Kips/ft)	Response function	Shift factors 75°F	100°F	120°F	Linear fit [$Y = a = b\ Log\ (t)$] (a)	(B)	r^2
0.9	Strain	1	10	40	1.94	0.23	0.93
	E(t)	1	10	40	0.44	-0.031	0.95
1.1	Strain	1	6	20	2.20	0.516	0.92
	E(t)	1	6	20	0.435	-0.047	0.95
1.5	Strain	1	8	25	3.41	0.715	0.96
	E(t)	1	8	25	0.37	-0.032	0.97
1.9	Strain	1	5	20	(*)	(*)	-
	E(t)	1	5	20	(**)	(**)	-

(*) Best fitted polynomial function : $y = 5.654 + 0.263\ Log(t) + 0.145\ (Log\ t)^2 - 0.01\ (Log\ t)^3$

(**) Best fitted polynomial function : $y = 0.332 - 0.011\ Log(t) - 0.012\ (Log\ t)^2 + 0.02\ (Log\ t)^3$

It should be noted that since the elasticity modulus of the geogrid polymer is directly proportional to temperature, a vertical shift of the modulus is expected due to modulus variation with temperature. A correction can be applied so that the change in mass per unit volume (ρ) as a function of temperature is accounted for. This correction can be written as *[33]*:

$$\frac{E(T_0, t)}{\rho(T_0)\ T_0} = \frac{E(T, t/a_T)}{\rho(T)\ T} \tag{8}$$

As the division by the density corrects the change of density with temperature variation. However , Morgan showed that, above the glass-transition range, the vertical shift are usually small and can be neglected *[34]* . In this analysis, no vertical shift was applied on the temperature curves to establish the master curve.

4. The shift factors are applied to higher temperatures to obtain the master curves for longer times:

The 10,000 hour master curves were established using test results at temperatures up to 49°C(120°F). Temperature shift was then applied to the results at higher temperatures up to 72°C (160°F) to predict creep strains for longer time intervals. The master curves for strains and elasticity moduli for creep loads 13 kN/m (0.9 Kips/ft), 16 kN/m (1.1 Kips/ft), and 22 kN/m (1.5 Kips/ft) are shown in figures 55-60. The figures show that the application of temperature-shift could extend the prediction of creep strains to up to 200,000 hours from the 1,000 hour test results.

5. The coefficients C_1 and C_2 are compared with the theoretical ones:

The shift factors obtained from the experimental results were shown in table 10. The relationship between the shift factors and temperature is shown in figure 61. The figure

shows that the shift factors (Log a_T) did not practically change with the change of the applied creep load. The figure can then be used to estimate the shift factors at other creep loads within the selected range.

The comparison between the shift factors established from the experimental results in figure 61 and the theoretical values of the shift factors in figure 44 shows that these values compared well and that a_T values have a reasonable form consistent with the theoretical formulation.

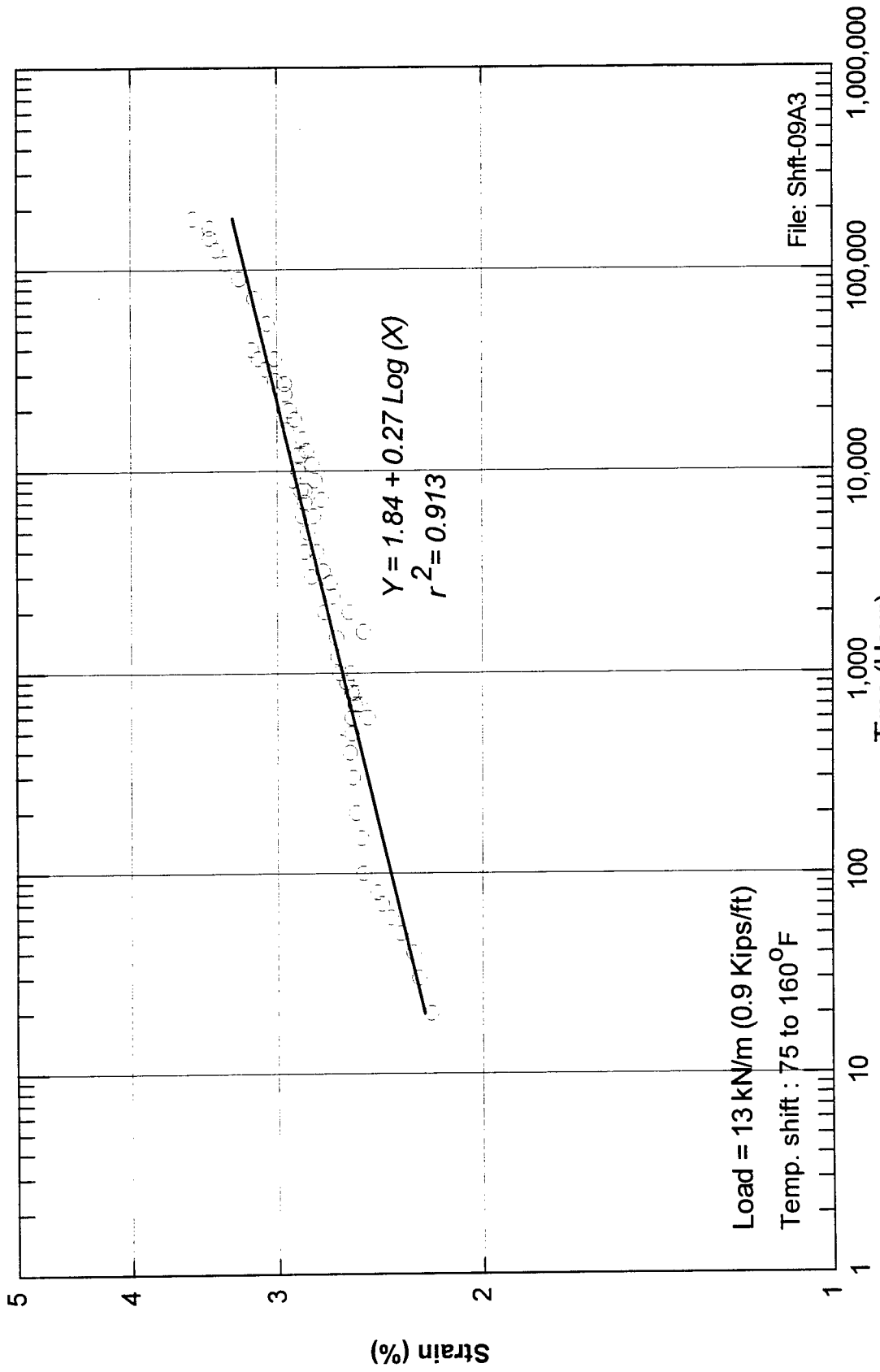

Figure 55

Predicted creep strain at load 13 kN/m

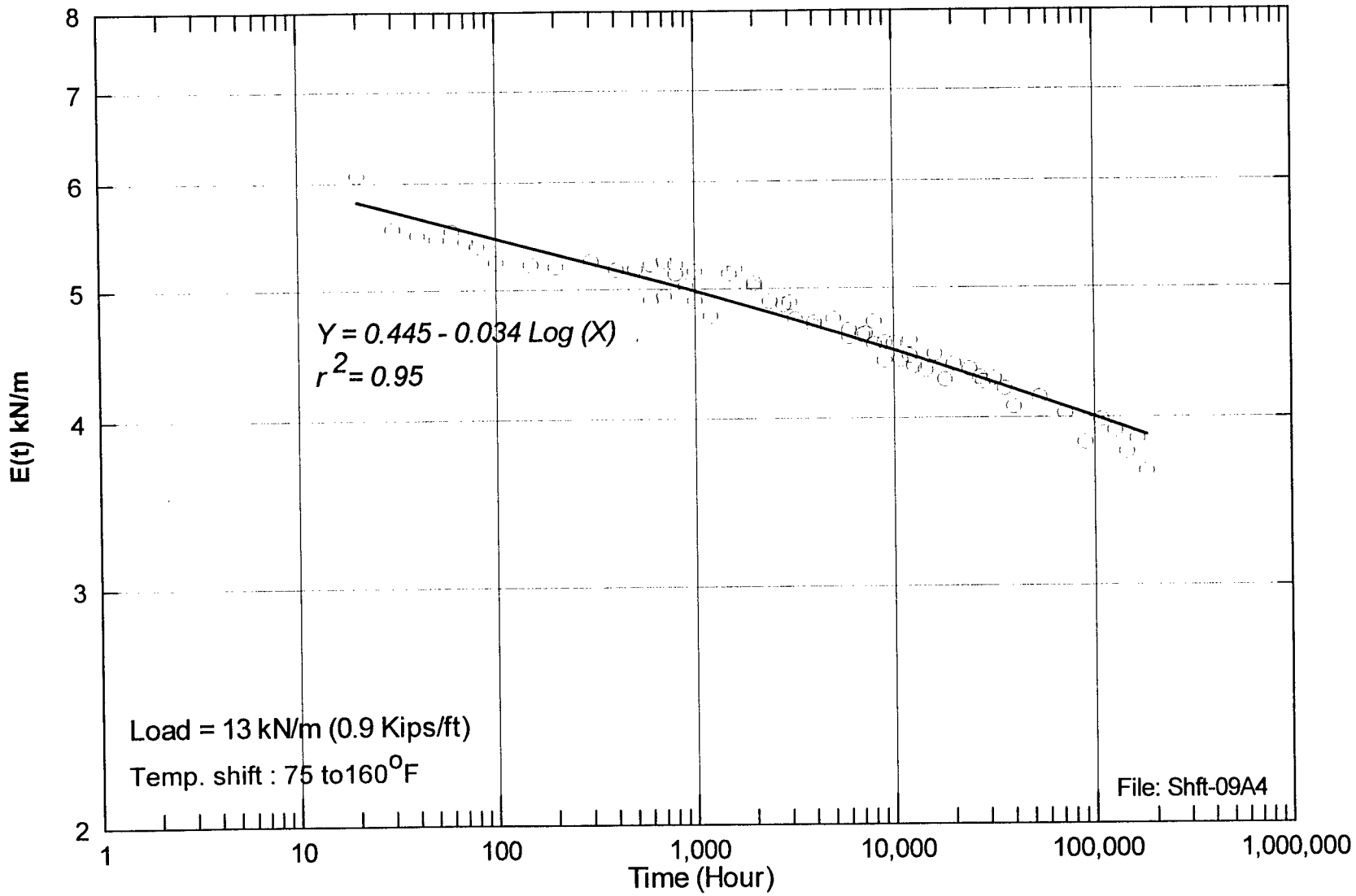

Figure 56

Predicted creep elasticity modulus at load 13 kN/m

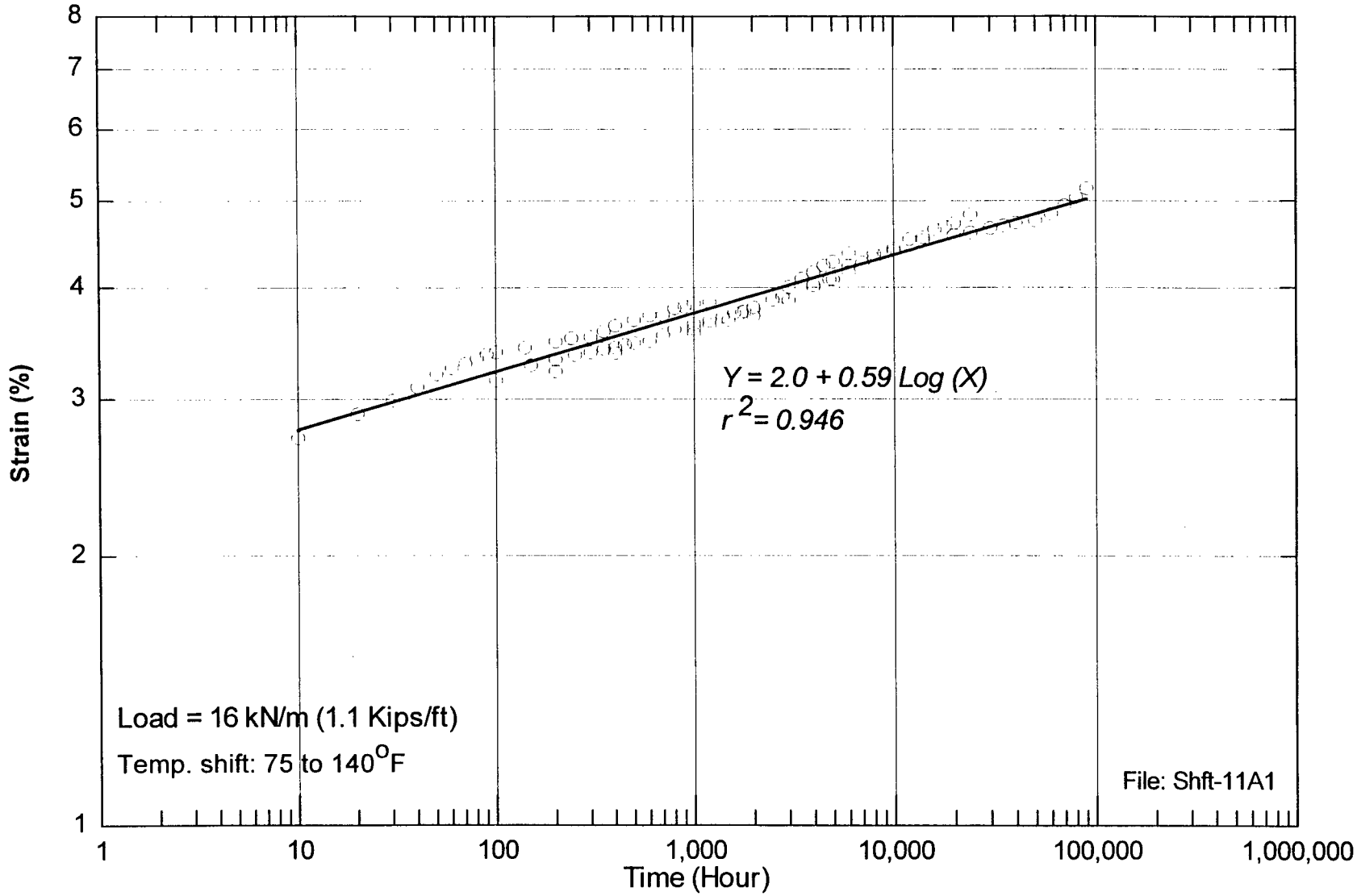

Figure 57

Predicted creep strain at load 16 kN/m

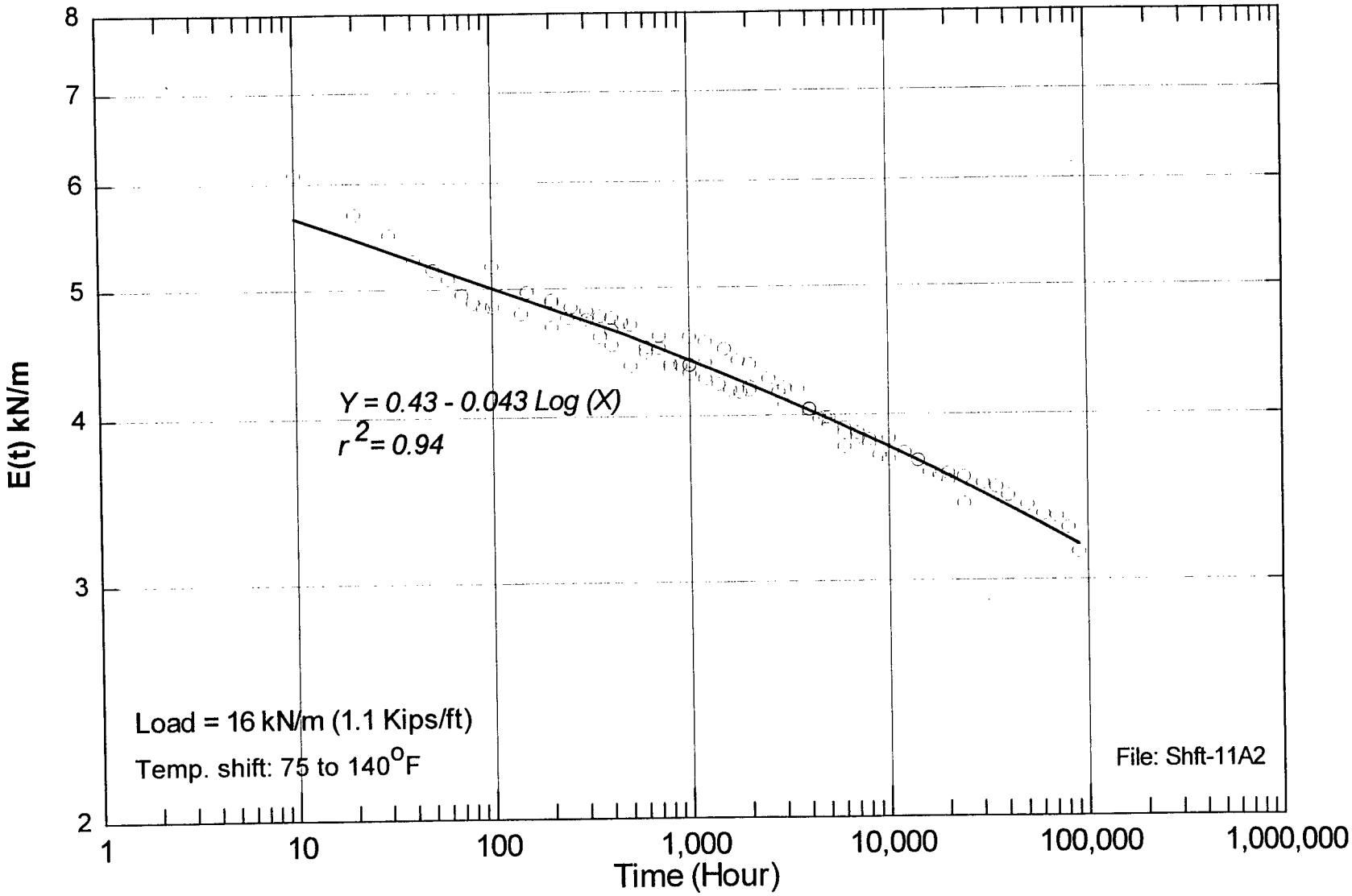

Figure 58

Predicted creep elasticity modulus at load 16 kN/m

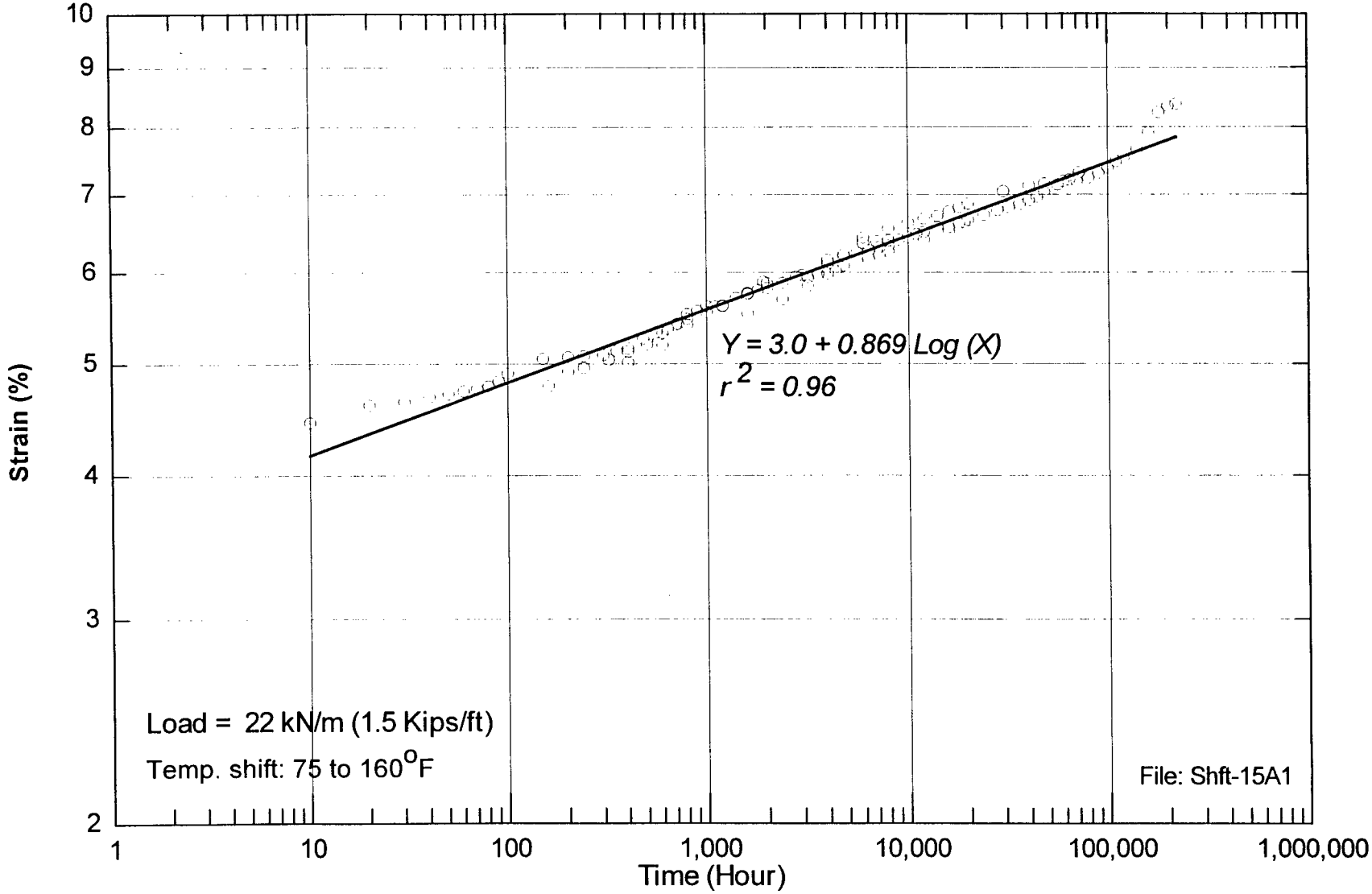

Figure 59

Predicted creep strain at load 22 kN/m

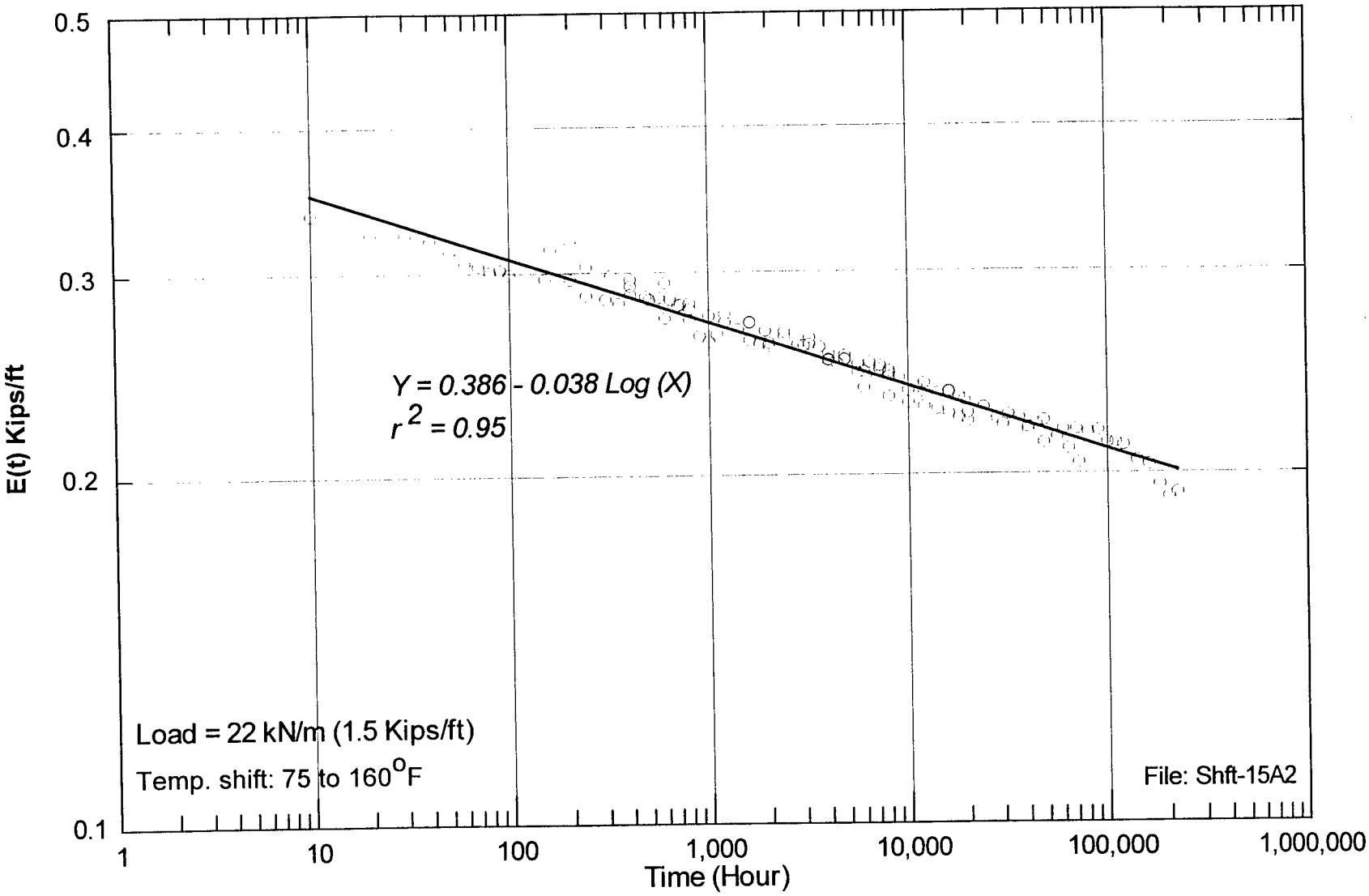

Figure 60

Predicted creep elasticity modulus at load 22 kN/m

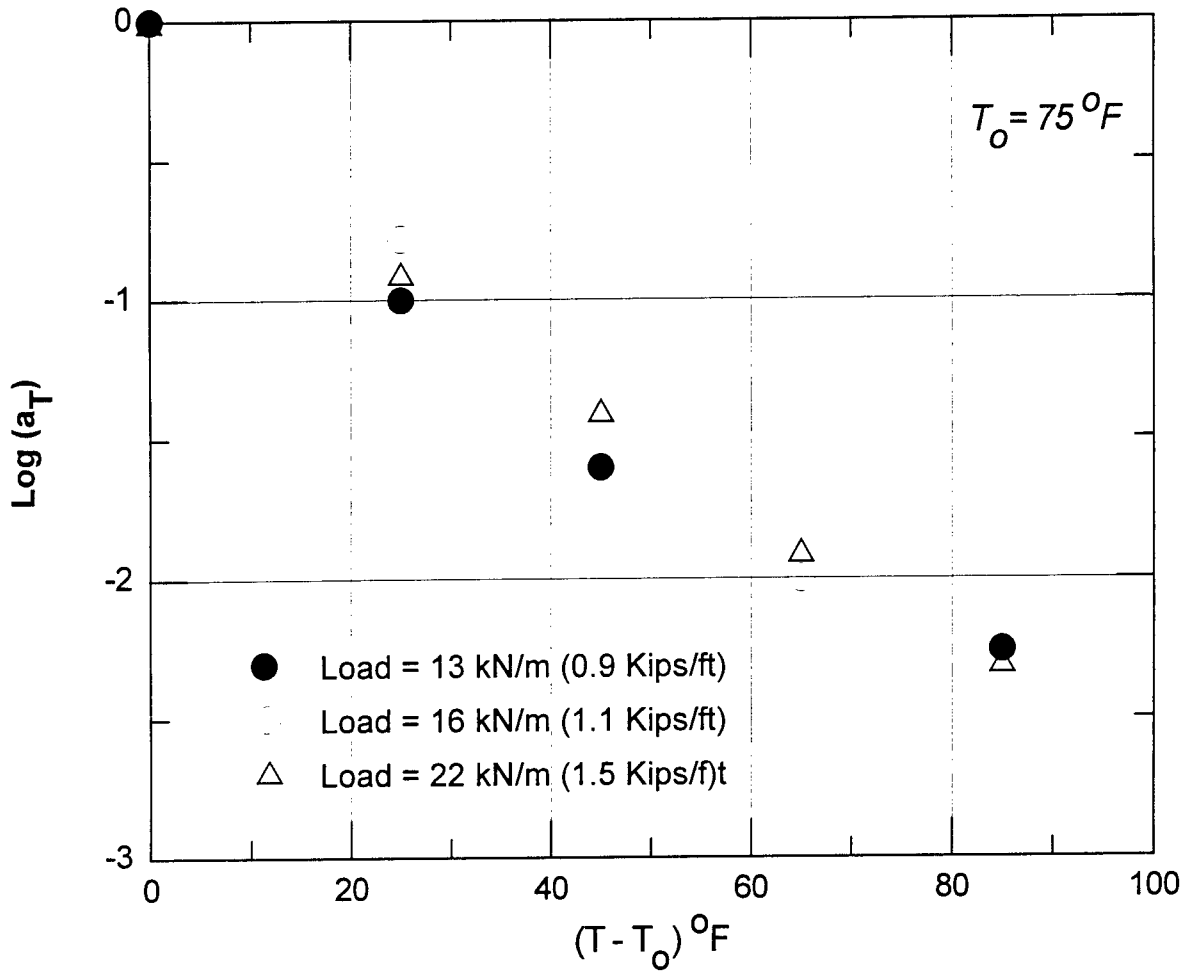

Figure 61

Temperature shift factors a_T from the experimental results

CHAPTER VI

DISCUSSION AND CONCLUSIONS

A creep testing equipment was constructed to test creep behavior of geogrids at room temperature and at elevated temperatures. A testing procedure was conducted for evaluating geosynthetics time-load-temperature relationships. The testing procedure was assessed by testing two different geogrids (HDPE and PET) at various creep loading levels and temperature ranges.

Temperature-creep relationships in geosynthetics vary for each type of geogrid and depend on many factors such as polymer structure, manufacture process, degree of crystallinity, and glass-transition temperature. The extrapolation procedures to predict creep strains from elevated temperature tests do not apply to all types of polymers used in the geosynthetics industry.

The PET geogrid was tested at elevated temperatures close to its glass-transition temperature (75^{o}C). Consequently, the changes in creep strains were not sufficient to successfully establish temperature-creep relationship. Tests at temperatures higher than 75^{o}C are suggested for the PET to evaluate the extrapolation procedures for predicting creep strains at higher temperature. The HDPE polymer had a glass-transition temperature well below room temperature and showed measurable creep response at elevated temperatures. Consequently, temperature-creep test results of the HDPE geogrid were employed in an interpretation procedure to extrapolate creep strains at longer time intervals.

The use of the Arrhenius equation in predicting creep strain-rates from temperature creep tests was presented. The results showed that the estimation of the activation energy was sensitive to the procedure of measuring strain-rates from test results at various temperatures. The evaluation of the procedure demonstrated the difficulty of properly estimating the activation energy that corresponded to each creep load and temperature range.

An interpretation procedure based on shifting creep-temperature curves along the log-time scale was evaluated to predict creep strains at longer times. The estimation of the shift factors was established from the experimental curves and was evaluated with the empirical procedure of the WLF equation. The temperature-shift procedure is summarized as follows:

1. Determine a temperature range for the testing program. The maximum temperature should be lower than the melting point of the polymer, and the temperature range should be within the temperature limit that does not change the physical properties of the geosynthetic. The procedure was evaluated on polymer geogrid performing above its glass transition temperature (HDPE polymer). For polymers in an operating state below the glass transition (as in the PET polymer), the procedure was not successful in shifting creep response curve to establish master curves.

2. Determine the loading range for the creep testing program. The applied loads should be in the visco-elastic range of the polymer tested. The procedure was successful in predicting creep response at loads up to about 40 percent of T_{max} for the HDPE polymer. Temperature-shift procedure failed to accurately estimate creep response at higher loading level that caused an accelerated creep failure of the HDPE polymer.

3. Establish the 10,000 hour creep response at room temperature and at the selected creep loads. The 10,000 hour creep test results are used in calibrating the shift factors from elevated temperature curves.

4. Conduct 1,000 hour creep tests within the established temperature range and creep loading levels.

5. Apply the temperature shift principal on the creep test results to establish the master curves according to the procedure in chapter V. The master curves up to 10,000 hours should compare well with he experimental test results.

6. The constants C1 and C2 of the shift factors should reasonably compare at various loading levels and have a reasonable form as established theoretically using the WLF equation.

It should be noted that the WLF equation was first developed for amorphous polymers at their transition zone and it has been found to apply to numerous amorphous polymers *[21],[22]*. However, polymers used in geosynthetics applications are generally semi-crystalline polymers. Published information has showed some limitations regarding the applicability of the temperature-shift principal in semi-crystalline polymers. However, shift principals could be applied to polymers with some degree of crystallinity *[35]*. Moreover, Plazek showed that it is correct for limited time-temperature ranges *[36]*. Hall evaluated tensile strain-rate-temperature relationships on PP polymers which had 55 percent crystallinity, at temperatures up to 60°C (140°F) *[37], [38]*. His studies showed the validity of the superposition principal for this material. Takaku also showed that the temperature-shift factor a_T of PP fibers followed the WLF equation *[32]* .

The interpretation procedure was evaluated on geogrid polymers of an operating temperature above their glass transition temperature. Further tests would be required to investigate the applicability on other types of polymers. Furthermore, temperature shift procedure was applied to predict the 200,000 hour creep response, which is about two cycles shift on the log-time scale. Further shifts to longer time intervals should be verified and correlated with experimental results.

The maximum range of temperature evaluation should be limited to within the temperature range of the physical state in which the polymer resides at service conditions *[18]*. The thermal transition limits of polymers used in geosynthetics were shown in table 1.

REFERENCES

1. FHWA, *Guidelines for Design, Specifications, and Contracting of Geosynthetic Mechanically Stabilized Earth Slopes on Firm Foundations*, FHWA-SA-93-025, 1993.

2. Task Force No. 27, *Design Guidelines for Use of Extensible Reinforcements (Geosynthetic) for the Mechanically Stabilized Earth Walls in Permanent Applications*, Joint Committee of AASHTO-AGC-ARBTA on Materials, 1989.

3. Allen, T.M., "Determination of the Long Term Tensile Strength of Geosynthetics: A State-of-the-art Review," *Geosynthetics'91 Conference*, Atlanta, 1991, pp. 351-379.

4. GRI-GG4 Standard Practice, "*Determination of the Long Term Design Strength of Stiff Geogrids*," Geosynthetics Research Institute, Drexel University, 1991.

5. Jewell, R.A., and Greenwood, J.H., "Long Term Strength and Safety in Steep Soil Slopes Reinforced by Polymer Materials," *Geotextiles and Geomembranes*, No. 7, 1988, pp. 81-118.

6. Bush, D.I., "Variation of Long Term Design Strength of Geosynthetics in Temperatures up to 40°C," *4th International Conference on Geotextiles, Geomembranes and Related Products*, The Hague, 1990, pp. 673-676.

7. Müller-Rochholz, J., and Kirschner, R., "Creep of Geotextiles at Different Temperatures," *4th International Conference on Geotextiles, Geomembranes and Related Products*, The Hague, 1990, pp. 657-659.

8. Rimoldi, P., and Montanelli, F., "Creep and Accelerated Creep Testing for Geogrids", *Geosynthetics'93 Conference*, Vancouver, Canada, 1993, pp. 773-787.

9. Yeo, K.C.,*The Behavior of Polymeric Grids used for Reinforcement*, Ph.D. Thesis, University of Strathclyde, Glasgow, UK, 1985.

10. Hall, C., *Polymer Materials*, John Wiley and Sons, Inc., New York, N.Y., 1981.

11. Thomas, R.W., and Cassidy, P.E., "An Introduction to Polymer Science for Geosynthetics Applications- Part one," *Geotechnical Fabrics Report*, July/August, 1993, pp. 32-36.

12. Cooke, T.F., and Rebenfeld, L., "*Effect of Chemical Composition and Physical Structure of Geotextiles on their Durability*," Geotextiles and Geomembranes, Vol. 7, 1988, pp. 7-22.

13. Rebenfeld, L., and Cooke, T.F., "Structure and Properties of Fibers in Relation to Durability of Geotextiles," *Durability and Aging of Geosynthetics*, 1989, pp. 48-64.

14. Den Hoedt, G., "Creep and Relaxation of Geotextile Fabrics", *Geotextiles and Geomembranes*, Vol. 4 , 1986, pp. 83-92.

15. Den Hoedt, "Principles of Creep and Relaxation," *Durability of Geotextiles*, 1988, pp. 34-38.

16. Aklonis, J.J. and MacKnight, W.J., *Introduction to Polymer Viscoelasticity*, John Wiley and Sons, 2nd edition, 1983.

17. Thomas, R.W., and Cassidy, P.E., "An Introduction to Polymer Science for Geosynthetics Applications- Part Two," *Geotechnical Fabrics Report*, September, 1993, pp.10-14.

18. Shelton, W.S., and Bright, D.G., " Using the Arrhenius Equation and Rate Expressions to Predict the Long-Term Behavior of Geosynthetic Polymers", *Geosynthetics'93*, 1993, Vancouver, pp. 789-802.

19. McCrum, N.G., Buckley, C.P., and Bucknall, C.B., *Principles of Polymer Engineering*, Oxford University Press, 1988.

20. Lord, A.E. and Halse Y.H., "Polymer Durability-The Materials Aspects," *Durability and Aging of Geosynthetics*, 1989, pp.293-329.

21. Williams, M.L., Landel, R.F., and Ferry, J.D., *Journal of American Chemical Society*, Vol. 77, 1955, pp. 3701-3707.

22. Ferry, J. D., *Viscoelastic Properties of Polymers*, 3rd edition, John Wiley and Sons, 1955.

23. GRI-GG3(a) Standard Practice, "*Tension Creep Testing of Stiff Geogrids*", Geosynthetics Research Institute, Drexel University, 1991.

24. GRI-GG3(b) Standard Practice, "*Tension Creep Testing of Flexible Geogrids*", Geosynthetics Research Institute, Drexel University, 1991.

25. Greenwood, J.H., "The creep of Geotextiles", *4th International Conference on Geotextiles, Geomembranes and Related Products*, The Hague, 1990, pp. 645-650.

26. Matichard, Y., Leclercq, B., and Segouin, M., "Creep of Geotextiles: Soil Reinforcement Applications", *4th International Conference on Geotextiles, Geomembranes and Related Products*, The Hague, 1990, pp. 661-665.

27. Miki, H., Hayashi, Y., Yamada, K., Takasago, T., Shido, H., "Plane Strain Tensile strength and Creep of Spun-Bonded Non-Wovens", *4th International Conference on Geotextiles, Geomembranes and Related Products*, The Hague, 1990, pp. 667-672.

28. Wrigley, N.E., "Durability and Long Term Performance of Tensar Polymer Grids for Soil Reinforcement," *Materials Science and Technology*, Vol. 3, 1987, pp. 161-170.

29. 1995 Specifier's Guide, *Geotechnical Fabrics Report*, Industrial Fabrics Associations International, December, 1994.

30. Sherby, O.D., and Dorn, J.E., "Anelastic Creep of Polymethyl Methacrylate", *Journal of Mechanics and Physics of Solids*, Vol. 6, 1958, pp. 145-162.

31. Segrestin, P., and Jailloux, J.M., "Temperature in Soil and its Effect on the Aging of Synthetic Materials," *Geotextiles and geomembranes*, No. 7, 1988, pp. 51-69.

32. Takaku, A., "Effect of Temperature on Creep Fracture of Polypropylene Fibers," *Journal of Applied Polymer Science*, Vol. 25, 1980, pp. 1861-1866.

33. Mercier, J.P., Aklonis, J.J., Litt, M. and Tobolsky, A.V., "Viscoelastic Behavior of the Polycarbonate of Bisphenol A," *Journal of Applied Polymer Science,* Vol. 9, 1965, pp. 447-459.

34. Morgan, C.J., and Ward, I.M., "The Temperature Dependence of Non-Linear Creep and Recovery in Oriented Polypropylene," *Journal of the Mechanics and Physics of Solids*, 1971, Vol. 19, pp. 165-178.

35. Hadely, D.W. and Ward, I.M., "Non-Linear Creep and Recovery Behavior of Polypropylene Fibers," *Journal of Mechanics and Physics of Solids*, Vol. 13, 1965, pp. 397-411.

36. Plazek, D.J.,"Temperature Dependence of the Viscoelastic Behavior of Polystyrene,", *The Journal of Physical Chemistry*, Vol. 69, 1965, pp. 3480-3487.

37. Hall, I.H., "The Effect of Temperature and Strain Rate on the Stress-Strain Curve of Oriented Isotactic Polypropylene," *Journal of Polymer Science*, 1961, Vol. 54, pp. 505-522.

38. Hall, I. H., "Temperature-Strain Rate Transformations with Isotactic Polypropylene at Finite Strains," *Journal of Applied Polymer Science*, Vol. 8, 1964, pp. 1577-1581.

This public document is published at a total cost of $1912.35. Three hundred copies of this public document were published in this first printing at a cost of $1360.35. The total cost of all printings of this document including reprints is $1912.35. This document was published by Louisiana State University, Graphic Services, 3555 River Road, Baton Rouge, Louisiana 70802, to report and publish research findings of the Louisiana Transportation Research Center as required by R.S.48:105. This material was printed in accordance with standards for printing by state agencies established pursuant to R.S.43:31. Printing of this material was purchased in accordance with the provisions of Title 43 of the Louisiana Revised Statutes.